Journal of Structural Biology: X 11 (2025) 100122

Contents lists available at ScienceDirect

Journal of Structural Biology: X

journal homepage: www.sciencedirect.com/journal/journal-of-structural-biology-x

Molecular biophysics and inhibition mechanism of influenza virus A M2 viroporin by adamantane-based drugs – Challenges in designing antiviral agents☆

Kyriakos Georgiou [a], Dimitrios Kolokouris [b], Antonios Kolocouris [a,*]

[a] Laboratory of Medicinal Chemistry, Section of Pharmaceutical Chemistry, Department of Pharmacy, National and Kapodistrian University of Athens, Panepistimiopolis-Zografou, Athens 157 71, Greece
[b] Structural Biology Section, Department of Drug Design and Pharmacology, Faculty of Health and Medical Sciences, University of Copenhagen, Copenhagen, Denmark

ARTICLE INFO

Edited by Andreas H Engel

Keywords:
influenza A M2
Amantadine
Rimantadine
Biophysics
Channel blockers

ABSTRACT

The influenza A matrix 2 (AM2) protein is a prototype viroporin that conducts protons through an array of water molecules and sidechains of ionizable amino acid residues, with His37 being the most important. Amantadine is a prototype AM2 channel blocker and inhibitor of influenza A AM2 wild type (serine-31) replication. Amantadine received approval for prophylaxis against the influenza virus A in 1966. However, the characterization of the mechanism of action of amantadine targeting AM2 came 50 years after its approval as an anti-influenza A drug. We present results from experimental biophysical methods and molecular dynamics simulations for the complexes of the AM2 WT and amantadine-resistant mutant channels (V27A, L26F, S31N) in complex with adamantane-based ligands. Additionally, we describe critical experimental evidence from biochemical/functional and molecular biology experiments. Previous debates on the mechanism of drug binding and inhibition were due to the different membrane mimetic environment, the excess of the drug, and the method used, rather than the accuracy of the experiments. The collective knowledge acquired can inspire research for the development of new antivirals against influenza viruses and provide experience on the application of molecular biophysics to other viroporins.

1. Introduction

1.1. Structural elements and function of influenza A M2 protein

Viruses present significant public health risks every year. Influenza A virus (IAV) causes global health problems with millions of symptomatic infections in the EU each year and thousands of deaths, straining public health systems logistically. (Paget et al., 2022).

The M gene of IAV encodes two conserved proteins, matrix 1 (M1), a capsid protein, and matrix 2 (M2), which homotetramerize forming an ion channel. M1 is a major component of viral particles, essential for virus assembly and structural integrity. (Martin and Heleniust, 1991) The homotetrameric M2 channel is a prototype viroporin of biological and medicinal interest. It is essential for viral replication through its proton channel (Pinto et al., 1992) and viral budding functions. (Rossman and Lamb, 2011) M2 consists of four regions (Fig. 1), a short disordered extracellular domain (ED, residues 1–21) (Park et al., 1998; Pinto and Lamb, 2007) which is very much conserved and suggested to assist M2 inclusion into the virion, 21) (Park et al., 1998) a transmembrane domain (AM2TM, residues 22–46), an amphipathic helix (AH, residues 47–62), and a largely disordered cytosolic tail (CT, residues 63–97) (Park et al., 1998) which interfaces through non-covalent bonding with the M1 protein. (Lamb et al., 1985) Post-translational palmitoylation alters the cytoplasmic tail (AM2CT), and mutagenesis experiments confirmed that Cys50 is the site of fatty acid acylation (palmitoylation). (Sugrue et al., 1990) Cross-linking experiments showed that inter-monomer disulfide bonds at Cys17 and Cys19 connect the four TM helices at the N-terminus. (Holsinger et al., 1995) The AHs maintain the TM helices together at their C-end, preventing the homotetramer from dissociating when the channel is activated by acid.

☆ This article is part of a special issue entitled: 'Virus-host interactions' published in Journal of Structural Biology: X.

* Corresponding author at: Laboratory of Medicinal Chemistry, Section of Pharmaceutical Chemistry, Department of Pharmacy, National and Kapodistrian University of Athens, Panepistimiopolis Zografou 15771, Athens, Greece.
E-mail address: ankol@pharm.uoa.gr (A. Kolocouris).

https://doi.org/10.1016/j.yjsbx.2025.100122
Received 21 November 2024; Received in revised form 26 January 2025; Accepted 2 February 2025
Available online 4 February 2025

(Schnell and Chou, 2008) In research with AM2 constructs, Cys50 is routinely mutated to Ser to facilitate peptide synthesis and purification and to prevent oligomerization through the formation of disulfide bonds.

The AM2TM is essential for proton conduction, protein tetramerization, and can be blocked by adamantane-based drug molecules. (Chizhmakov et al., 1996; Wang et al., 1994) AM2TM monomers contain hydrophobic residues (e.g., Leu, Ile, Val, Ala), polar or ionic amino acid residues (Ser, His, Trp, Asp, Arg) and Gly that stabilize the tetrameric bundle with hydrophobic and polar interactions. The closed state of the channel is formed by the four monomeric TM α-helices. Proton selective ion channel activity is dependent on the pore formed by four TM α-helices (Ser31, His37, Trp41, Asp44, and Arg45) according to electrophysiology (EP) experimental studies. (Pinto et al., 1992; Chizhmakov et al., 1996; Wang et al., 1994; Sakaguchi et al., 1997; Lin and Schroeder, 2001; Mould et al., 2000; Shimbo et al., 1996; Pinto and Lamb, 2006; Chizhmakov et al., 2003; Pinto et al., 1997; Tang et al., 2002; Acharya et al., 2010; Holsinger et al., 1994; Hu et al., 2006) The polar and charged amino acid residues (Ser31, His37, Trp41, Asp44, and Arg45) have their side chains pointing inside the channel pore. The side chains of the hydrophobic residues point towards the lipid bilayer except for Val27, Ala30, and Gly34, which also orient inside the channel pore. (Sugrue and Hay, 1991; Holsinger and Alams, 1991) The TM domain's lipid-facing residues are mostly composed of lipophilic residues that interact with the lipid acyl chains of the bilayer via weak hydrophobic interactions.

The H37xxxW41 motif, which is characteristic of influenza proton channels, is essential for AM2 proton conductance. (Pinto and Lamb, 2006; Acharya et al., 2010; Hu et al., 2006) Four His37 residues, known as the heart of the proton conducting channel, are in the middle of the TM bundle and are critical to the proton transport mechanism. (Hu et al., 2006) The homotetrameric AM2 channel's α-helical bundle (Duff et al., 1992) has a structurally rigid closed state at pH > 7.5 with His37 and Trp41 functioning as gates, and it opens under slightly acidic endosomal pH (pH 6).

The His37 tetrad in the middle of the TM domain has a + 3 net charge at pH 6. (Hu et al., 2006) Protonation of the imidazole rings of His37 results in electrostatic repulsion between charged His37 residues. This repulsive force perturbs helix-helix packing causing a quaternary structure destabilization and enlargement of the pore. The Trp41 gate opens and protons enter from the outside of the virus (Fig. 1**A**). (Pinto et al., 1992) It was suggested (Okada et al., 2001) that the protonated imidazole side chains of His37 and the electron-rich indole rings of Tpr41 side chains have the proper orientation to form strong π-cation interactions. This interaction stabilizes the Trp41 gate in the open conformation upon His37 protonation. AM2 is characterized by asymmetry in the conductance direction regulated by Trp41, since only when the external pH is acidic ($pH_{out} < pH_{in}$) can the Trp41 gate open favoring

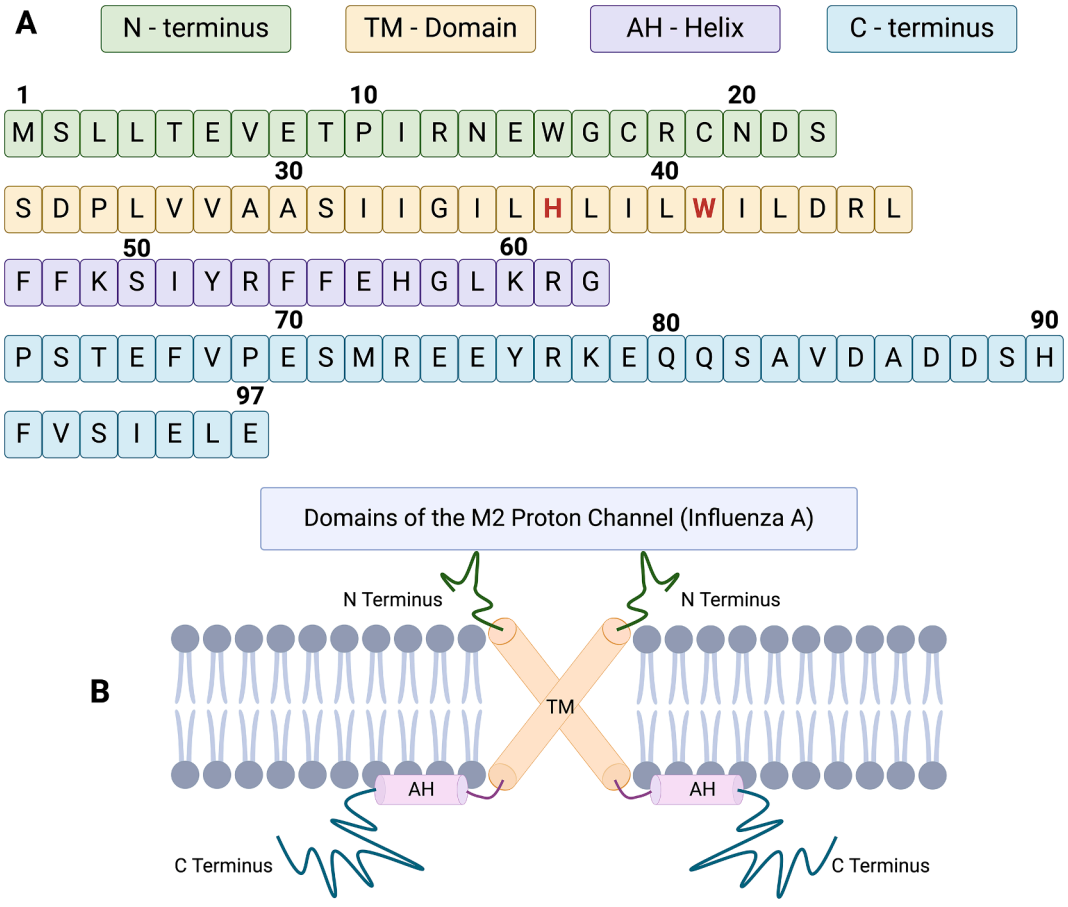

Fig. 1. (A) Structure and amino acid sequence of the influenza wild-type (WT) Udorn/72 AM2 protein. The N-terminus (residues 1–22) is positioned outside the membrane, has a substantial β-sheet structure, and stabilizes the tetramer by inter-monomer disulfide bonds between Cys17 and Cys19. (Holsinger et al., 1995) Amino acids 23–46 form a TM helix, featuring the characteristic H37xxxW41 motif in the C-terminal half, which contains the essential His37 and Trp41 residues (red). The C-terminal half, which has 35 amino acid residues, binds to the AM1 protein. (Jin et al., 1997) Residues 47–62 make up the juxtamembrane amphipathic helix (AH). Residues F47-48 are at the junction between TM and AHs. The disordered C-terminus consists of residues 63–97. The combination of the TM and AHs forms the conductance domain of AM2 (AM2CD) which produces the channel properties of the full protein AM2 (AM2FL) and amantadine drug binding of AM2 WT. (B) Graphical representation of AM2′s domains and the membrane bilayer (only two TM monomers embedded in the bilayer are shown for clarity). (For interpretation of the references to color in this figure legend, the reader is referred to the web version of this article.)

proton transport. (Chizhmakov et al., 2003; Mandala et al., 2017).

AM2TM + AH (AM2CD), dubbed the conductance domain (CD), (Schnell and Chou, 2008) is the functional core containing all the residues and necessary interactions to replicate the conductance properties of the native full-length M2 (M2FL) protein. (Ma et al., 2009) The AHs (residues 47–62) are in the inner membrane interface (Fig. 2), between the TM α-helix and the AM1-binding domain. The inner membrane interface location of the AHs creates the wedge-like shape of M2CD, promoting the M2 membrane curvature in the host cell, critical for viral budding. (Rossman and Lamb, 2011) Different studies show slight discrepancy in the definition of the AM2CD domain, involving residues 18–60 (Andreas et al., 2010) or 21–61 (Ma and Polishchuk, a L., Ohigashi, Y., Stouffer, a L., Schon, a; Magavern, E., Jing, X., Lear, J. D., Freire, E., Lamb, R. a; DeGrado, W. F., Pinto, L. H. , 2009) or 22–62 (Sharma et al., (1979) 2010).

EP experiments have revealed that amantadine, (Wang et al., 1993) rimantadine, (Thomaston et al., 2021; Drakopoulos et al., 2017) and adamantyl amine analogs, (Tzitzoglaki et al., 2017; Drakopoulos et al., 2018; Kolocouris et al., 2014; Torres et al., 2012; Barniol-Xicota et al., 2017) or other cage amine analogs, (Torres et al., 2014; Rey-Carrizo et al., 2015; Rey-carrizo et al., 2013; Rey-Carrizo et al., 2014; Hu et al., 2006) inhibit the proton translocation of the wild-type (WT) AM2 channel, with serine at position 31. The antiviral potency of amantadine was initially reported in 1963 After this, amantadine received approval for prophylaxis against the influenza virus A in 1966. However, due to the occurrence of mutant strains resistant to amantadine, with mutations L26F, V27A and the prevalent S31N in the AM2 transmembrane domain, amantadine and rimantadine usage has been abrogated in the clinic. To this end, a second generation of adamantane-based drugs was developed. These compounds are conjugates of amantadine with an aryl group, connected through a methylene linker and can block the AM2 S31N channel-mediated proton current according to EP. (Wang et al., 2013; Hu et al., 2018; Wang et al., 2018; Tzitzoglaki et al., 2020) Some adamantyl amines (Torres et al., 2012; Barniol-Xicota et al., 2017; Rey-Carrizo et al., 2014; Stampolaki et al., 2023; Hu et al., 2017; Wang et al., 2011; Balannik et al., 2009) or conjugates of adamantyl amines with an aryl group (Tzitzoglaki et al., 2022) can also block the AM2 V27A- and/or L26F-mediated proton current according to EP.

The structure, dynamics and function of AM2 in complex with ligands has been explored by various biophysical and biochemical techniques. Applications include neutron diffraction, Nuclear Magnetic Resonance (NMR) spectroscopy, solid state NMR (ssNMR), solution NMR, X-ray crystallography, small-angle and wide-angle X-ray scattering (SAXS and WAXS, respectively), native mass spectrometry (nMS), Differential Scanning Calorimetry (DSC), Analytical Ultracentrifugation (AUC), Ultraviolet (UV) resonance Raman spectroscopy, Circular Dichroism (CD) spectroscopy, electron paramagnetic resonance (EPR) spectroscopy and molecular dynamics (MD) simulations. Additionally, EP, liposome proton flux, isothermal titration calorimetry (ITC), surface plasmon resonance (SPR) assays and molecular biology (e.g., mutagenesis) experiments have been applied.

While the experimental structures in most cases did not correspond to AM2FL, various M2 constructs in complex with adamantane-based compounds have been studied, but a different membrane mimetic environment was applied for structure determination, e.g., different synthetic bilayers or detergent micelles, and different molar excess of drugs to the AM2 tetramer. The results caused many contradictions in the way drugs bind and inhibit the channel. For example, the drug binding site within the channel pore or on the surface of the protein, as well as the orientation of the drug, caused a significant debate which stimulated functional experiments and structural biology investigations. Relevant information is also available elsewhere, e.g., see review articles in refs. (Cross et al., 2012; Pielak and Chou, 2011; Jalily et al., 2020; Wang et al., 2011; Kumar and Sakharam, 2024; Aledavood et al., 2022; Georgiou and Kolocouris, 2025). This manuscript incorporates updated information about liganded AM2 structures that have been deposited in

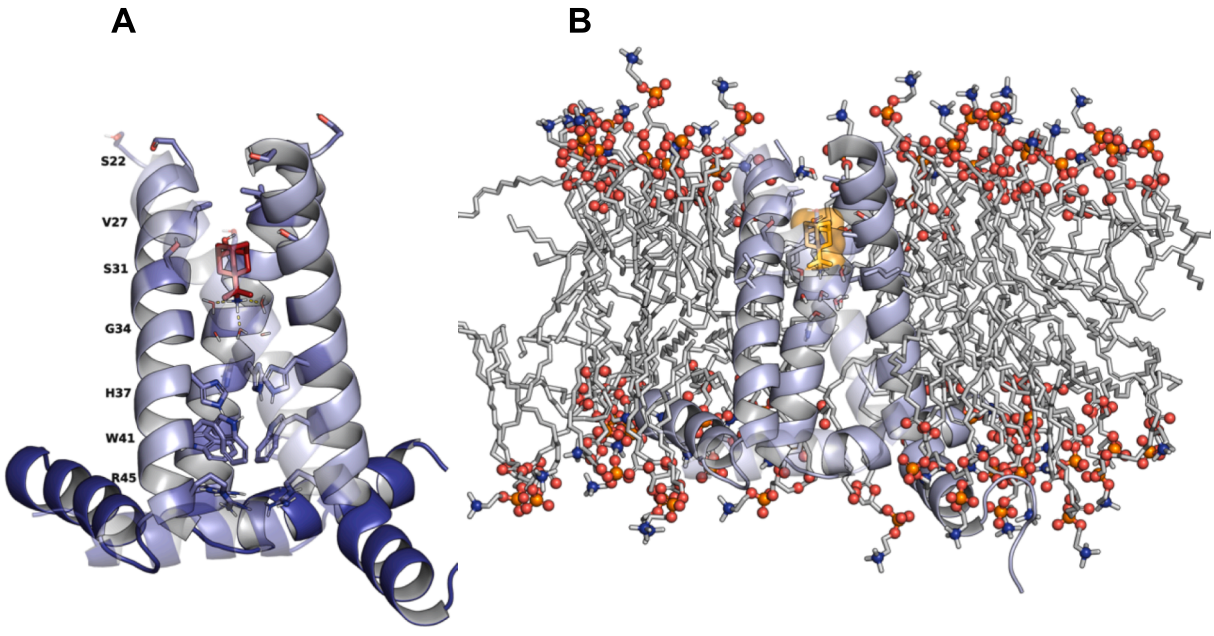

Fig. 2. (A) Structure of AM2CD WT (residues 22–62) in complex with an adamantyl amine, a rimantadine analog bearing a methyl group substitution at carbon bridge of rimantadine (see Drakopoulos et al., 2018), in its functional binding site (inside the AM2 pore) revealed from research in refs. (Cady et al., 2010; Cady et al., 2011; Thomaston et al., 2018). Residues F47-48 are at the connection between TM and AHs. It is shown the juxtamembrane AH (residues 47–62). The structure of the complex resulted from our 500 ns-MD simulations, using the amber19sb force field (ff19sb) (Tian et al., 2020) for protein, CHARMM36m for the lipids (Huang et al., 2016) and generalized Amber force field (GAFF) (Sprenger et al., 2015) for the ligand, of AM2CD – adamantyl amine complex embedded in 1-palmitoyl-2-oleyl-*sn*-glycero-3-phosphocholine (POPC) bilayers. The starting structure for the simulations was prepared based on PDB ID 2L0J (Sharma et al., (1979) 2010) after superposition with PDB ID 2KQT (Cady et al., 2010), eliminating the AM2TM and build the rimantadine analog instead of amantadine. The complex was embedded in a pre-equilibrated hydrated POPC bilayer. The bilayer extended 20 Å beyond the solute in the x-y plane while waters extended 20 Å beyond the solute in the z-axis perpendicular to the membrane normal. (B) The structure of AM2CD WT in complex with the rimantadine analog after 500 ns-MD simulations in the POPC bilayers.

the Protein Data Bank (**Table S1**). An attempt was made to provide results in accordance with the many biophysical methodologies employed, as well as to portray the investigative progress in chronological order.

2. The pharmacological binding site of adamantyl amine drugs against AM2 WT

2.1. Indirect evidence from adamantyl amine drugs binding to AM2 WT

2.1.1. Molecular biology

Hay and collaborators originally described in their studies in 1978 (Skehel et al., 1978)and 1985 (Hay et al., 1985) that resistance to inhibition of influenza A virus by amantadine, is related to mutations in the AM2 WT protein's TM domain. The types of drug-resistant mutations that can be tolerated are limited by the homotetrameric structure of the AM2 WT channel, as described by DeGrado and collaborators in 2008 (Stouffer et al., 2008) and Arkin and collaborators in 2011. (Astrahan and Arkin, 2011) Because the binding site was assumed to be inside the TM of the pore having a C4 symmetry axis, a single mutation that changes four positions per tetramer can cause large changes on drug binding but also on the channel's function, as reported by Pinto and collaborators in 2010. (Balannik et al., 2010) Pinto and collaborators used TEVC in oocytes in 2010 (Balannik et al., 2010) to study the effect of different mutations on amantadine sensitivity. Only four AM2 mutants (V27W, V27T, S31A, and S31G) at the N-terminal of the His37 gate showed more than 75 % inhibition by 100 μM amantadine. AM2 W41F lacks Trp41′s electron-rich ring, which is required for AM2′s structure, pH activation, and rectification. This mutant, like W41A, has lower sensitivity to amantadine. It seems that because of their distant location inside the pore from the amantadine binding site, most mutants on Asp44 and Trp41 residues showed minimal or no effect on amantadine inhibition.

The few amantadine- or rimantadine-resistant mutations are L26F, V27A, A30T, S31N and G34E in the transmembrane pore (22–46) of AM2 WT. (Furuse et al., 2009; Bright et al., 2005; Lan et al., 2010; Abed et al., 2005; Brown et al., 2010; Li et al., 2009; Dong et al., 2015; Garcia and Aris-Brosou, 2014; Furuse et al., 2009) The mutations that induce the largest decrease in inhibition are S31N and V27A, which enhance the polarity of the pore. Indeed, most of the resistant viruses (95 %) have the S31N mutation in AM2, whereas only 1 % have V27A, and L26F, A30T. The G34E is a rare mutant. (Dong et al., 2015; Garcia and Aris-Brosou, 2014) Between the influenza A viruses currently circulating, the AM2 S31N mutant, which is one of the most conserved viral proteins, maintains almost similar channel function to the AM2 WT while being resistant to amantadine and its analogs. The mutation V27A occurred mainly because of drug selection pressure (Furuse et al., 2009; Furuse et al., 2009) and the rest of mutations are natural. These mutations can be found in transmissible viruses, (Furuse et al., 2009; Bright et al., 2005; Lan et al., 2010) while other mutations are easily detected *in vitro*. The prevalence of globally circulating influenza A L26F, V27A, and mainly S31N mutant viruses drives the hunt for new ion channel blockers that target these resistant AM2 channels with higher activity.

2.1.2. EP, liposomal proton flux assay

Duff and Ashley in 1992 (Duff and Ashley, 1992) showed that AM2TM WT proton channels in glycerophospholipid bilayers consisting of POPC and 1-palmitoyl-2-oleyl-*sn*-glycero-3-phosphoserine (POPS) are blocked by 20 μM amantadine in EP experiments.

The most straightforward method to determine the blocking effect of M2-mediated proton current is EP in AM2CD WT expressed in oocytes. In 1993, Lamb and coworkers characterized (Wang et al., 1993) the blocking of AM2FL WT-mediated proton current by amantadine. The Udorn AM2FL WT showed a $K_i = 9$ μM at pH 7.5 compared to $K_i = 13$ μM at pH 6.2. Thus, amantadine binds with the highest affinity to the closed form of the channel. A TEVC assay using X. laevis oocytes microinjected with RNA expressing the AM2 WT protein was used. (Wang et al., 1994) Continuing this work, in 1996, Lamb and coworkers (Tu et al., 1996) performed additional EP studies to characterize the blockage by other analogs of amantadine, e.g., of 2-[3-azaspiro (5,5)undecanol]-2-imidazoline (BL-1743). TEVC studies of AM2 WT in oocytes performed by Lamb and coworkers in 1994 (Wang et al., 1994) revealed that deletion of the four residues 28–31 in the TM domain (AM2 WT-del28-31) results in a proton channel that was insensitive to pH and blockage by 100 μM amantadine. (Wang et al., 1993)Indeed, this sequence (AM2 WT-del28-31) was identified in influenza virus that was amantadine resistant. (Wang et al., 1994) In 1997, Pinto and collaborators used site-directed mutagenesis combined with Cys scanning, EP and periodicity analysis to suggest (Acharya et al., 2010) that amantadine binds inside the AM2TM pore (residues 26–43) close to Gly34 where the largest space of the pore is present. (Pinto et al., 1997).

In EP assays conducted by Schroeder and collaborators in 2005, (Schroeder et al., 2005) amantadine inhibits proton flux through AM2FL WT in liquid crystalline lipid bilayers containing 30 % cholesterol. However, EP investigations in *Escherichia coli* membranes and liposomes without containing cholesterol revealed that cholesterol was not necessary to make the proton channel sensitive to amantadine blockage. (Schroeder et al., 2005).

Chou and Schnell in 2009 (Pielak et al., 2009) showed with proteoliposomal proton flux assays that rimantadine quickly blocks proton currents through the fully functional cytoplasmic helices of the AM2CD WT construct (residues 18–60).

Pinto, DeGrado and collaborators in 2009 (Ma et al., 2009) applied AUC to measure the stability of AM2TM WT compared to AM2FL WT in the pH range pH 6–9. To measure the proton conductance mediated by AM2TM WT or AM2CD WT (residues 18–60), the pH of activation, and drug-inhibition properties a liposome proton flux assay was applied with AM2 construct embedded in small liposomes composed by unilamellar 2:1 POPC/1-palmitoyl-2-oleyl-sn-glycero-3-[phospho-rac-(1-glycerol)] (POPG) vehicles. It was shown that AM2CD WT (residues 18–60) exhibits amantadine-sensitive proton fluxes. (Ma et al., 2009) It was demonstrated (Ma et al., 2009) that AM2TM WT is the minimal construct required for tetramerization, selective proton transport, and amantadine channel blockage. The AM2TM WT domain's proton flux rate and amantadine inhibitory characteristics were found to be identical to those of the AM2FL WT.

2.1.3. Neutron diffraction

Bradshaw and collaborators in 1994 (Duff et al., 1994) used neutron diffraction with both deuterium-labeled amantadine and AM2TM WT (d6-V27) and showed amantadine lying 5 Å from the bilayer's center in an area between Val27 and Ser31, in line with the findings from Pinto and collaborators (Pinto et al., 1997). In this position amantadine can sterically block the ion channel proton transportation according to this assumed model of channel inhibition. However, such experiments with amantadine and the amantadine-resistant mutant AM2TM V27A revealed no such interaction. (Duff et al., 1994).

2.1.4. Thiol-disulfide interchange experiments

In 2003, DeGrado, Lear and collaborators applied (Cristian et al., 2003) thiol-disulfide exchange assays under equilibrium conditions in AM2TM WT (residues 19–46) embedded in glycerophospholipids POPC, 1,2-dimyristoyl-*sn*-glycero-3-phosphocholine (DMPC), and 1,2-dilauroyl-*sn*-glycero-3-phosphocholine (DLPC) bilayers. The experiments aimed at measuring the thermodynamics of AM2TM WT tetramer formation in different phospholipid bilayers with or without amantadine. The peptide AM2TM WT (residues 19–46) has a single native Cys residue. This Cys residue can form reversibly inter-monomer disulfide bonds in the tetramer. The resulting tetramer with the S-S bonds still binds amantadine. Because the AM2TM WT exists in equilibrium between monomers and tetramers, the peptide's redox capacity depends on the peptide/ phospholipid ratio. The reduced form of AM2TM WT

(residues 19–46) peptide was reconstituted with different peptide/phospholipid molar ratios into phospholipids and glutathione (GSH) redox buffer containing known quantities of oxidized glutathione (GSSG) and reduced GSH. The reaction reached equilibrium before being treated with HCl to stop thiol exchange and oxidation. The contents of the equilibrium mixture were separated and measured using analytical RP-HPLC. By increasing peptide concentration, the population of the tetramer increases and the AM2TM WT peptide was oxidized easier. While the disulfide formation was increased according to the trend POPC > DMPC > DLPC in agreement with the CD experiments, (Salom et al., 2000) amantadine increased tetramer stability and promoted the formation of more homogeneous helical bundles. (Cristian et al., 2003).

CD, AUC, fluorescence spectroscopy, solution ^{1}H NMR spectroscopy

DeGrado and collaborators studied in 2000 (Salom et al., 2000) the equilibrium between monomer and tetramers of AM2TM WT peptide in dodecyl phosphocholine (DPC) micelles using CD, AUC, fluorescence spectroscopy and ^{1}H NMR. The tetramerization as well as binding by amantadine increased the ellipticity (223 nm) in the AM2TM CD spectrum. For example, when [AM2TM]/[DPC] = 1/2000 the monomer was the predominant constituent, when [AM2TM]/[DPC] = 1/100 an equilibrium with ~ 60 % tetramers existed, and for an equilibrium containing mainly tetramers bound to amantadine the sample contained [AM2TM]/[DPC]/[amantadine] = 1/100/10. It should be noted that in various biophysical experiments with various AM2 WT constructs the molar ratio tetramer/lipid can have increased values, e.g., 1:25 or even 1:8 to ensure the tetramer formation of the studied AM2 WT construct. When amantadine binds AM2TM WT it shifts the equilibrium toward tetramer. The tetramer formation and binding of AM2TM WT by amantadine were more favorable at elevated pH, e.g., pH = 8 where all His37 are unprotonated and the AM2TM WT adopts a C_{closed} conformation. Additionally, using ^{1}H NMR spectroscopy a p*K*α of 6.4 was measured for the AM2TM WT tetramer without amantadine. The drug was found to decrease the p*K*α of the tetramer to 5.8 suggesting its presence at a binding site close to the His37 tetrad.

Hay and collaborators developed in 2004 (Czabotar et al., 2004) an assay to measure the binding affinity of adamantyl amines at acidic pH against the C_{open} conformation of AM2FL. The assay used the quenching of Trp41 fluorescence by His37 protonation below pH 6 in the AM2 channel in LDAO (N,N-dimethyldodecylamine-N-oxide) detergent. The quenching is reversed by adamantyl amine blockers. The assay was used by Kolocouris in 2010 [258] and Cournia, Kolocouris in 2013. (Gkeka et al., 2013).

DeGrado and collaborators applied AUC in 2005 (Stouffer et al., 2005) to measure the difference in thermodynamic stability of the oligomeric state of AM2TM WT (Udorn peptide), caused by ten different mutations in residues with side chains lying in the helix–helix interface (Leu26, Ile33, Leu38, Ile40), or Ser31 with a side chain lining the hydrophilic pore, to either alanine or phenylalanine. Interestingly, these mutations didn't cause destabilization of the corresponding tetramers suggesting that AM2 adjusts its conformational stability to preserve gating and proton conduction which requires quick interchange between the involved conformations. The binding constant for amantadine was measured K_d = 11 μM which was very close to that determined by Lamb and co-workers using EP in 1993. (Wang et al., 1993) The most destabilizing mutations in the presence of amantadine were L26A and L26F, suggesting that L26 could engage amantadine. Thus, a model of the amantadine complex was suggested in which amantadine binds near the center of the pore between the side chains of residues Val27, Ala30, Ser31, Gly34, and His37 that line the pore.

The solution NMR spectra of AM2CD WT (residues 18 − 60) solubilized in micelles obtained by Chou and Schnell in 2008 (Schnell and Chou, 2008) showed that the apo-AM2 exhibited broad NMR lines that become narrower upon rimantadine addition making the conformational mixture more homogeneous stabilizing the tetramer, as observed in previous thiol disulfide exchange experiments. (Cristian et al., 2003).

2.1.6. Raman spectroscopy

Takeuchi and collaborators in 2001 (Okada et al., 2001) used Raman spectroscopy and confirmed that, at acidic pH, AM2TM WT in 1-palmitoyl-2-oleyl-*sn*-glycero-3-phosphoethanolamine (POPE)/POPS has its Trp41 gate stabilized in the open conformation upon His37 protonation via a His37-Trp41 cation-π interaction. The protonation of His37 and the Raman intensity change of Trp41 were not seen in the presence of amantadine, which may inhibit the M2 ion channel adjacent to His37, the main titratable residue in the pore. This finding was in line with previous data showing reduction of the channel's p*K*α with amantadine and suggests that amantadine affects the protonation equilibrium of the His37 tetrad.

2.1.7. ITC

Pinto and collaborators in 2009 (Ma et al., 2009) applied ITC for the titration of tetrameric AM2TM WT (Udorn sequence) reconstituted in POPC/POPG bilayers, using 1:100 peptide/phospholipid which ensured the formation of M2TM WT tetramers quantitatively at pH 7.4 in the presence of amantadine and reported a K_d = 2.3 μM for the interaction between amantadine and AM2TM WT, which was the highest affinity measured to date and under biochemically controlled, *in vitro* conditions.

2.1.8. SPR

In 2010 (Rosenberg and Casarotto, 2010) Casarotto and colleagues conducted a series of SPR studies to correctly assess the affinity of amantadine and rimantadine for AM2TM WT ion channels in DMPC liposomes.

They found that these adamantyl amine drugs can bind AM2TM WT with two distinct affinities in the order of 10^{-4} (K_d = 0.40 mM) and 10^{-7} M (K_d = 0.91 μM) suggesting that both sites are present. They suggested that the binding site with the higher affinity which is responsible for the biological activity of the drugs corresponds to the adamantyl amine position inside the AM2 ion channel pore, and that the secondary binding site with the lower affinity corresponds to the lipid facing position. In this study, drug binding to mutant AM2TM (V27A, S31N, and D44A) was investigated to probe further the position of the two binding sites. Thus, by measuring a K_d = 0.13 μM for amantadine against AM2TM D44A, compared to K_d = 0.91 μM for AM2TM WT, they argued that the drug binds AM2TM D44A only inside the pore. Only AM2TM WT (K_d = 0.40 mM), and AM2TM V27A (K_d = 0.38 mM) bind amantadine at high concentrations in the low affinity binding site, but not AM2TM S31N or D44A. (Rosenberg and Casarotto, 2010) These findings suggest that the latter pore-lining residue mutations affect the low affinity binding site's accessibility via an intricate allosteric network.

2.1.9. Solution NMR

Broadhurst, Kolocouris and collaborators in 2004 (Kolocouris et al., 2004) used the lineshape of 3-fluoro-amantadine in ^{1}H NMR spectra of this ligand, with AM2TM WT peptide in DMPC liposomes. At pH 5–7 the ^{1}H NMR signals of 3-fluoro-amantadine were clearly observed since it has been shown that, at this pH range, AM2TM WT exists mainly as monomers in a lipid environment. Above pH 7.5, when the tetrameric AM2TM WT forms and binds the ligand, the ^{1}H NMR resonances of 3-fluoro-amantadine became too broad to be detected (Fig. 3).

It was used (Kolocouris et al., 2004) a molar ratio DMPC/AM2TM = 25 that ensured the formation of M2TM WT tetramers at pH 7.5. The binding of 3-fluoro-amantadine with AM2TM WT was successfully detected with ^{1}H NMR spectroscopy, because the interaction between the fluorinated drug and DMPC was weak allowing the drug to interact efficiently with AM2TM WT in the concentration applied in these experiments.

Broadhurst, Kolocouris and collaborators in 2007 (Kolocouris et al., 2007)studied the interaction between amantadine or 3-

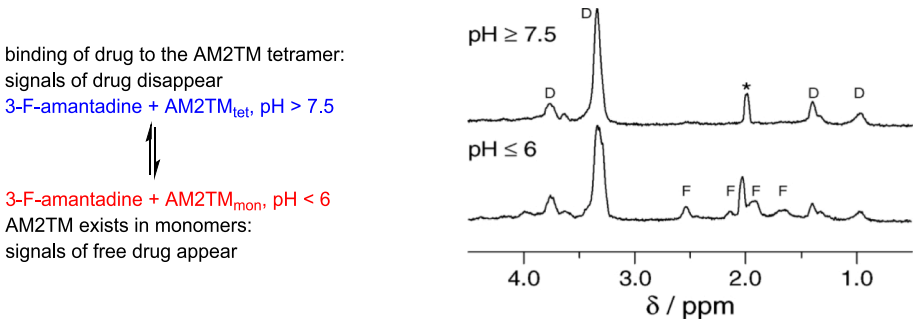

Fig. 3. ^{1} H NMR spectra of samples at 298 K containing 3-fluoro-amantadine, DMPC and AM2TM WT monomer in phosphate buffer at pH ≥ 7.5 and pH ≤ 6 (D, DMPC peaks; F, 3-fluoro-amantadine peaks; *, free acetate (drug concentration and AM2TM WT peptide was 0.6 mM).

fluoroamantadine with 5-F-Trp41 AM2TM WT in dodecylphosphocholine (DPC) micelles using ^{19}F NMR in the range between pH 5 and 8. Above pH 7, when the F-AM2TM WT tetramer is formed and ligand is bound, in addition to the ^{19}F-Trp41 signal of the free AM2TM WT tetramer, a second signal from the AM2TM WT tetramer bound state was detected (Fig. 4).

2.1.10. ssNMR spectroscopy

In 2006 [23], Cross and collaborators titrated ^{25}labeled ^{15}N His37 AM2TM WT (Udorn strain S_{22}SDP-LVVAASIIGILHLILWILDRL$_{46}$) in different pH values using cross-polarized magic-angle spinning (CP-MAS) ssNMR. They employed single ^{15}Nδ1- and ^{15}Nε2-labeled His37 AM2TM WT in DPMC/DMPG bilayers. A 230-ppm signal indicated a neutral His37 tetrad at pH 8.6, which exists as equilibrated τ-tautomers (Nε-H) and π-tautomers (Nδ-H). The signal disappeared at a high pH of 7, which was considered remarkable given the normal p*K*α = 6.5 for His side chains in aqueous solution. This is due to the strong hydrogen bonds between protonated and neutral imidazole rings of His37 side chains at the + 2 charge of His37 tetrad at pH 7, i.e., the formation of two imidazole–imidazolium dimers (i.e., His − HisH^{+} dimers) that stabilize the AM2TM WT tetramer. After analyzing the population of charged and uncharged His37 side chains in the titration curve, the p*K*αs were determined as: pKα,1 = 8.2 ± 0.2, pKα,2 = 8.2 ± 0.2, pKα,3 = 6.3 ± 0.3, and pKα,4 < 5.0. Amantadine binding (in 2.5-molar excess to AM2TM WT tetramer) changed the titration curve of the His37 tetrad by reducing imidazole His37 basicity. In the presence of amantadine, the His − HisH^{+} dimer's ^{15}N signal disappeared, indicating that neutral tautomers were generated directly from biprotonated histidines when amantadine is present. This agreed also with the 230 ppm unprotonated ^{15}N signal that persists at a significantly lower pH of 6.0 in the presence of amantadine, indicating a decrease in His37 imidazole basicity. Analysis of the intensities revealed that the bound form has a single pKα ~ 5.4.

In their work in 2007 (Hu et al., 2007) Cross and collaborators using OS ssNMR studied the structure of AM2TM WT in the presence of amantadine (in 2.5-molar excess to AM2TM WT tetramer) at pH 8.8 in DMPC bilayers. A peptide:phospholipid = 1:16 which corresponds to tetramer:phospholipid = 1:64 was used (while peptide:phospholipid = 1:32 also did not cause spectral changes). Relaxation measurements of nuclear spins and polarization inversion spin exchange at the magic angle (PISEMA) experiments were applied to obtain orientational constraints (orientation of individual amide peptidic-groups). The comparison of the CP-MAS ssNMR for the His37 ^{15}Nδ1 signal in the presence or absence of amantadine was used to study the effect of amantadine binding (2.5-molar excess) on the side-chain motion and protonation of His37. It was discovered (Hu et al., 2007) that amantadine reduces significantly the His37 p*K*α values (by three orders of magnitude) in comparison to the His37's p*K*α in apo AM2TM WT and that the His-HisH^{+} dimer was not formed when amantadine was present. (Hu et al., 2007) It was proposed (Hu et al., 2007) that amantadine affects the chemical characteristics of the His37 tetrad and reduces proton conductivity, rather than solely amantadine sterically blocking the AM2TM WT pore. Amantadine's ammonium group aligns with the channel's C-terminus, resulting in a perturbation of His37 pKα. The absence of His-HisH + dimers in the presence of amantadine suggests that low-barrier His-HisH^{+} hydrogen bonds are required to transport protons via the pore's water network.

A kink at Gly34 in the TM helix just C-ward of what was thought to be

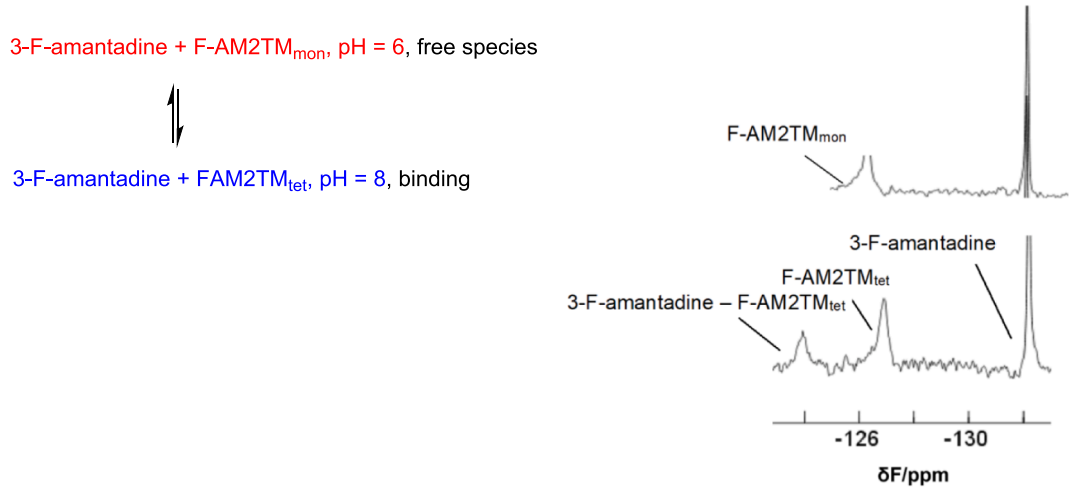

Fig. 4. ^{19} F NMR spectra at 298 K of samples including 3-fluoro-amantadine (1 mM), and 1 mM 5-F-Trp41 M2TM WT monomer in DPC micelles and phosphate buffer (pH 6 or 8); mon: monomer, tet: tetramer. (Kolocouris et al., 2004).

the binding site of amantadine is the main structural effect of drug binding, according to the PISEMA experiments in refs. (Hu et al., 2007) and (Li et al., 2007). The kink at Gly34 between the two helical fragments of each AM2TM WT monomer is ~ 10-11° such that the C-terminal half of each monomer in the tetramer has a tilt angle ~ 21° (Hu et al., 2007; Li et al., 2007) and the N-terminal half ~ 31° (Hu et al., 2007) or 32° (Li et al., 2007) with respect to membrane normal (Fig. 5). In the first experimentally determined structure of the AM2TM WT peptide was measured an α-helix tilted by 38° with respect to the bilayer normal (PDB ID 1MP6 (Wang et al., 2001) and the same value was measured in the tetrameric AM2TM WT reconstituted in phospholipid bilayers (PDB ID 1NYJ (Nishimura et al., 2002). The tilt of the N-terminal region of the helix seemed to be very slightly affected by the kink caused by amantadine (going from 38° to 31–32°), while the tilt of the C-terminal portion was significantly decreased to 21° at pH 8.8. The spectral comparison of the AM2TM S31N with and without amantadine, as illustrated in ref. (Hu et al., 2007) revealed a little spectral change in the backbone and thus no conformational change, compared to the significant tilt angle change for the C-terminal portion of the TM helix in the AM2TM WT when amantadine binds. AM2TM WT in DMPC bilayers adopts the C_{closed} conformation at alkaline pH and based on the constraints obtained at pH 8.8 in ref. (Hu et al., 2007) Cross and collaborators reported the structure with PDB ID 2H95 (Hu et al., 2007) for AM2TM WT when amantadine is bound.

The N-terminal portion tilted 35° in the apo-state (Cady and Hong, 2008) and slightly larger at 38° (Cady et al., 2007; Cady and Hong, 2008) in the amantadine-bound state, according to Hong and colleagues' study in 2008 (Cady and Hong, 2008) of AM2TM WT reconstituted in DLPC bilayers with and without amantadine. This suggests that the drug pushes the N-end to open slightly, enlarging the pore vestibule. They also studied in 2009 (Cady et al., 2009) the apo-protein and amantadine-bound structure of AM2TM WT in DLPC bilayers at pH 7.5 using MAS ssNMR at 30 °C or 40 °C, and amantadine/tetramer ratio 32:1. Comparison of the chemical shift perturbations (CSPs) in the apo-form (PDB ID 2KAD (Cady et al., 2009) and bound AM2TM WT indicated that amantadine most significantly alters the AM2TM WT conformation at Ser31, where a substantial ^{15}N CSP of 7 ppm strongly suggests drug binding. (Cady et al., 2009) While the C-terminal L38 and Asp44 were very slightly impacted, the CSP is likewise strong on Gly34 and Val28.

Overall, the ssNMR studies by Cross and collaborators using OS ssNMR in 2007, (Hu et al., 2007; Li et al., 2007) and Hong and collaborators with MAS ssNMR in 2008, (Cady and Hong, 2008) 2009 (Cady and Hong, 2009) of AM2TM WT reconstituted in phospholipid bilayers. Apo-AM2TM WT depicted NMR lines that were uniformly widened by the large-amplitude, microsecond-time scale motion of the protein. In the presence of amantadine inside AM2TM WT pore the structural stability is enhanced. Amantadine promotes the formation of more homogeneous helical bundles, by increasing the motional rate of most of the backbone Cα sites at pH 7.0 and 7.5. This was demonstrated by the substantial line-narrowing, i.e., the reduction of the exchange broadening of the NMR signals. The spectra showed that amantadine reduced conformational freedom and stabilizes the polypeptide backbone and His37 side chains. It slightly alters the helix orientation and has low impact on the average backbone and side chain conformations. However, the functional complexity of the AM2 ion channel including the opening, gating, and proton conduction, depends on the kinetics and structural flexibility. Indeed, DeGrado and co-workers using AUC in micelles systems in 2000 (Salom et al., 2000) or thiol disulfide equilibria in lipid bilayers in 2003 (Cristian et al., 2003) showed that both amantadine and cholesterol shift the equilibrium to AM2TM WT (residues 22–46 or 19–46, respectively) towards tetramers. Thus amantadine promotes the formation of a structurally rigid tetrameric helical bundle, lacking the conformational flexibility necessary for physiological proton conduction.

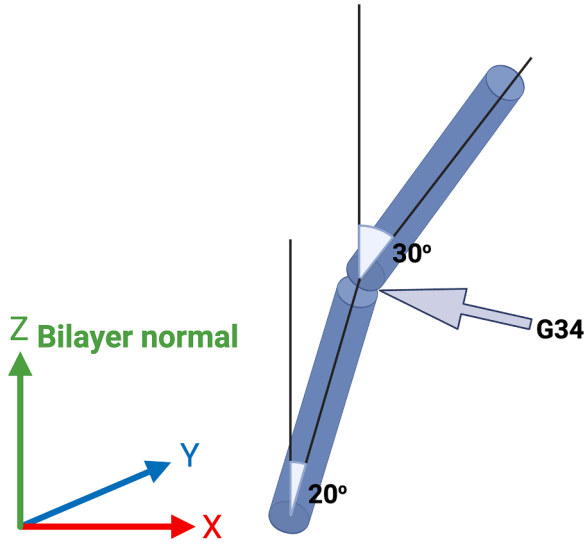

Fig. 5. The 11° kink close to Gly34 is highlighted by the monomer structure with cylinders along the helical fragment axes. (Hu et al., 2007).

Griffin and collaborators in 2010 (Andreas et al., 2010) studied the MAS NMR spectra of AM2CD WT (residues 18–60), both in the apo-form and as a complex with rimantadine, in POPC or 1,2-diphytanyl-*sn*-glycero-3-phosphocholine (DPhPC) bilayers. At pH 7.8 and 0 °C, ^{15}N-^{13}C and ^{13}C–^{13}C spectra were acquired using a protein tetramer:phospholipid = 1:24. Numerous peaks in the spectra were doubled, such as Val27, Ser31, Gly34, and Pro25 for the apo-AM2CD WT and Pro25, Val28, and Ala29 for the rimantadine-bound version. This supported both a dimer-of-dimers symmetry for the H37xxxW41 tetrad and a dimer-of-dimers conformation for the TM domain. The resonances of the rimantadine-bound form accounted for around 25 % of the total intensity when one rimantadine molecule was added per channel. When four rimantadine molecules per channel were added, the rimantadine-bound AM2CD WT complex was the primary species, with less than 10 % of the total intensity still being attributed to apo-AM2CD WT. When 16 rimantadine molecules per channel were added only the bound form was observed. It should be mentioned that rimantadine or amantadine are partitioned strongly into the membrane, as was shown by experimental biophysics (Wang et al., 2004; Li et al., 2008; Konstantinidi et al., 2018; Cady et al., 2011; Cady et al., 2010) and MD simulations (see **Subsection 3.1**). (Li et al., 2008; Chee et al., 2008; Konstantinidi et al., 2018) The authors noticed significant (> 2 ppm ^{15}N, > 1 ppm $^{13}C\alpha/C\beta$) CSPs in TM helix residues 24 to 41. The pore-lining residues 27, 34, 37, and 41 as well as the lipid-facing sites and helix-helix interface residues 24, 25, 28, 29, 31, 32, and 35 all showed significant CSPs. (Schnell and Chou, 2008) Chemical shift perturbations of > 1 ppm in $^{13}C\alpha/C\beta$ and > 2 ppm in ^{15}N were not seen in any of the assigned residues, except for 30 and 42. It was suggested that these CSPs were due to allosteric effects since they are expanded by a length scale that was several times greater than that of the ~ 5 Å rimantadine drug. The largest ~ 7 ppm CSP at Ser31, that was previously observed from Cross or Hong and collaborators for AM2TM WT, (Hu et al., 2007; Cady and Hong, 2008; Cady et al., 2009; Hu et al., 2007) was also observed for AM2CD WT in complex with rimantadine as well as a ~ 3.5 ppm shift in His37 Cα. The chemical shift data suggested an allosteric effect and agreed with the proposed sites of drug binding (Ser31 and Asp44).

2.1.11. MD simulations

Zhou, Cross and collaborators in 2008 (Yi et al., 2008) ran MD simulations for 10 ns of the AM2TM WT embedded in 110 DMPC lipids using as starting structure the ssNMR structure without (PDB ID 1NYJ (Nishimura et al., 2002) or with amantadine (PDB ID 2H95 (Hu et al., 2007). In the presence of amantadine, it was shown that the helix

bundle's packing tightened, which led to a noticeable decrease in pore size. Additionally, a secondary gate and a constriction are formed by the Val27 sidechains extending into the pore. (Yi et al., 2008) They further explored in 2009 (Yi et al., 2009) with MD simulations of 15–22 ns the conformational plasticity of the AM2TM WT proton channel embedded in 110 DMPC lipids. They suggested that at high pH conditions the apo-form exhibited a distribution of conformations with Gly34 helix-kink angle at 0° and 40°, with the former being predominant. Upon amantadine binding to AM2TM WT in DMPC bilayers, AM2TM WT showed a significant kink at Gly34 with a tilt angle of 31° for the N-terminal part and 20° for the C-terminal part (PDB ID 2H95 (Hu et al., 2007). Thus, the amantadine-bound form shows a predominant conformation with a Gly34 helix-kink angle of 10°.

2.2. Direct evidence of adamantyl amine drugs binding

2.2.1. X-ray crystallography

In 2008 DeGrado and collaborators published (Stouffer et al., 2008) the first X-ray crystal structure of AM2TM WT with a 1.3:1 AM2TM tetramer:amantadine molar ratio at pH 5.3. AM2TM WT was in β-octyl glucoside detergent micelle and bared the stabilizing mutation Gly34Ala (PDB ID 3C9J (Stouffer et al., 2008) to facilitate crystallization. The TM domain's N-terminal half had a tilt angle of ~ 35°, which agreed with previous ssNMR data. In accordance with the low pH of 5.3, the TM helices of the C-terminal half were straight and diverged apart toward the C-terminus, capturing the open, conducting state of the channel. A well-resolved electron density inside the pore was observed, near Ser31 and enclosed by other drug-resistant residues, which was attributed to bound amantadine. The assumed amantadine binding site and stoichiometry of the X-ray structure verified the pore blocking model for channel inhibition, agreeing with the original EP data by Lamb and coworkers in 1993. (Wang et al., 1993).

2.2.2. Solution NMR

The solution NMR structure of AM2CD WT (residues 18–60) in 1,2-dihexanoyl-*sn*-grycero-3-phosphocholine (DHPC) detergent micelles (PDB ID 2RLF (Schnell and Chou, 2008), solved by Chou and Schnell in 2008, (Schnell and Chou, 2008) revealed the unexpected finding that the antiviral drug rimantadine binds to an external site on each chain of the tetramer rather than inside the pore. Specifically, a rimantadine molecule was proposed to bind at a lipid-facing site close to the C-terminal side of the channel domain, further stabilizing the closed conformation populations. The intermolecular NOEs between rimantadine and the lipid-facing site at position 44 indicated that the ammonium group of rimantadine forms a salt bridge with the Asp44 carboxylate and perhaps hydrogen bonds with the neighboring Arg45. Moreover, rimantadine's adamantyl group was found to interact with Leu40 and Leu43 from the neighboring helix via hydrophobic interactions and Ile42 from one TM helix.

2.2.3. The controversy regarding the amantadine binding site

With a maximum diameter of approximately 3.4 Å for the roughly spherical adamantyl cage, the X-ray structure's low resolution of 3.5 Å proved insufficient for the unequivocal identification of small compounds, like amantadine. Chou and colleagues therefore questioned the structure, proposing an exterior location and an allosteric mechanism of channel blockage for rimantadine and amantadine based on a solution NMR structure of AM2CD WT in DPC micelles (PDB ID 2RLF (Schnell and Chou, 2008). However, for the solution NMR structure determination PDB ID 2RLF, (Schnell and Chou, 2008) a ~ 210-fold excess of rimantadine to AM2CD WT was used. This significant excess allows ligand molecules to reach and bind potentially lower affinity pockets, explaining the unprecedented Asp44 salt bridge findings. Therefore, it was argued that this secondary lipid-facing position corresponds to a not specific binding site. Based on only CSPs from ssNMR (see **Subsection 2.1.10**) the specific pharmacological binding site of amantadine and rimantadine couldn't be identified unambiguously. The relationship between the amantadine binding site and channel inhibition was debated for about three years. (Pielak and Chou, 2010).

2.2.4. The effect of experimental conditions on AM2 protein conformation

In the PDB ID 2L0J (Sharma et al., (1979) 2010) (see Fig. 2) the structure of AM2CD WT published in 2010 (Sharma et al., (1979) 2010) by Cross and collaborators the AH's binding to the membrane interface was discovered. The cavity formed by the two hydrophobic amino acids Val27 and Ala30 (Yi et al., 2008; Nishimura et al., 2002) reveals a binding site that, when AM2 is in the virion or in DMPC bilayers, accommodates amantadine or rimantadine in the AM2 pore, as is shown with the structure PBD ID 2KQT. (Cady et al., 2010) In contrast, the AHs in PDB ID 2RLF (Schnell and Chou, 2008) (see **Subsection 2.2.2**) form a distinct water-soluble four-helix bundle that is fully H/D interchangeable rather than being positioned in the membrane interface.The latter result was not in agreement with the H/D exchange results for AM2CD WT obtained by Cross and collaborators using ssNMR in 2003 (Tian et al., 2003) for the AM2CD WT (residues 18–60) and in 2021 (Zhang et al., 2021) for AM2CD WT in phospholipid bilayers. Also, the packing of TM helices is altered in detergent DHPC environment having small tilt angles, smaller than 20°, relative to the pore axis compared to the tilt angle 32° measured with OS ssNMR in the apo-M2CD WT (residues 18–60; PDB ID 2L0J (Sharma et al., (1979) 2010) and with X-ray crystallography in the apo-M2TM WT (residues 25–46; 3LBW (Acharya et al., 2010). As a result, the secondary gate made up of the Val27 residues—which was initially suggested in 2008 using MD simulations (Yi et al., 2008) (see Subsection 2.1.9) —seems to be more tightly closed, making it impossible for the drug to pass through. The necessity for precise native membrane mimetics that can similarly constrain the membrane protein structure is highlighted by this. (Cady et al., 2011) Nevertheless, the solution NMR structure of the AM2CD V27A structure in DHPC micelles (PDB ID 2KWX (Pielak and Chou, 2010), published by Chou and Pielak in 2010, (Pielak and Chou, 2010) did not show this deviation. Nevertheless, in the detergent-based crystal structures of AM2TM WT, like PDB ID 3C9J (Stouffer et al., 2008) or PDB ID 3LBW, (Acharya et al., 2010) amantadine can also bind inside the channel pore (see **Subsection 2.3.3**).

2.3. The adamantyl amine drugs pharmacological binding site

2.3.1. ssNMR

Hong and collaborators published in 2010 (Cady et al., 2010) the MAS ssNMR structure of AM2TM WT in complex with amantadine in DMPC lipids at pH 7.5 (PDB ID 2KQT (Cady et al., 2010). The structure PDB ID 2KQT (Cady et al., 2010) was derived using the experimentally determined side chain dihedral restraints in PDB ID 2H95, (Hu et al., 2007) published by Cross and collaborators in 2007. (Hu et al., 2007) In ref. (Cady et al., 2010) the authors used a perdeuterated amantadine and applied distance measurements between TM α-helices as well as between the drug and the TM α-helices from rotational-echo double-resonance (REDOR) experiments. When they used an amantadine/tetramer molar ratio 1:1 they clearly identified the pore as the primary amantadine binding site (PDB ID 2KQT (Cady et al., 2010). The backbone structure of PDB ID 2KQT ssNMR structure (Cady et al., 2010) and the high-resolution X-ray structure of apo-AM2TM WT (PDB ID 3LBW (Acharya et al., 2010) differ only by RMSD ~ 0.35 Å. It was shown that amantadine binds the AM2TM WT pore and is positioned between the Val27 secondary gate and the His37 tetrad. In the lumen of the four-helix bundle of AM2TM WT, the 1-adamantyl group of amantadine was situated in a hydrophobic pocket that was primarily made up of the side chains of the pore-lining residues Val27 and Ala30, as previously suggested by Cross and collaborators (Yi et al., 2008; Hu et al., 2007) using ssNMR or Lamb, Pinto and collaborators using functional assays (Jing et al., 2008) or DeGrado using X-ray crystallography. (Stouffer et al., 2008) The drug-binding in the lipid facing position was also

observed as Asp44 dephasing in REDOR measurements (Cady et al., 2010) using a higher amantadine/tetramer molar ratio of 4:1 (Fig. 6). One should consider for the used drug:tetramer ratio that amantadine is also partitioned into the membrane (Cady et al., 2010; Wang et al., 2004; Li et al., 2008; Konstantinidi et al., 2018; Cady et al., 2011; Chee et al., 2008) (see **Subsection 3.1**). These sites, pore and lipid-facing, correspond to the high affinity binding site (K_d = 0.91 μM) and secondary low affinity binding site (K_d = 0.40 mM), respectively, measured by Casarotto and collaborators in 2010 (Rosenberg and Casarotto, 2010) using SPR in DMPC bilayers (see **Subsection 2.1.8)**. Thus, the first equivalent of amantadine binds inside the AM2 channel pore with much higher affinity compared to the external protein binding site which is accessed by the excess of amantadine partitioned in the lipid membrane, likely through lateral diffusion. These SPR experiments provide additional insight into the previous disagreement regarding the type of inhibition mechanism (occlusion of the M2 pore or allosteric inhibition).

Hong and collaborators additionally determined (Hu et al., 2007) the direction of the ammonium group of rimantadine inside AM2TM WT at pH 8 using MAS ssNMR in 2011. (Cady et al., 2011) They used ^{13}C-labeled AM2TM WT in DMPC lipid bilayers and methyl-deuterated rimantadine and measured distances with ^{13}C–^{2}H REDOR experiments. It was shown that the rimantadine ammonium group points to the C-end of the channel pore, facing the His37 tetrad, while the methyl group is positioned close to the Gly34 (Fig. 6). The proximity of the rimantadine methyl group to the Gly34 backbone (Hu et al., 2007)the higher affinity of rimantadine for AM2 compared to amantadine previously reported. This increase of binding affinity was measured by Kolocouris and collaborators in 2016–2018 using Isothermal Titration Calorimetry (ITC) and EP (Drakopoulos et al., 2017; Drakopoulos et al., 2018; Ioannidis et al., 2016)and by Kolocouris, DeGrado and collaborators in 2021 using EP (Thomaston et al., 2021) (see **Subsection 2.4.2**). At stoichiometric drug concentration, rimantadine binds inside the pore with the adamantyl molecular axis about parallel to the bilayer normal similar to amantadine.

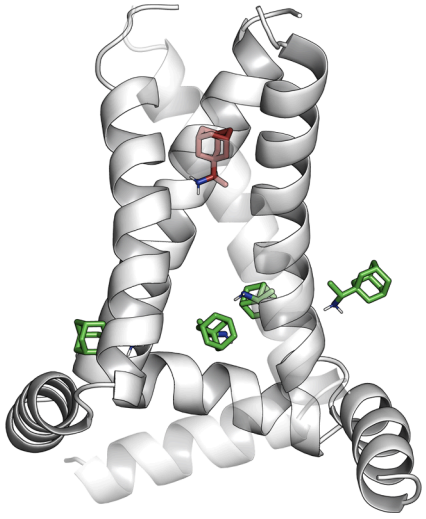

Fig. 6. Binding positions of rimantadine molecules to AM2CD WT. To generate this model we superimposed the solution NMR structure of AM2CD WT in complex with four peripheral rimantadine molecules solved in micelles (PDB ID 2RLF (Schnell and Chou, 2008) and the ssNMR structure of apo-AM2CD WT solved in phospholipids (PDB ID 2L0J (Sharma et al., (1979) 2010) and deleted 2RLF (Schnell and Chou, 2008) protein. The resulting structure includes AM2CD WT (PDB ID 2L0J (Sharma et al., (1979) 2010) with four peripheral rimantadine molecules. We then superimposed this structure with the X-ray structure of AM2TM WT in complex with rimantadine inside the AM2TM WT pore (PDB ID 6US9 (Thomaston et al., 2021) and deleted 6US9 (Thomaston et al., 2021) protein to obtain the complex of AM2CD WT (PDB ID 2L0J (Sharma et al., (1979) 2010) with 5 rimantadine molecules; 4 peripheral rimantadine molecules (carbons colored in green) are in contact with the side chains of the 4 Asp44 residues (not shown) and one rimantadine molecule (carbons colored in red) binds to its pharmacological important position blocking the AM2 pore. (For interpretation of the references to color in this figure legend, the reader is referred to the web version of this article.)

In 2011 (Cady et al., 2011) Hong and collaborators also conducted (Tian et al., 2020)MAS ssNMR experiments using the extended functional construct, AM2CD WT (residues 21–61), (Tian et al., 2020) in DMPC bilayers to investigate the effects the AHs may have on the binding of amantadine to the pore. They performed ^{13}C–^{2}H REDOR distance measurements of perdeuterated amantadine drug complexed with AM2CD WT. Amantadine was shown to still bind inside the pore in its canonical binding site previously showed with AM2TM WT – amantadine complex (PDB ID 2KQT (Cady et al., 2010) embedded in the same membrane. Thus, it was demonstrated that in the fully functional AM2CD WT, the pharmacologically significant drug-binding site is located inside the TM pore. Surprisingly, the lower affinity lipid-facing site at Asp44 observed in AM2TM WT was not seen, suggesting it is disfavored in the longer AM2CD WT peptide. This does not mean the secondary site is necessarily artificial, but likely, that the AHs' membrane deforming behavior may alter the membrane geometry and fluidity that these ligands depend on to access the secondary site.

Griffin and collaborators in 2013 (Andreas et al., 2013) further studied rimantadine binding to AM2CD WT (residues 18–60) in DPhPC bilayers using a drug/tetramer ratio of 4:1 at room temperature using dynamic nuclear polarization (DNP) MAS ssNMR. The ^{15}N-labeled ammonium of rimantadine was observed in proximity to A30 ^{13}Cβ and G34 ^{13}Cα. It was discovered that the distance between the drug's amino group N and A30 carbonyl oxygen varied between 2.4 to 3.5 Å, indicating a potential hydrogen bond to A30 carbonyl. The weaker external binding site close to Asp44 was also observed in the room temperature DPhPC environment. This supports the hypothesis that lack of its observation by Hong and collaborators may have been due to the combination of DMPC and the lower temperatures employed (243 K) for MAS ssNMR, resulting in increased stiffness of the membrane environment.

2.3.2. *Solution NMR*

A rimantadine-bound solution NMR structure of a AM2-BM2 chimeric tetramer with a rimantadine:tetramer ratio ~ 100:1 (solubilized in DHPC micelles at pH 7.5) was solved by Chou and coworkers in 2011. (Pielak et al., 2011) The 35-residue AM2-BM2 peptide incorporated residues 18–37 of AM2 linked to residues 20–34 from BM2. This structure revealed the drug binding location inside the pore (PDB ID 2LJC (Pielak et al., 2011). The controversy regarding the drug binding site seemed to firmly settle on the pore site.

2.3.3. *X-ray crystallography*

DeGrado, Kolocouris, and coworkers provided the X-ray structures of the AM2TM WT in the presence of amantadine in 2018 (Thomaston et al., 2018) as the most concrete proof of the pore binding site for adamantyl amine drugs. Furthermore, the X-ray structures of AM2TM WT bound enabled the high-resolution investigation of the crucial water network involved in drug binding, previously only discernible at a the more modest resolution of 3.5 Å from work in 2010 (PDB ID 3C9J (Stouffer et al., 2008). These experimental structures of higher resolution in 2018 (Thomaston et al., 2018) made possible the detection of the crystallographic important waters that facilitate the potent inhibition of AM2 by inhibitors targetting key waters. Overall, four X-ray structures of the AM2TM WT homotetrameric channel bound to adamantyl amines blockers were solved using lipidic cubic phase (LCP) crystallization (Fig. 7). A maltose-neopentyl glycol (MNG) amphiphile was used as a detergent additive in crystallization experiments to stabilize the crystal structures. (Thomaston et al., 2018) These structures correspond to AM2TM WT bound to: (a) rimantadine, in the C_{closed} state (PDB ID 6BKL; 2.00 Å (Thomaston et al., 2018) at pH 4.5 (b) amantadine, in the C_{closed} state (PDB ID 6BKK; 2.00 Å (Thomaston et al., 2018) at pH 5.6 (c) spiro-

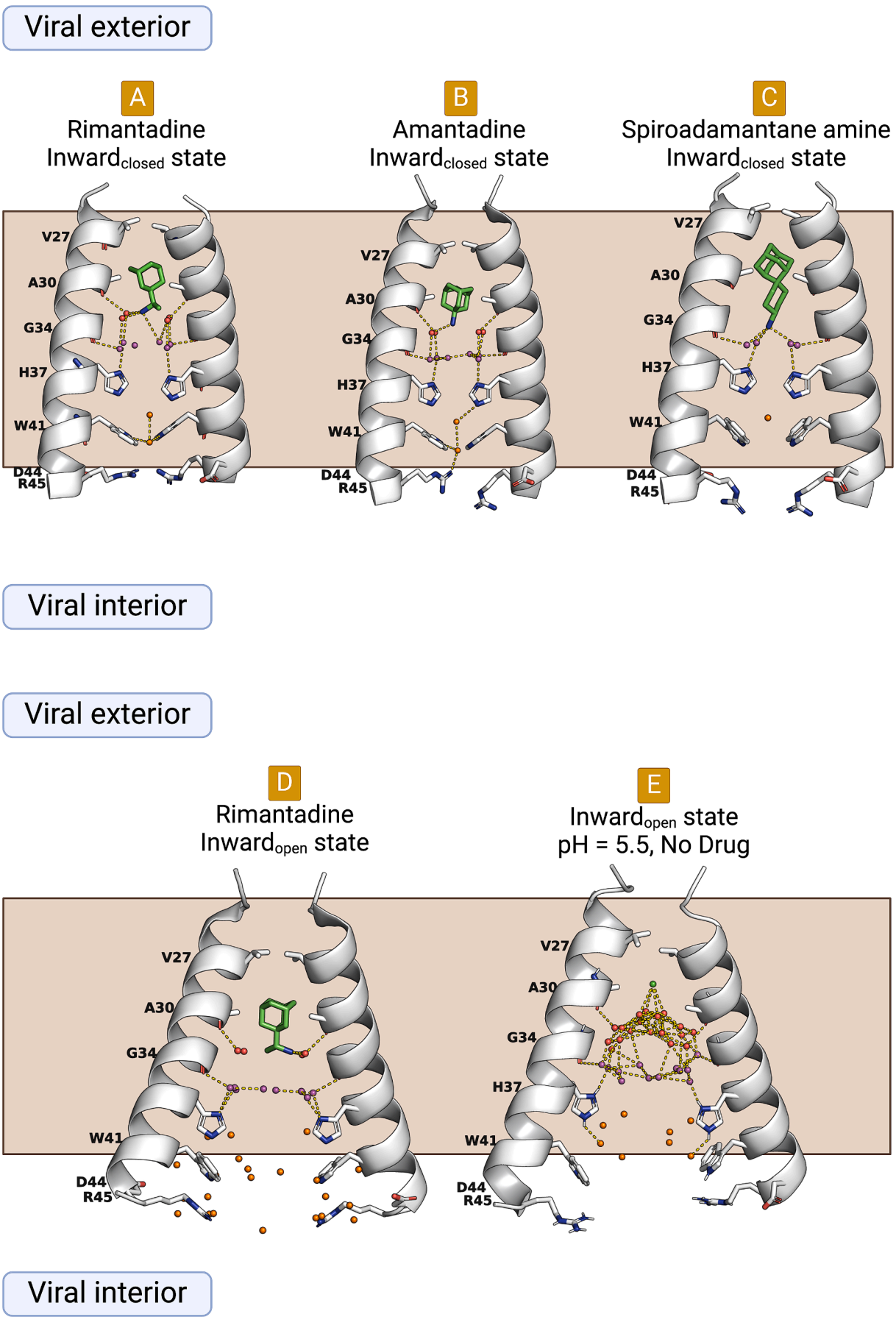

(caption on next page)

Fig. 7. X-ray structures of the AM2TM WT homotetramer in complex with drugs and inhibitors (Thomaston et al., 2018) (the contents of the channel pore are visible after the front and rear monomers have been removed). Yellow dashes represent hydrogen bonding. The water layer that forms hydrogen bonds with Ala30 carbonyls is shown by red spheres, whereas the water layer that forms hydrogen bonds with Gly34 carbonyls is represented by purple spheres. Top, left to right: (A) AM2TM WT bound to rimantadine in the C_{closed} state; PDB ID 6BKL, (Thomaston et al., 2018) pH 4.5, 2.00 Å resolution. (B) AM2TM WT bound to amantadine in the C_{closed} state; PDB ID 6BKK, pG 5.6, 2.00 Å resolution. (C) AM2TM WT M2 bound to spiro-adamantyl amine in the C_{closed} state; PDB ID 6BMZ, (Thomaston et al., 2018) pH 7, 2.63 Å resolution. Bottom, left to right: (D) AM2TM WT bound to rimantadine in the C_{open} state; PDB ID 6BOC, (Thomaston et al., 2018) pH 3.5, 2.25 Å resolution. (E) X-ray structure of the previously solved apo-AM2TM WT in the C_{open} state; PDB ID 5JOO, (Thomaston et al., 2017) pH 5.0, 1.41 Å resolution. (For interpretation of the references to color in this figure legend, the reader is referred to the web version of this article.)

adamantyl amine in the C_{closed} state (PDB ID 6BMZ; 2.63 Å (Thomaston et al., 2018) at pH 7, (d) rimantadine in the C_{open} state (PDB ID 6BOC; 2.25 Å (Thomaston et al., 2018) at pH 3.5. The binding of amantadine drugs stabilizes the C_{closed} state and reduces the pKα of His37 as was observed by Cross and co-workers using ssNMR in DMPC bilayers at pH 8.8. (Hu et al., 2007)The adamantane cage fits tightly into the N-end of the pore in both the amantadine-bound and rimantadine-bound X-ray structures, pushing out the water layer close to Val27.

The location of the different adamantyl amines and waters within the pore in the X-ray crystal structure of the AM2 complexes remained stable throughout the 200 ns-MD simulations (Thomaston et al., 2018) using the OPLS2005 force field (Thomaston et al., 2017; Wright et al., 2016) (available from Schrödinger) with the AM2TM WT complex (PDB IDs 6BKK and 6BMZ (Thomaston et al., 2018) embedded in a hydrated-bilayer containing 200 DMPC lipids. The drugs dehydrate the N-part of the pore close to Val27 and disrupt the continuous water network in the pore, which is necessary for proton conductance in the drug-free state,. (Thomaston et al., 2018; Hu et al., 2006) Between the inhibitor's ammonium group and His37, two layers of ten waters are formed. These water layers were unperturbed by drug binding and formed networks identical to those captured previously in the drug-free state. (Acharya et al., 2010) The first layer, termed the "Ala30 layer", is made up of four water molecules that establish hydrogen bonds with surrounding Ala30 carbonyls, and the second layer, the "Gly34 layer", is made up of two bridging water molecules and four carbonyl-associated water molecules. Proximally next to the four waters of the Ala30 layer, the ammonium group of amantadine and rimantadine is stabilized by three hydrogen bonds with these waters, uncovering the role of the water network in ligand affinity. Yet, the longer dehydrates the Ala30 layer and forming hydrogen bonds directly with the Gly34 layer instead (Fig. 7**)**. The solved X-ray structure of rimantadine bound to the C_{open} state (PDB ID 6BOC; 2.25 Å (Thomaston et al., 2018) at pH 3.5 agreed well with the low-resolution X-ray structure (3.5 Å) of AM2TM WT-amantadine complex in the C_{open} conformation (PDB code 3C9J (Stouffer et al., 2008)) solved previously at pH 5.3. Similar drug binding mode between the C_{closed} and the C_{open} states were shown by the crystal structures, with RMSD (Cα) = 0.98 Å. This can explain how these drugs can inhibit the channel in the pH range 6–8 in which the AM2 changes its state from open (pH 6) closed (pH 8) with comparable affinity. (Wang et al., 1993; Ma et al., 2009) Collectively, the drug ammonium group is oriented toward His37 and binds to water-lined sites, which are thought to stabilize transient hydronium ions formed in along the proton-conduction pathway (Fig. 7**)**. The ammonium group of these inhibitors electrostatically mimics the hydronium cation when it binds to the channel pore, as demonstrated in ref. (Thomaston et al., 2018). This suggests that the adamantane-like compounds act as mechanism-based inhibitors because they take advantage of structural aspects of the channel that are linked to native proton transport.

2.4. Binding of rimantadine enantiomers to AM2

2.4.1. ssNMR

Cross and collaborators in 2016 (Wright et al., 2016) studied with MAS ssNMR the binding of rimantadine enantiomers to AM2FL WT. AM2FL WT was reconstituted in DMPC/DMPG bilayers at a tetramer protein/lipid ratio 1:30. Except for early *in vivo* studies in mice that demonstrated comparable antiviral activity of the enantiomers, (Aldrich et al., 1971) rimantadine's antiviral activity was always assessed as a racemic mixture prior to this study. To uncover possible stereospecific rimantadine binding interactions to the AM2 proton channel and support the development of new inhibitors, it was crucial to characterize protein–ligand interactions at the atomic level for each enantiomer independently. Based on the isotropic chemical shift changes at −10 °C and ^{13}C–^{2}H REDOR experiments, Cross and collaborators suggested the differential binding of the rimantadine enantiomers to the proton channel. To obtain a binding pose for the complexes of rimantadine enantiomers with AM2FL WT, they used the distance restrains from ^{13}C–^{2}H spectra for position restrained MD simulations of rimantadine enantiomers bound to AM2CD WT (PDB ID 2L0J (Sharma et al., (1979) 2010). The simulations revealed that the (R)-rimantadine enantiomer forms a more stable complex with AM2CD WT compared to (S)-rimantadine. However, to suggest a differential complex with each rimantadine enantiomers only unrestrained MD simulations are appropriate.

2.4.2. EP, ITC and antiviral assays

To investigate the possible differential binding, blocking efficiency and inhibition of virus replication by rimantadine enantiomers Kolocouris, Wang and collaborators in 2017 (Drakopoulos et al., 2017) applied TEVC in oocytes injected with AM2CD WT and antiviral assays, as well as ITC experiments and alchemical binding free energy calculations on AM2TM WT. In contrast to the ssNMR results obtained by Cross and collaborators for rimantadine enantiomers on AM2FL WT, (Wright et al., 2016) it was found that the two enantiomers didn't exhibit notable differences. In contrast, both rimantadine enantiomers shared the same binding affinity constant (K_d) for AM2TM WT (K_d ~ 0.33 μM) (Drakopoulos et al., 2018) in agreement with EP and functional assays measured for AM2CD WT. (Drakopoulos et al., 2018).

Kolocouris, DeGrado and collaborators in 2021 (Thomaston et al., 2021) further used TEVC in oocytes to perform more accurate binding kinetic measurements on rimantadine enantiomers compared to previous equilibrium measurements in ref. (Drakopoulos et al., 2017).The (Thomaston et al., 2021; Thomaston et al., 2021)best-fit values from the kinetic experiments in ref. (Thomaston et al., 2021) are included in Table 1 showing that rimantadine enantiomers have equal binding k_{on} and k_{off} and channel blockage against AM2.

Enantiomers were also tested against the amantadine-sensitive strain (A/H1N1/Soloman Island/3/2006) (Thomaston et al., 2021) to confirm previous antiviral results (ref. (Drakopoulos et al., 2017) showing that the (R)- and (S)-enantiomers of rimantadine have the same inhibition

Table 1
Summary of the binding kinetics results of rimantadine enantiomers and amantadine and against AM2CD WT (Udorn sequence). (Thomaston et al., 2021).

	rimantadine (racemic)	(R)-rimantadine	(S)-rimantadine	amantadine
Concentration tested	50 μM	50 μM	50 μM	100 μM
k_{on} ($min^{-1}M^{-1}$)	19600 ± 300	20800 ± 700	22500 ± 300	20500 ± 300
k_{off} (min^{-1})	(9.1 ± 0.8) *10^{-4}	(9 ± 2)*10^{-4}	(8.8 ± 0.8) *10^{-4}	(119 ± 2)* 10^{-4}
$K_d = k_{off}/k_{on}$ (nM)	46 ± 4	41 ± 9	39 ± 4	580 ± 20

potency for the influenza A virus. (Tzitzoglaki et al., 2017) The cellular assays confirmed slight differences between the (R)- and (S)-rimantadine antiviral potencies, EC_{50} = 19.62 and EC_{50} = 24.44 nM, respectively.

2.4.3. X-ray crystallography and MD simulations

Kolocouris, DeGrado and collaborators in 2021 (Thomaston et al., 2021) reported the X-ray crystal structures of the (R)- rimantadine (PDB ID 6US9 (Thomaston et al., 2021) and (S)-rimantadine (PDB ID 6US8 (Thomaston et al., 2021) in complex to the AM2TM WT and observed slight differences in the waters inside the pore between the two complexes (Fig. 8).

300 ns-MD simulations were performed using the ff99sb (Lindorff-Larsen et al., 2010) for the protein, CHARMM36 force field (Huang and Mackerell, 2013) for the lipids, while the GAFF (Sprenger et al., 2015) was applied to the ligand. For the MD simulations the structures of the complexes with PDB ID 6US9 (Thomaston et al., 2021) and PDB ID 6US8 (Thomaston et al., 2021) were embedded in hydrated POPC bilayer consisting of 200 lipids. The radial distribution function (RDF) between the ammonium group and water oxygen atoms for (R)-rimantadine and (S)-rimantadine was calculated from the MD simulations (Fig. 8). The rimantadine showed a strong water population at 2.7 Å from rimantadine's nitrogen, which describes the upper (N-ward) layer that consists of 4 waters. These waters form hydrogen bonds with rimantadine's ammonium group and the Ala30′s carbonyl groups. The bottom (C-ward) layer consists of 5–6 mobile waters and is represented by the second broader population peak at 4.8 Å; these waters form hydrogen bonds with the His37 imidazole groups and the Gly34 carbonyl groups.

The water structure was assessed using Grand Canonical Monte Carlo combined with MD simulations (GCMC/MD) for increased sampling. Each water's chemical potential was calculated to investigate the impact of the hydration of the AM2TM WT pore on drug binding affinity. (Samways et al., 2023) During the titration of the binding cavity with waters the chirality of the drug was initially masked by the two layers of ordered water molecules that lie between the bound drug and the gating His37 residues of the channel. The drug sinks to the lower water layer where the chemical potential increases, making the interaction more susceptible to chirality (Fig. 9). According to this research, it may be possible to displace the upper water layers by drugs targeting the upper lower layer, a result supported by the spiro-adamantyl amine AM2TM

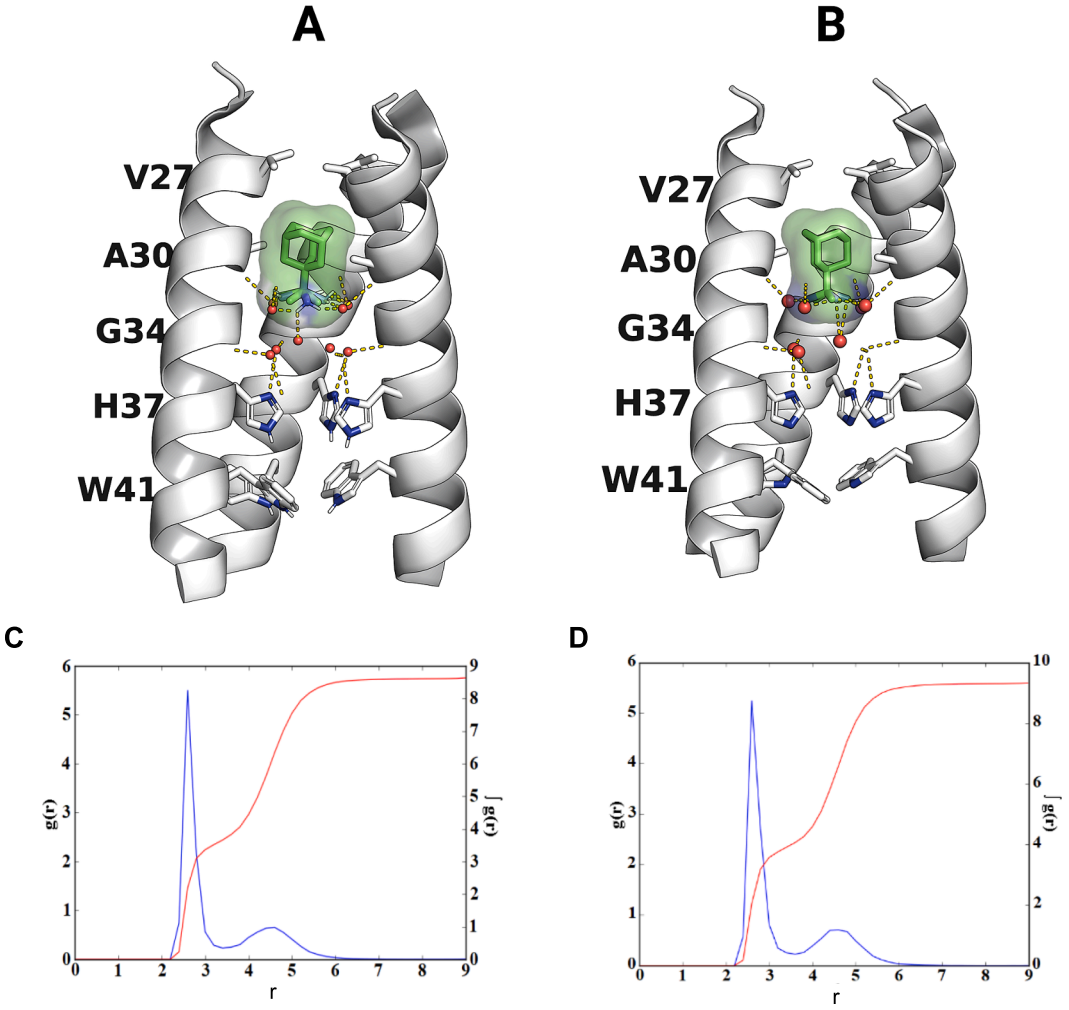

Fig. 8. X-ray crystal structures of (A) (R)-rimantadine and (B) (S)-rimantadine in complex with AM2TM WT (Thomaston et al., 2021) (the contents of the pore are visible due to the removal of the front and rear monomer helices). Between the bound rimantadine and the gating His37 residues, it is shown a network of organized waters. These waters form vertical H-bond networks that lead to the gating His37 residues and establish also hydrogen bonds with pore-facing carbonyl groups. In (C), or (D) are shown plots of calculated g(r) (RDF) for the complexes between the ammonium group and water oxygen atoms for (C) (R)-rimantadine and (D) (S)-rimantadine inside the AM2TM WT pore and cumulative integrated intensity ∫g(r), which is displayed on the right axis. The rimantadine enantiomers showed a strong peak at 2.7 Å from rimantadine's nitrogen, which describes the upper (N-ward)-four waters layer and a second broad peak at 4.8 Å which indicates the bottom (C-ward) layer which consists of 5–6 waters. For the MD simulations the X-ray structures PDB ID 6US8 (Thomaston et al., 2021) or PDB ID 6US9 (Thomaston et al., 2021) were used as starting structures.

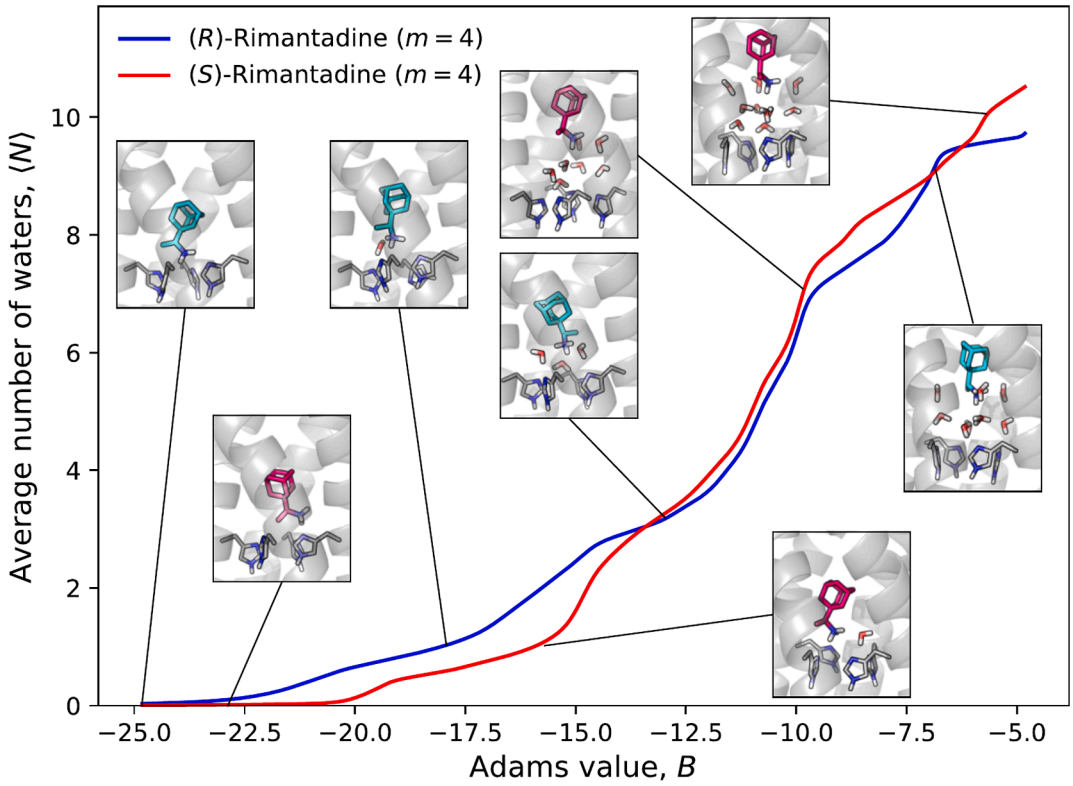

Fig. 9. Calculated titration curves for the two enantiomers with the average number of waters observed plotted against the chemical potential that describes the water binding free energy profiles B value; see theoretical methods in ref. (Thomaston et al., 2021)). Comparing the two titration plots, the B value (water binding free energy profiles) is plotted against the average number of waters detected. The rimantadine enantiomer results are displayed as inset pictures that have been created to illustrate typical structures from various curve points. The (S)-enantiomer is displayed in pink, whereas the (R)-enantiomer is displayed in blue. A total of four sigmoid functions were fitted to the data, as shown by the symbol m = 4 in the legend. (reproduced from Kolocouris, DeGrado and collaborators work in ref. (Thomaston et al., 2021) with permission by American Chemical Society). (For interpretation of the references to color in this figure legend, the reader is referred to the web version of this article.)

WT crystal structure.

3. Interactions of AM2 WT system with adamantyl amines in membranes

3.1. Interactions of adamantyl amines with membranes using NMR and MD simulations

Adamantyl amine drugs that block the AM2 WT proton channel are lipophilic amines that can partition and concentrate in lipid bilayers. The partitioning of adamantyl amines in lipid bilayers was shown for amantadine by Chou and collaborators in 2004 (Wang et al., 2004) using solution NMR (Cady et al., 2011; Cady et al., 2010) and Cross and collaborators in 2008 (Li et al., 2008) using ^{15}N and ^{31}P ssNMR and MD simulations with the CHARMM27 force field (Feller and MacKerell, 2000) and 68 DMPC lipids bilayer (12.6 ns). Additionally, Biggin and coworkers in 2008 studied with umbrella sampling (US) potential of mean force (PMF) calculations (Chee et al., 2008) the permeation of amantadine, rimantadine, memantine through a 52 POPC lipid membrane (runs were also performed with membranes consisting of 128 and 256 POPC lipids). For the PMF/US calculations, 190 windows each separated by a width 0.5 Å were included and the duration of the unrestrained MD simulations in each window was 15 ns, performed with the OPLS force field, (Kaminski et al., 2001; Rizzo and Jorgensen, 1999) in each window. It was concluded that the drugs prefer to stay in the interfacial with water lipid bilayer with their protonated form, but the permeant form is the neutral.

Dong, Zhou and collaborators ran simulations in 2021 (Yang et al., 2021) for amantadine interaction with a membrane bilayer consisting of 256 DMPC lipids or 174 supplemented with 82 cholesterols in the presence of 16 amantadine molecules in their protonated form. The amantadines were randomly placed in each system to improve sampling efficiency: eight of which were in the aqueous phase, and the other eight were inside the lipid bilayer. MD simulations for 400 ns were performed using the CHARMM36 force field (Huang and Mackerell, 2013) for lipids and CHARMM general force field (CGenFF) (Vanommeslaeghe et al., 2010) for amantadine. To determine the free energy landscape of the permeation along the distance (z) between the center of mass of amantadine and the bilayer center, they generated the PMF using the adaptive biasing force (ABF) method. The range of z from 0 (at the center of the bilayer) to 32 Å (in the aqueous phase) was sampled in 28 windows, with a width of 1 Å for z from 0 to 24 and 2 Å for z from 24 to 32 Å. A structure for each window was subjected to MD simulations for 50 ns with z under restraint to relax the membrane and PMF profile was calculated for 10 ns. At low cholesterol mole fractions, the drug molecule stably binds to DMPC bilayers. Cholesterol at a high mole fraction results in the expulsion of the drug molecule from the lipid bilayer to the aqueous phase. This finding was supported by ssNMR data in 2011 (Cady et al., 2011) by Hong and collaborators with 100 % amantadine bound to the DMPC bilayers at a drug–lipid molar ratio of 1:15. When a virus-mimetic membrane containing 30 % cholesterol, a sharp isotropic peak, appeared and assigned to amantadine in bulk water, accounted for 18 % of total intensity. The isotropic peak was cholesterol-dependent and its intensity was reduced significantly when the cholesterol fraction was lowered to 23 %. It was shown using ^{2}H ssNMR spectra of Rmt-d_{15} in comparison to Amt-d_{15} bound to AM2TM WT reconstituted in DMPC at the 1:1 drug:tetramer ratio that ~ 27 % of Rmt is embedded in the lipid phase, (Cady et al., 2011) while only 14 % of Amt is partitioned

into the lipid bilayer. (Cady et al., 2010) The results showed also that excess amantadine in the bilayer increased membrane viscosity.

Kolocouris, Mavromoustakos and collaborators in 2018 (Konstantinidi et al., 2018) studied the perturbation of DMPC bilayers induced by amantadine and the synthetic adamantyl amine, spiro[pyrrolidine-2,2′-adamantane], (Tzitzoglaki et al., 2017; Stamatiou et al., 2001). They applied DSC, SAXS/WAXS, ^{1}H MAS/^{13}C CPMAS 1D ssNMR and MD simulations in DMPC bilayers at pH 8. It was shown that the two adamantyl amines perturbed significantly the DMPC bilayers. The spiranic amine perturbed more effectively at high concentrations and partitioned also in lipid bilayers at very high concentrations, while amantadine crystallized. This finding suggests a significant limitation in the incorporation of amantadine in drug delivery formulations such as targeted liposomes. The significant interactions of the adamantyl amine drugs at the interface between the phosphoglycerol backbone and lipophilic regions were revealed by 500 ns-MD simulations using the (Hu et al., 2011)CHARM36 force field (Huang and Mackerell, 2013) in a bilayer of 256 DMPC lipids (Fig. 10). In their free-base amine form, the two adamantyl amines engage with *sn*-2 carbonyls and water by hydrogen bonding, while in their protonated ammonium form, they connect with phosphate oxygens and water through hydrogen bonding. This drugs localization explains the reorientation of DMPC bilayers and their potent perturbing action, which is demonstrated by all used biophysical techniques (see also **Subsection 3.2.5**).

3.2. *Variation of AM2 construct, lipid environment, ligand structure and method*

3.2.1. *EP*

EP measurements by Pinto and collaborators in 2009 (Ma et al., 2009) or Lamb and collaborators in 2009 (Ohigashi et al., 2009) on AM2CD WT and truncated AM2 constructs were performed. The experiments demonstrated that ectodomain-truncated AM2 (residues 21–97) variants had a slower onset of amantadine inhibition while retaining proton channel properties like those of the AM2CD WT protein. (Ohigashi et al., 2009; Rossman et al., 2010)Further the IC_{50} of amantadine, measured after incubation of amantadine with AM2FL WT for 2 min at pH 5.5, is higher for ectodomain-truncated AM2(21–97) (46 μM) than for AM2CD WT (16 μM). These IC_{50} values showed that the drug has a stronger affinity for the AM2CD WT. Kolocouris and collaborators revealed (Drakopoulos et al., 2018) that even small changes in amino acid residue at position 28 of AM2 WT (e.g., V28I), which does not point inside the pore, significantly impacts the kinetics of AM2 WT blocking by adamantyl amines.

3.2.2. *ssNMR*

A. AM2TM WT and AM2CD WT

Hong and collaborators in 2009 (Cady et al., 2011) and 2011 (Hu et al., 2011; Cady et al., 2011) performed MAS ssNMR experiments at

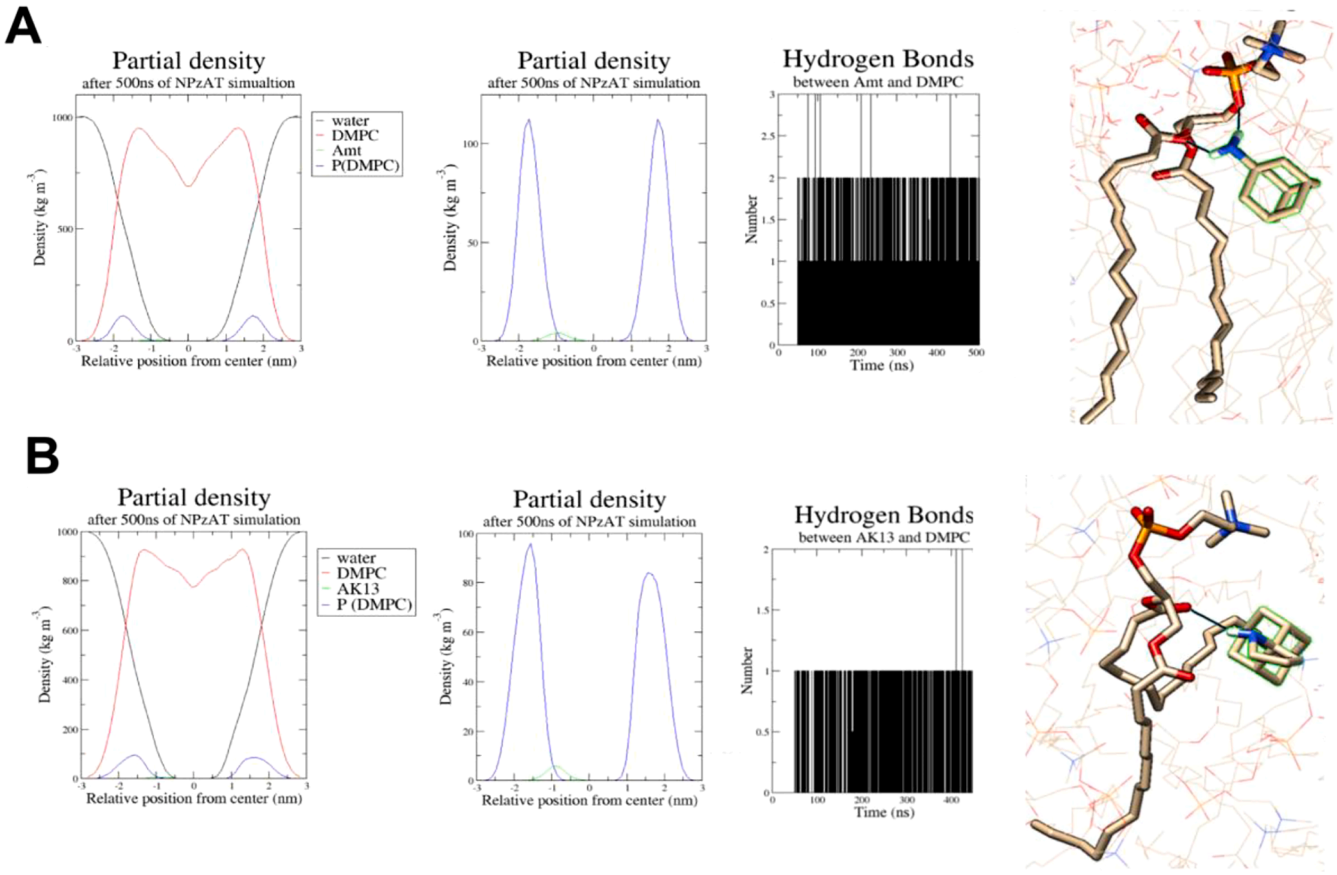

Fig. 10. Results from 500 ns-MD simulations in NPT ensemble of (A) amantadine or (B) spiro[pyrrolidine-2,2′-adamantane] (neutral forms) inside DMPC bilayers at pH7. The two plots on the left suggest the partial density profiles depicting the relevant positions of adamantyl amine (green), DMPC (red), water (black), and the phosphorus atom of the lipid polar head (blue). The partial density profile of the adamantyl amine group and P atom clearly show that the adantantyl amine is most of the time located ~1 nm from the center of the DMPC bilayer. On the right-hand side are shown the number of hydrogen bonds changed by time and snapshots showing the adamantyl amine forming hydrogen bonds with DMPC (reproduced by Kolocouris, Mavromoustakos and collaborators work in ref. (Konstantinidi et al., 2018) with permission by American Chemical Society). (For interpretation of the references to color in this figure legend, the reader is referred to the web version of this article.)

alkaline pH examining in detail the effect of the composition of membrane on the conformations of AM2TM WT (Cady et al., 2011; Hu et al., 2011) and AM2CD WT (residues 21–61), (Cady et al., 2011) focusing on the binding mode of amantadine inside the pore. EPR data suggest that lipid selection influences the conformation of AM2 due to the protein's conformational plasticity. (Duong-Ly et al., 2005) Hong and collaborators tested various bilayers bilayers at a protein–lipid molar ratio of 1:15, e.g., DMPC, POPC and two virus mimetic (VM) membranes containing cholesterol, egg sphingomyelin (SM) and glycerophospholipids (e.g., POPC, POPS) using a drug/tetramer ratio 1:5. They showed in refs. (Cady et al., 2011; Hu et al., 2011) that the thicker POPC bilayer shifts the conformational equilibrium for AM2TM WT to favor amantadine binding compared to the thinner DMPC bilayer, in agreement with EPR. (Duong-Ly et al., 2005) In AM2CD WT reconstituted in DMPC bilayer three amantadine sites with a population ratio 47:45:7 was observed, corresponding to species bound to the AM2CD protein, the bilayers, and the aqueous phase, respectively. Recall that according to ssNMR by Hong and collaborators in 2011 (Cady et al., 2011) amantadine was 100 % bound to the DMPC bilayers. Part of the loss in the bilayer population of amantadine can be attributed to the presence of the AHs that are known to alter the membrane curvature inducing negative gaussian curvature (NGC), and this effect is favored by the presence of cholesterol according to molecular biology and virology experiments performed by Lamb and collaborators in 2010 (Rossman et al., 2010) and CG/MD simulations performed by Kolocouris and collaborators in 2024. (Kolokouris et al., 2024) Interestingly, in ref. (Cady et al., 2011) was shown that when AM2CD WT was embedded in a VM membrane that contains 30 % cholesterol, chemical shift changes present by addition of amantadine were not observed at 30 °C in residues pointing into the pore, in comparison to AM2TM WT in VM membrane that showed chemical shift changes effected by the drug. (Hu et al., 2011; Cady et al., 2011) This result provides some support for the hypothesis that at least a subpopulation of the amantadine molecules bound in the M2 pore comes from exchange with the membrane-bound population. In DMPC bilayers the conformational equilibrium of AM2CD WT favors slightly the drug-free state compared to AM2TM WT, showing ~ 85 % bound form compared to 95 % for AM2TM WT based on Val27 and Ser31 peak ^{13}C signal intensities. These experiments (Cady et al., 2011) revealed that in the longer AM2CD WT construct the VM membrane shifts the conformation equilibrium to the unbound state. Compared to the bound conformation of AM2TM WT in VM membrane, AM2CD WT in VM membrane presents a Val27 gate that is tightly packed, energetically disfavoring drug entrance to the pore. The packed Val27 gate is likely due to the small helix tilt angle, seen in the structure of AM2CD WT (residues 18–60) in DHPC micelles (PDB ID 2RLF (Schnell and Chou, 2008).

Griffin and collaborators in 2010 (Andreas et al., 2010) performed MAS ssNMR in AM2CD WT (residues 18–60) reconstituted in POPC bilayers and one rimantadine per tetramer. Their spectra showed rimantadine existing mainly in the unbound state with only 25 % in the AM2CD-bound state at alkaline pH and 0 °C.

Andreas and collaborators performed in 2020 (Movellan et al., 2020) and 2023 (Tekwani Movellan et al., 2023) MAS ssNMR experiments in AM2CD WT (residues 18–60), in the apo-from or in complex with rimantadine (drug:tetramer ratio ~ 3:1 mol), in DPhPC lipid bilayers at pH 7.8. In this alkaline pH the His37 tetrad has a neutral charge. In ref. 2023 (Tekwani Movellan et al., 2023) they also studied AM2CD WT (residues 18–60) at pH 7.8 embedded in DPhPC/30 % cholesterol or in a VM membrane. Collectively, (Elkins et al., 2017; Ekanayake et al., 2016) Andreas and collaborators reported proton resonances at 14.3, 11.7 ppm for the His37 Nδ1, Nε2 of apo-AM2CD WT due to His-His^{+} dimer-of-dimers formation (Nδ1-H···Nε2 and Nδ1···H-Nε2 forms) and showed an intermolecular coupling (J_{NN} = 8.9 ± 0.3 Hz) due to hydrogen bonding between Nε and Nδ of adjacent His37. (Movellan et al., 2020; Tekwani Movellan et al., 2023) They reported the dimer-of-dimers conformation of AM2CD WT encompasses all the TM residues based on the double peaks they found and that this feature is characteristic for the protein in all membrane lipid compositions. In the presence of bound rimantadine to AM2CD WT pore the His37-Nε2 proton resonances at 14.3 and 11.7 ppm shifted upfield. When rimantadine was added to AM2CD WT in DPhPC bilayers or in VM bilayers or in DPhPC-30 % cholesterol bilayers at 4 °C, the spectra did not show pore binding at all, as observed previously by Hong and collaborators in AM2CD WT (residues 21–61) reconstituted in VM at 30 °C using a drug:tetramer ratio 5:1. (Cady et al., 2011) Pore binding was observed only at 40 °C by measuring the intensity reduction of the side chain His37 peaks in the (H)NH spectra compared to the apo-AM2CD WT signals. While binding took place over three days at 40 °C, complete binding was seen in just a few hours at 55 °C. In accordance with its pore blocking mode of AM2CD WT inhibition, the rimantadine-bound sample also showed a disruption of the J_{NN} hydrogen bond between His37 Nε and Nδ at 40 °C, offering a novel NMR assay for the detection of inhibition by adamantyl amines. The slow kinetics reported for rimantadine by NMR contrast the fast blocking of AM2CD WT (residues 18–60)-induced proton currents by either rimantadine or amantadine observed in liposomal proton flux assays by Chou and Schnell in 2009 (Pielak et al., 2009) or Pinto and DeGrado in 2009, (Ma et al., 2009) respectively. At pH 6 however, i.e. around the pH found in the Golgi lumen (pH 6.0–6.7) (Kellokumpu, 2019) where the AM2 channel adopts its activated + 3 charge state, the rimantadine pore-binding kinetics were faster. (Tekwani Movellan et al., 2023).

These findings also demonstrated how the AHs, as well as the membrane environment and cholesterol, can modify the conformation of TM helices to promote (or not) drug binding to the channel pore.

Indeed, using ssNMR it was shown by Cross or Hong and collaborators that AHs strongly interact with cholesterol. (Elkins et al., 2017; Ekanayake et al., 2016; Elkins et al., 2018) However, as mentioned in **Subsection 2.1.2**: (a) in the functional assays conducted by Schroeder and collaborators in 2005, (Schroeder et al., 2005) amantadine inhibits proton flux mediated by AM2FL WT in liquid crystalline lipid bilayers containing 30 % cholesterol. Additionally, the EP experiments in cholesterol-free liposomes and cholesterol-free *Escherichia coli* membranes demonstrated that cholesterol is not necessary for drug-sensitive proton channel activity. (Schroeder et al., 2005) (b) Using liposomal proton flux assay in liposomes composed of POPC, POPG and cholesterol, Pinto and DeGrado in 2009 (Ma et al., 2009) showed that AM2CD WT (residues 18–60) exhibited amantadine-sensitive proton fluxes. (c) In ref. (Tekwani Movellan et al., 2023) the rimantadine pore-binding kinetics at 40 °C were faster with DPhPC-30 % cholesterol compared to DPhPC or VM (which also contains 30 % cholesterol) showing that membrane bilayer constituents also affected the pore entry kinetics. Therefore, it seems that the absence of amantadine or rimantadine binding is not caused solely by excessive cholesterol levels. However, the conformational equilibrium of the cytoplasmic helix-containing AM2 may be such that amantadine and rimantadine can bind to the pore at low enough cholesterol levels.

B. N-terminal ectodomain and ectodomain-truncated M2 WT

The previous data indicated that AM2 WT drug binding is construct-dependent since rimantadine did not bind AM2CD WT compared to AM2TM WT. Thus, in the AM2 construct that contains the TM domain and AHs (residues 21–61) rimantadine binding is not observed. (Cady et al., 2011) However, Hong and collaborators reported CSPs in 2018 (Liao et al., 2019) demonstrating that the presence of the whole cytoplasmic domain in AM2 (21–97) restores the pore-binding site. This finding indicates that the curvature-effecting AHs distorted the TM structure and obstructed drug binding, while the cytoplasmic tail alleviates this effect. (Liao et al., 2019).

Hong and coworkers studied in 2016 (Kwon and Hong, 2016) the ectodomain-containing AM2 WT (residues 1–49) tetramer reconstituted in DMPC with MAS ssNMR. They found that the electrostatic repulsion

between the acidic residues lying in the random coils of the ectodomain favored a drug-bound like conformation in the TM bundle. Both amantadine and random coil residues 1–21 shift the AM2TM WT toward a conformation kinked at Gly34 and increase the diameter of the AM2 pore at Ser31. Furthermore, the ectodomain enhances drug entrance since it is located near the drug's path of entry into the TM pore. Since amantadine has been demonstrated to tighten the four-helix bundle generated by the AM2TM WT peptide, the observed interhelical Ala30–Ile35 cross-peaks in ref. (Kwon and Hong, 2016), which showed a well-packed four-helix bundle, are consistent with the synergistic action of the ectodomain and drug binding. (Hu et al., 2007; Cady and Hong, 2009; Cristian et al., 2003) The reduced affinity for the synthetic ectodomain-truncated M2(21–97) (Liao et al., 2015) compared to AM2CD WT is explained by this conformational selection, as seen by the three-fold larger IC_{50} of the truncation mutant's determined by EP (Ohigashi et al., 2009) (see **Subsection 3.2.1**). Fig. 11 illustrates the impact of the ectodomain and amantadine binding, which has been demonstrated to tighten the TM four-helix bundle, on the conformational equilibrium of the AM2TM WT helix bundle.

3.2.3. EPR spectroscopy

EPR was applied in AM2TM WT (residues 21–49) labeled at L46C by Georgieva, Freed and collaborators in 2016. (Georgieva et al., 2016) They confirmed that this AM2TM WT construct in DOPC/POPS (1:10,000 peptide/phospholipid molar ratio), in the presence or absence of amantadine, forms a mixture of monomers, dimers, and tetramers. It was suggested that the dimer configuration acts as an intermediate in the assembly of the AM2TM WT tetramer, suggested also in their previous work. (Georgieva et al., 2015) Double electron–electron resonance (DEER) showed that amantadine changes the oligomer equilibrium in favor of tetramers, as evidenced by an increase in DEER modulation depth for peptide/phospholipid molar ratio ranging from 1:18,000 to 1:160. This was shown by DeGrado in 2000 (Salom et al., 2000) with AM2TM WT (22–46) in DPC micelles using CD, AUC, fluorescence spectroscopy and ^{1}H NMR. Additionally, amantadine binding causes the inter-spin distances (for nitroxide labels) to decrease by 5–8 Å, which suggests that the drug caused the channel to close its C-terminal part. The thinner membrane containing DLPC/1,2-dilauroyl-*sn*-glycero-3-phospho-serine (DLPS) did not exhibit this effect, highlighting the significance of bilayer thickness. The analysis of continuous wave (cw) ESR spectra of spin-labeled L46C AM2TM WT suggested a more conformationally constrained helix bundle when amantadine binds AM2TM WT. Compared to apo-AM2TM WT, the amantadine-bound form did not show any observable conformational alterations in the case in the AM2TM G34A mutant present in several drug-resistant influenza strains. (Georgieva et al., 2016).

3.6.4. nMS

A recent and first application of native mass spectrometry (nMS) showed that AM2TM WT and AM2FL WT form polydisperse and previously unobserved oligomers. The local chemical environment (lipids and pH) highly affects the multiplicity of these dynamic oligomers. (Townsend et al., 2021) The findings demonstrated that nMS is suitable to recommend an appropriate lipid environment to favor the most physiological oligomer (tetramer) raises the possibility that AM2 may exist in nature as a mixture of various oligomeric states that are shifted to the channel's active oligomer (tetramer) by amantadine and low pH.

3.2.5. SAXS

Kolocouris, Mavromoustakos and coworkers in 2020 (Konstantinidi et al., 2020) performed SAXS, WAXS, and DSC to investigate the partitionining of AM2TM WT and AM2TM WT/adamantyl amine drug systems. It has been observed in 2018 (Konstantinidi et al., 2020) by Kolocouris, Mavromoustakos and coworkers using DSC and MD simulations that both amantadine and spiro[pyrrolidine-2,2′-adamantane] perturbed the DMPC bilayer's biophysical characteristics in a similar manner when adamantyl amine:lipid molar ratio is $x = 0.05$. According to ^{31}P or ^{13}C ssNMR, and MD simulations, these adamantyl amines affect the phosphate groups in their ammonium form or the glycerol backbone and the carbonyl area of the headgroup region in their amine form, respectively.

Two bilayer nanodomains emerged at low AM2TM WT protein concentration (x = 0.03); one for bulk lipids and another for non-annular lipids/annular lipids attached to AM2TM WT tetramers. The latter is the lipid domain which makes up nearly all the lipids at high peptide density (x = 0.06). It was demonstrated that amantadine, as

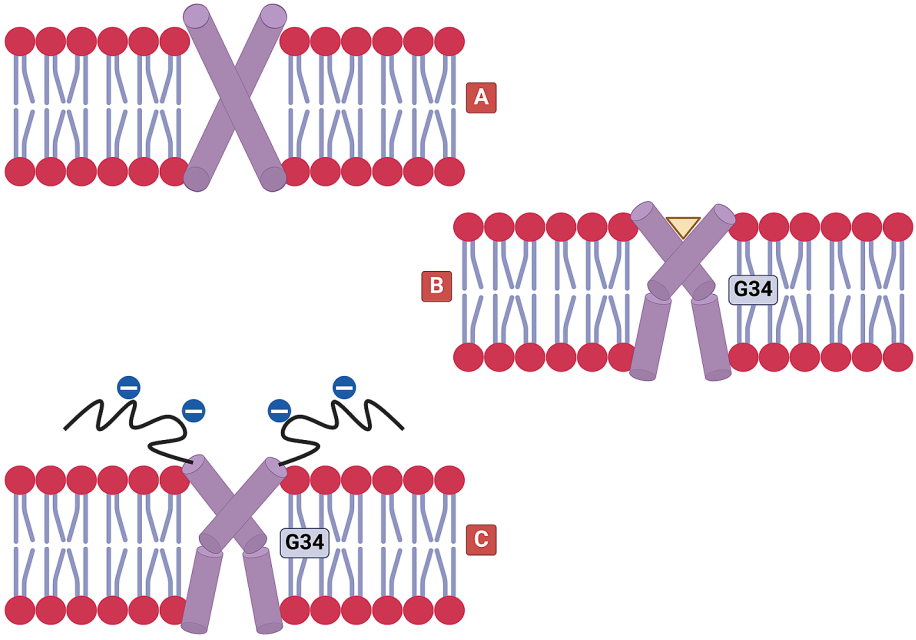

Fig. 11. Schematic illustrating of how the ectodomain affects the AM2TM WT helix's conformational equilibria (two tetramer TM helices are shown). **(A)** Drug-free AM2TM WT domain. **(B)** Amantadine bound to the AM2TM WT domain, which causes a kink at Gly34. **(C)** Even when the drug is not present, the ectodomain moves the TM domain in the direction of the drug-bound conformation. This is probably because the acidic residues in the ectodomain electrostatically repel one another.

opposed to spiro[pyrrolidine-2,2′-adamantane] (x = 0.05), may significantly disrupt chain-stacking through ionic hydrogen bonding interactions between their ammonium and phosphate groups; this affects the formation of two lipid domains, which most likely represent bulk lipids and AM2TM WT boundary lipids (Fig. 12). The apo-form or drug-bound form of AM2TM WT spans the membrane and exhibits significant interactions with lipid acyl chain-tails and the phosphate groups of the polar head surface, as shown by ^{1}H and ^{31}P ssNMR. Excess drug molecules can be inspected and their effects on the lipid head group area evaluated thanks to the ^{13}C ssNMR spectra.

3.2.6. *MD simulations*

Arkin in 2011 (Leonov et al., 2011) applied 20 ns-MD simulations with the united atoms GROMOS96 53a6 force field (Oostenbrink et al., 2004) and PMF(US) calculations, using as starting structure the AM2TM WT (PDB ID 3BKD (Stouffer et al., 2008), to investigate AM2TM WT – amantadine or rimantadine complexes embedded in 100 DMPC lipids. It was suggested (Leonov et al., 2011) that because of their positively charged amino group, adamantyl amines electrostatically hinder AM2 proton channel function; in contrast, conductivity is unaffected by the hydrophobic adamantyl moiety alone. Recall that in ref. (Thomaston et al., 2018) DeGrado, Kolocouris and coworkers (see **Subsection 2.3.3**) showed that when adamantyl amines bind to the channel pore, their ammonium group can mimick a hydronium, indicating that the adamantyl amines act as mechanism-based inhibitors exploiting structural elements of the channel natively involved in proton transport.

Klein and collaborators in 2011 (Khurana et al., 2011) performed MD simulations of amantadine or rimantadine – AM2TM WT WT complexes in 0, +3, +4 charge states embdded in 218 DMPC lipids bilayer for ~ 20 ns using the CHARMM27 for protein, (Mackerell et al., 2004) and CHARMM27 force field for lipids, (Pastor and MacKerell, 2011) starting from crystallographic and solution NMR structures and different protonation states of His37 (e.g., 3C9J (Stouffer et al., 2008) with charge states + 3, +4 and 2RLF (Schnell and Chou, 2008), 3BKD (Stouffer et al., 2008) with charge state 0). The MD simulations showed that amantadine is stable inside the tetrameric bundle, which spans the area between residues Val27 and Gly34, at both low and high charge states. It was proposed that amantadine's amino group is oriented toward the His37 gate at low pH levels (equiv. high charge states), interacting with water molecules that bridge the side chains of His37 imidazole, but at high pH levels (equiv. neutral His37 tetrad), its orientation shows fluctuations in direction. Additionally, according to these MD simulations, the molecules of amantadine and rimantadine did not exhibit a high affinity for the lipid facing binding site. (Khurana et al., 2011).

Liu, Wei and collaborators performed elegant PMF(US) calculations in 2011 (Gu et al., 2011) to compare the free energy path of a protonated rimantadine molecule through a lipid bilayer of 128 1,2-dipalmitoyl-*sn*-glycero-3-phosphocholine (DPPC) lipids without and with AM2CD WT (residues 18–60), using as starting structure the PDB ID 2L0J, (Sharma et al., (1979) 2010) to reach the Asp44 side chain (peripheral binding site). They also investigated the free energy path along the collective variable connecting rimantadine from the bulk water to the pore-binding site. For the PMF/US calculations a relaxed protein (after 15 ns of MD simulations) and 90 windows were used, and the duration of the unrestrained MD simulations was 5 ns with the OPLS force field (Kaminski et al., 2001; Rizzo and Jorgensen, 1999) in each window. The GROMOS96 united-atom (UA) force field (Berendsen et al., 1995) and Berger's UA force field (Berger et al., 1997)were used for describing the

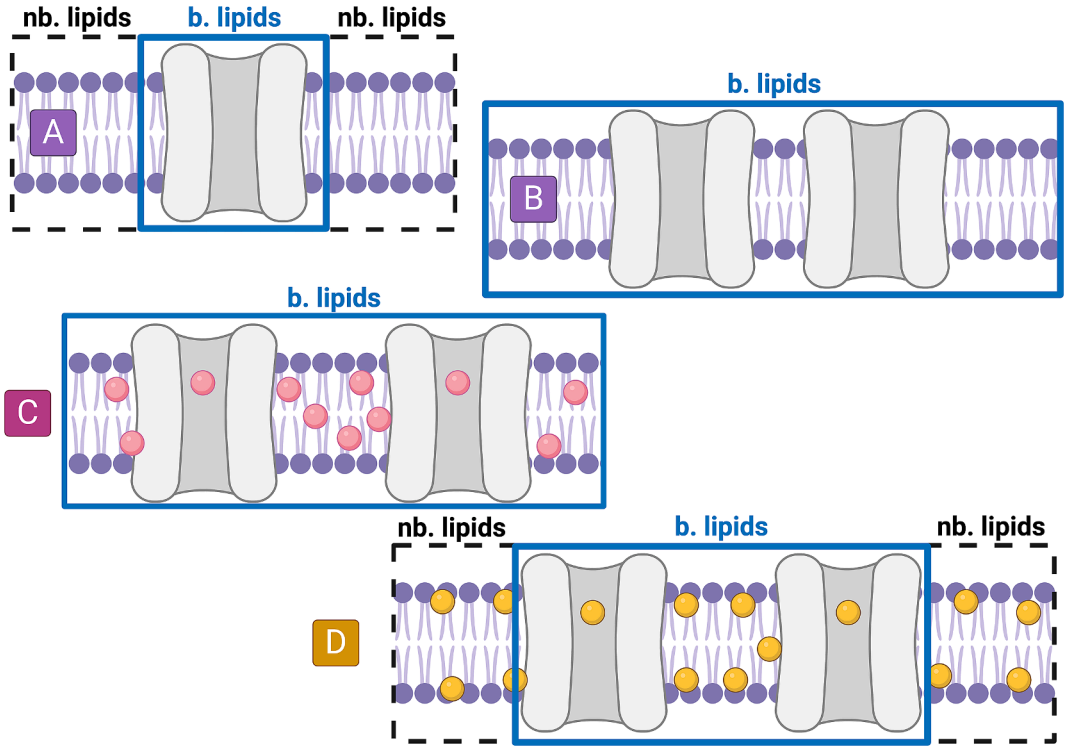

Fig. 12. **(A)** Two domains emerged at low concentrations of embedded AM2TM WT protein (x = 0.03), which is displayed as a tetrameric surface. One domain corresponds to bulk lipids (lipids are represented as a head with two tails), while the other domain relates to lipids attached to AM2TM WT tetramers (annular and non-annular). **(B)** At higher AM2TM WT concentrations (x = 0.06), the second domain vanishes, suggesting that AM2TM WT is evenly distributed across the lipid bilayers and that all lipid molecules act as boundary lipids at this concentration. **(C)** The excess of the more lipophilic spiro[pyrrolidine-2,2′-adamantane] (shown in pink spheres), interacts with AM2TM WT's lateral surfaces more so than the lipid polar head region, in contrast **(D)** the extra amantadine, which is not bound to the protein shown as yellow spheres, attaches to the lipid polar head region via its ammonium group. The presence of AM2TM WT drives the formation of the two lipid nanodomains shown in the DSC and SAXS scans because amantadine has a stronger effect on bilayer geometry than the more lipophilic spiro[pyrrolidine-2,2́-adamantane] (b. lipids: boundary lipids; nb. lipids: non boundary lipids which are the bulk lipids). (For interpretation of the references to color in this figure legend, the reader is referred to the web version of this article.)

protein or rimantadine and the lipids, respectively. It was found that the pore binding is more thermodynamically favorable than the surface binding site by ~7 kcal/mol but requires a higher energy barrier of ~10 kcal/mol to be overcome. Using the OPLS force field (Kaminski et al., 2001; Rizzo and Jorgensen, 1999) for protein and rimantadine and Berger's UA force field (Berger et al., 1997) for lipids, similar results were obtained. In comparison, the less energetically stable surface binding site can be easily accessed by rimantadine molecules. It was suggested that rimantadine prefers to enter the AM2 pore from water than to reach Asp44 through diving into the membrane bilayer.

Voth and collaborators in 2020 (Watkins et al., 2020) applied for 2–4 ns Multiscale Reactive Molecular Dynamics (MS-RMD) and quantum mechanics/molecular mechanics to describe the dynamics of the mechanism-based inhibition of AM2 WT. They applied an explicit parametrization to describe the hydronium cations while the region spanning from ammonium group of the ligand to His37-tetrad was calculated with a QM theory level and CHARMM36 force field. (Huang and Mackerell, 2013) This QM/MM model was a continuation of a longtime effort to describe features of the conductance mechanism with QM/MM multiscale MD simulations, initially using the multistate empirical valence-bond (MS-EVB) model. (Wu and Voth, 2005) The MS-EVB model was developed to describe the hydrated excess proton (hydronium-like) which exists in a complex hydrogen bonded network that rearranges dynamically as bonds break and form according to the Grotthuss shuttling mechanism (thus possible hydronium states of waters inside AM2TM WT can be e.g., $H_5O_2^+$, $H_9O_4^+$ etc). Voth and collaborators improved the initial MS-EVB to the MS-RMD model that could more adequately describe the formation and breakage of bonds during proton transportation and applied this QM/MM model a decade later, e.g., in 2014–2019 with the longer AM2CD WT construct (see refs (Liang et al., 2014; Liang et al., 2016; Watkins et al., 2019) to describe proton-induced conformational and hydration dynamics in the AM2 channel. Voth and collaborators showed in 2016 (Liang et al., 2016) that under low pH_{in} and high pH_{out}, the reverse proton current in AM2 WT is blocked by steric hindrance and a desolvation penalty at Trp41, explored experimentally with ssNMR by Hong and collaborators in 2018. (Mandala et al., 2017).

3.2.7. ITC and alchemical binding free energy calculations

Kolocouris and collaborators in 2018 (Drakopoulos et al., 2018) evaluated the binding affinity of rimantadine analogs bearing progressively larger alkyl groups (with dimethyl, diethyl and dipropyl in the carbon bridge) and tested the blocking efficiency against the AM2FL WT and S31N protein channel and virus replication using TEVC and antiviral assays, respectively. Their results showed that compared to amantadine (K_d = 2.7 μM), and rimantadine (K_d ~ 0.33 μM), the dimethyl analog had enhanced affinity against AM2TM WT (Udorn sequence) in DPC micelles by ITC (K_d = 0.13 μM), and against AM2CD WT according to the kinetic binding measurements by EP. This was confirmed also by alchemical relative binding free energy (RBFE) calculations with a free energy perturbation coupled with 2 ns-MD simulations (FEP/MD) method in the NPT ensemble using the OPLS2005 force field. It was found that the diethyl and dipropyl rimantadine analogs showed reduced affinity and potency (Fig. 13). (Drakopoulos et al., 2018) Similarly, the antiviral potency (EC_{50}) evaluation showed the same ranking. Kolocouris and collaborators in ref. (Drakopoulos et al., 2017) showed that the calculated RBFE with FEP/MD calculations was $\Delta\Delta G_{FEP/MD}$ (**3** → **2-R**) = 0.62 ± 0.14 kcal/mol with $\Delta\Delta G_{ITC}$ (**3** → **2-R**) = 0.33 ± 0.50 kcal/mol while $\Delta\Delta G_{FEP/MD}$ (**3** → **2-S**) = 0.68 ± 0.15 kcal/mol with $\Delta\Delta G_{ITC}$ (**3** → **2-R**) = 0.42 ± 0.48 kcal/mol. In ref. (Drakopoulos et al., 2018) the 80-MD simulations with the OPLS2005 force field (Thomaston et al., 2017; Wright et al., 2016) of the ligand-AM2TM WT complexes embedded in ~ 50 DMPC lipid bilayers showed that in diethyl and propyl analogs (**4** and **5**; respectively, see Fig. 13) the alkyl groups appear to better occupy the space between the ligand and the pore walls. For these compounds' binding, the ITC data indicated that constrained motion and the resulting entropy cost of binding are important quantities and reduced the binding affinities

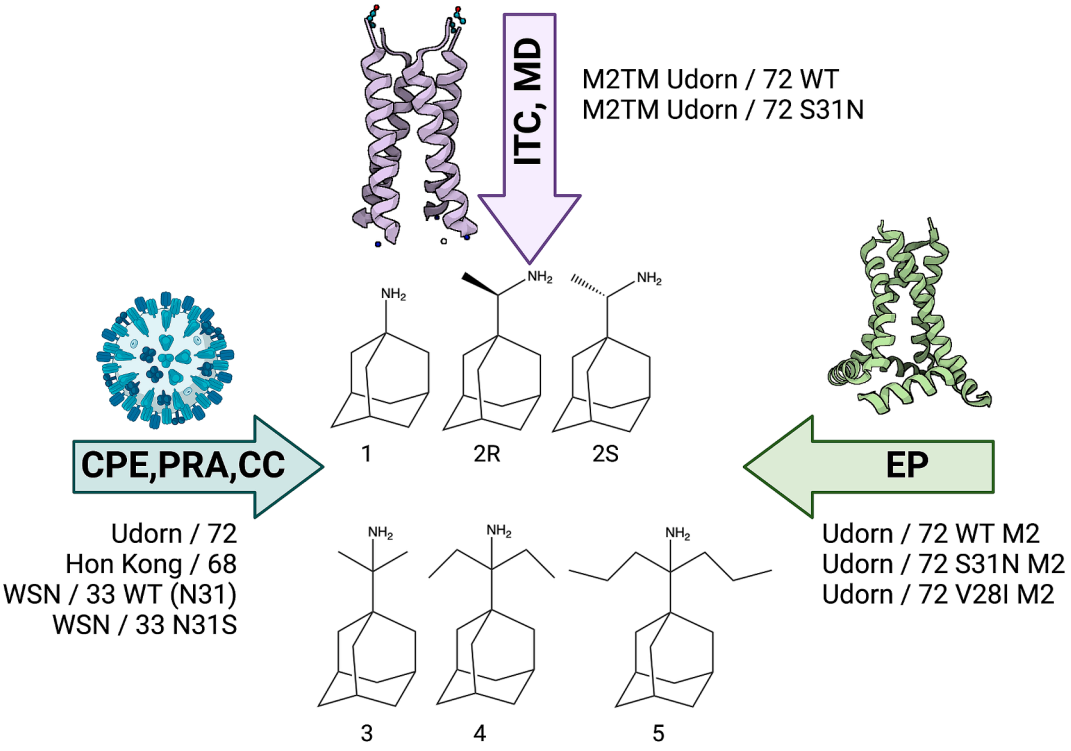

Fig. 13. Evaluation of the binding affinity and proton blockage against the AM2FL WT and S31N protein channels of rimantadine analogs which include in their structures progressively larger alkyl groups. The applied methods employed different constructs of AM2. These methods were the ITC and MD simulations that investigate binding to AM2TM WT, EP that used AM2CD WT, and cell-based antiviral assays. (Drakopoulos et al., 2018).

compared to **3** (see Table 1 in ref. (Drakopoulos et al., 2018). The proton blocking action of the adamantyl amines is consistent with the fact that no water molecules were detected in the area above the adamantane core (i.e., toward the N-terminus) in any of the examples.

Kolocouris, Gohlke, Cournia and collaborators in 2016, (Ioannidis et al., 2016) and Kolocouris and collaborators in 2024 (Georgiou et al., 2024) used ITC for the titration of tetrameric AM2TM WT (Udorn sequence) reconstituted in DPC micelles (~ 1:57 peptide/lipid to maintain tetramers) in its closed state (pH 8), by amantadine and various adamantyl amines. The K_d values were used as experimental probes for the FEP/MD calculations of alchemical RBFEs in the NPT ensemble. Cournia, Kolocouris and collaborators in 2012 (Gkeka et al., 2013) performed FEP/MD simulations in the NPT ensemble of AM2TM WT at acidic pH using as probes experimental K_d values measured at acidic pH against the C_{open} conformation of AM2CD WT. The experimental assay was based on inhibition by adamantyl amines of the quenching of Trp41 fluorescence by His37 protonation below pH 6 in AM2CD WT in detergent environment developed originally by Hay and collaborators. (Czabotar et al., 2004) This assay was previously tested in the adamantyl amine-AM2 WT system by Kolocouris and collaborators. [258] Gohlke, Kolocouris and collaborators in 2016 (Homeyer et al., 2016) also measured with ITC several adamantyl amines against AM2TM WT Weybridge strain (with V28I, L38F mutations compared to Udorn) and found a $K_d = 0.74$ μM for amantadine. They observed that the Molecular Mechanics-Poisson Boltzmann Surface Area (MM-PBSA) method with amber14sb force field (ff14sb) (Tian et al., 2020) can at least fairly provide the relative importance of the binding free energy components of adamantyl amines against AM2TM WT Weybridge, which are useful for the interpretation of the thermodynamic profiles measured experimentally, after decomposition of the calculated binding free energies. It was concluded (Homeyer et al., 2016) that MM-PBSA can help in prospectively prioritizing amantadine variants derivatives.

As continuation of the work in 2016 with FEP/MD simulations in the NPT ensemble, (Ioannidis et al., 2016) Kolocouris and collaborators in 2023 (Georgiou et al., 2024) published the ITC-based binding free energies of 27 adamantyl amines against the closed form of AM2TM WT tetramer in DPC micelles, and antiviral potencies (EC_{50}) with whole cell-assays. The range of the experimental K_d values was ~ 44 and the range of the EC_{50} values was ~ 750; these sets of values showed a good correlation (r = 0.76) between their corresponding binding free energies, computed using either the K_d or EC_{50} values. 250 ns-MD simulations with ff19sb (Tian et al., 2020) or CHARMM36m force field (Huang et al., 2016) and different experimental starting structures of AM2TM WT-complexes embedded in ~ 60 or 200 phospholipids were applied to investigate the binding mode of adamantyl amines that bind strongly, moderately or tightly to AM2TM WT embedded in DMPC, DPPC, POPC or a VM membrane (Fig. 14).

Kolocouris and collaborators in 2023 (Georgiou et al., 2024) carried out 2 ns-TI/MD simulations in the NVT ensemble with ff19sb and the MBAR estimator and FEP/MD NPT simulations with OPLS2005 force field (Thomaston et al., 2017; Wright et al., 2016) and the BAR estimator, on AM2TM WT-adamantyl amine complexes embedded in ~ 60 DMPC, DPPC, and POPC lipid bilayers, to precisely predict experimental RBFEs measured with ITC in DPC micelles. Dual topology and single topology alchemical transformations were used, respectively. The pairs of ligands considered beared subtle changes in the ligands' structures. With all lipid types tested, it was found that both approaches exhibited a very good correlation between the calculated and experimental relative binding free energies (r = 0.77–0.87, mue = 0.36–0.92 kcal/mol), with FEP/BAR performing the worst in DMPC bilayers and TI/MBAR performing the best (Fig. 15). The experimental RBFEs were also calculated using antiviral potencies rather than K_d values, and both FEP/BAR (r = 0.83, mue = 0.75 kcal/mol) and TI/MBAR (r = 0.69, mue = 0.77 kcal/mol) performed well for AM2TM WT − adamantyl amine complexes embedded in POPC bilayers. (Georgiou et al., 2024).

4. Interactions of adamantane-based drugs with AM2 mutants

Mutations that cause amantadine resistance are found at the interhelical interfaces at the N-terminal half of the channel (L26F), at the pore-facing positions (V27A, A30T, S31N, and G34E), and outside the drug-binding site at the interhelical interfaces (L38F, D44).

4.1. *Adamantyl amine drugs against AM2 V27A, L26F*

4.1.1. *MD simulations*

Arkin and collaborators in 2011 (Astrahan and Arkin, 2011) suggested that certain drug-resistant mutants (e.g., L26F, V27A, A30T, S31N) have an expanded drug binding pocket. (Leonov et al., 2011) Therefore, even after drug binding to the channel, the drug is still mobile enough so as to not induce a positive electrostatic repulsion that blocks protons. This was suggested as a simple mechanism for proton flow

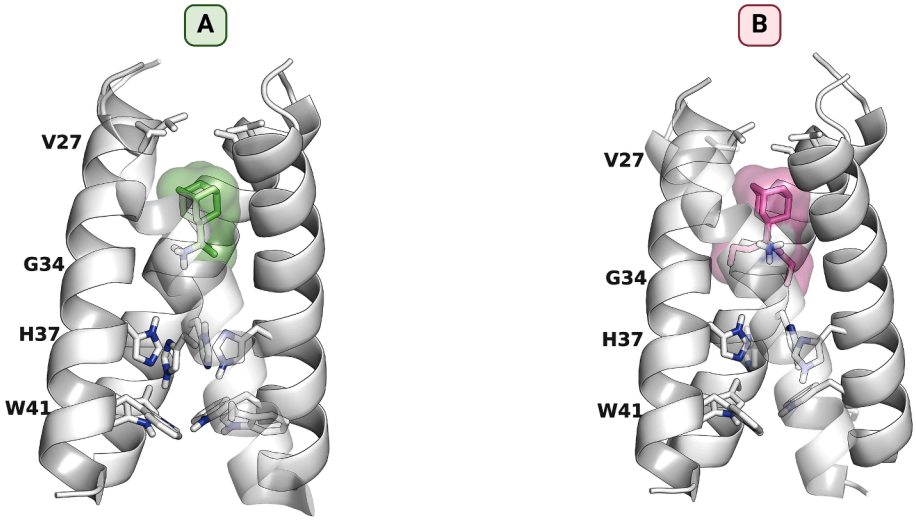

Fig. 14. Representative structures from 80 ns-MD simulations with ff19sb (Tian et al., 2020) of rimantadine analogs (A) 3, (B) 5 (see Fig. 13) in complex with AM2TM WT in DMPC bilayers. (Drakopoulos et al., 2018) In the Figure the protein is shown with white cartoon and the ligands with sticks and red color. The water molecules are shown with sticks. White color is used for hydrogens, red for oxygen and blue for nitrogen; yellow dotted lines show the hydrogen bonds. (For interpretation of the references to color in this figure legend, the reader is referred to the web version of this article.)

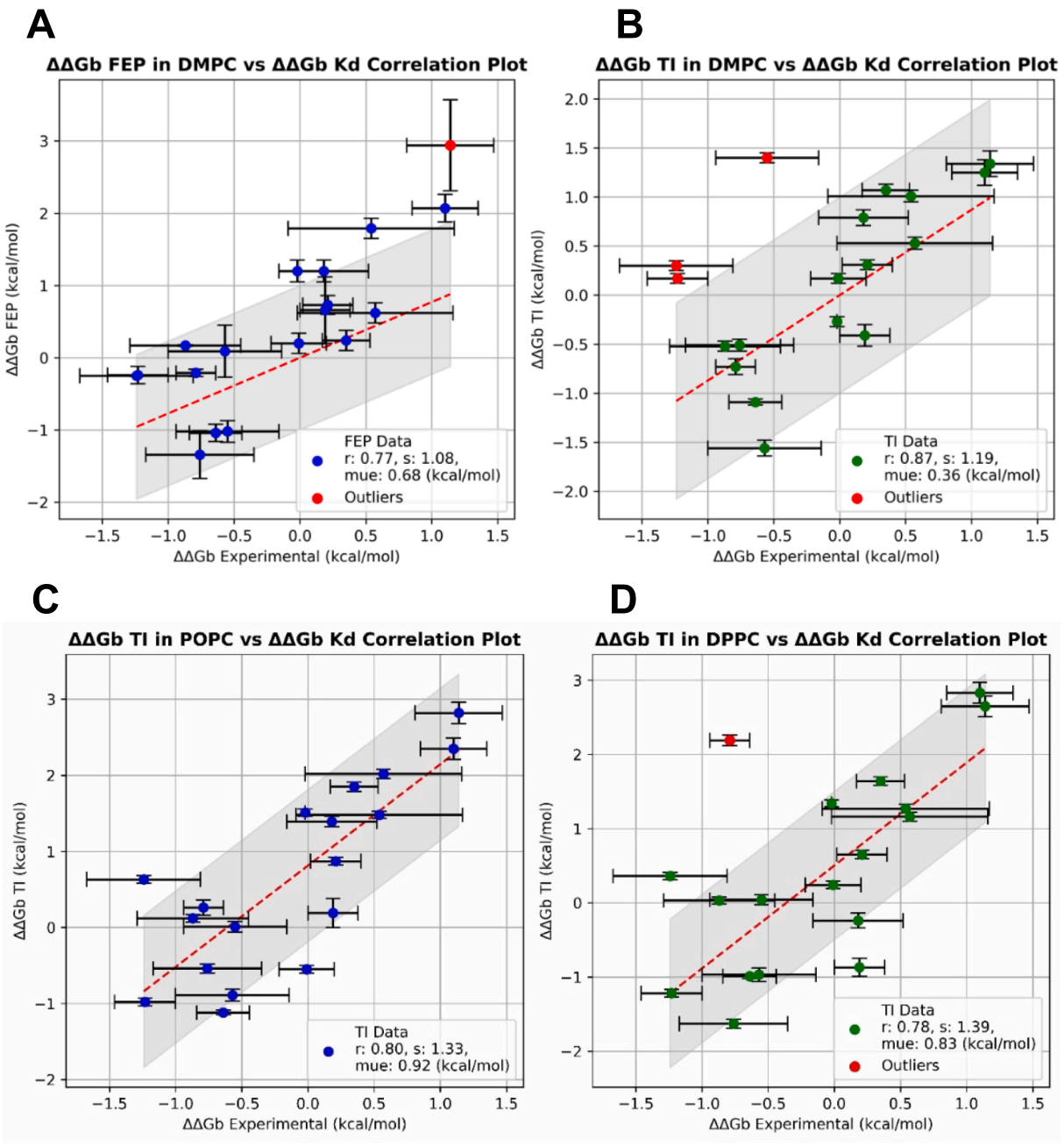

Fig. 15. Relative binding free energies obtained from ITC data ($\Delta\Delta G_{b,exp}$) versus calculated relative binding free energies with perturbative free energy methods for AM2TM WT-adamantyl amine complexes in phospholipid bilayers. **(A)** $\Delta\Delta G_{b,FEP/MD}$ calculated for complexes embedded in DMPC bilayers and **(B)-(D)** $\Delta\Delta G_{b,TI/MD}$ calculated for complexes embedded in **(B)** DMPC, or **(C)** POPC, or **(D)** DPPC bilayers. The correlation line (dashed red line), error bars, and Pearson *r*, *p*, slope (*s*) values are displayed, based on the linear least-squares fit of the data. The outliers correspond to deviation of calculated values larger than the method's error (1 kcal/mol) with the best case shown in panel **(C)**. By comparing **(A)-(D)**, the outliers may reflect inconsistencies due to the calculation models. (For interpretation of the references to color in this figure legend, the reader is referred to the web version of this article.)

blocking by amantadine in ref. (Leonov et al., 2011).

The AM2 V27A mutation which confers resistance to amantadine and rimantadine channel blocking is becoming important in circulating populations of influenza A virus. (Lindorff-Larsen et al., 2010) Luque, Cavalli and collaborators in 2016 (Llabrés et al., 2016) performed fifty 50 ns-metadynamics simulations of AM2CD WT and V27A (residues 18–60), based on the PDB ID 2L0J (Sharma et al., (1979) 2010) structure, in the His37 + 2 charge state embedded in 260 POPC lipids with the ff99sb (Lindorff-Larsen et al., 2010) force field to explore in detail the potential energy surface of the channel's pore with amantadine drug inside the pore. Using a starting structure with amantadine in the C-ward orientation they derived a sequential mechanism for the (un) binding of amantadine and its variants to the AM2 WT channel at the + 2 state (pH 7). To reach the thermodynamically preferred C-ward (inward) binding mode in the channel pore, amantadine's dynamics include the adoption of a transiently populated intermediate with the drug's amino group oriented towards the N-end (outward). Additionally, they proposed that, despite the absence of a significant population of chloride anions in the pore interior, chloride anions are crucial in maintaining the inward binding mode of amantadine to the AM2 WT channel, which is achieved by the electrostatic repulsion between the protonated amine of amantadine and the doubly protonated His37 tetrad. It was also proposed that the recovery of hydrating water molecules during the transition from the N-ward state to the C-ward binding

mode is what causes amantadine to bind to the AM2CD WT channel, in addition to the electrostatic stabilization provided by chlorine ions. These interactions lead to kinetic trapping, which favors amantadine's "pseudo-irreversible" blockage of the AM2 WT channel as seen in experiments. (Llabrés et al., 2016) Using a starting structure with amantadine in the C-ward orientation of the AM2 V27A pore the drug rotates quickly to the N-ward orientation. The study revealed that the drug is very flexible inside the pore and the potential energy surface of the complex is characterized by low energy barriers and many minima with similar energies. It was proposed that this would explain the sharp decrease in inhibitory effectiveness against the AM2 V27A variant. (Llabrés et al., 2016).

4.1.2. X-ray crystallography

Using X-ray crystallography Thomaston, Kolocouris, DeGrado and collaborators in 2020 (Thomaston et al., 2020) solved the crystal structures of AM2TM V27A (Fig. 16**A**) and AM2CD V27A (residues 21–61) in complex to a spiroadamantyl amine inhibitor of AM2 V27A. The structure of the spiroadamantyl amine bound to AM2TM V27A (PDB ID 6NV1 (Thomaston et al., 2020) in the C_{closed} conformation revealed the mechanism of amantadine resistance. Specifically, compared to the structure of the spiroadamantyl amine bound to AM2TM WT (PDB ID 6BMZ (Thomaston et al., 2018) in (Fig. 16**B** (see also Fig. 7**C**)), the AM2TM V27A channel pore in PDB ID 6NV1 (Thomaston et al., 2020) is wider at its N-terminus because of the Val27Ala mutation. This mutation eliminates the hydrophobic interactions on the Val27 side chain that are necessary for amantadine or rimantadine binding. Since the spiroadamantyl amine inhibitor is longer than amantadine, it may effectively block proton conductance in the AM2 WT and AM2 V27A mutant channels by translocating the binding site in the pore based on which residue is present at position 27. In ref. (Thomaston et al., 2020) a starting structure was prepared after applying the V27A mutation to the structure of spiro-adamantyl amine in complex with AM2TM WT in the $inward_{closed}$ closed conformation (PDB ID 6BMZ (Thomaston et al., 2018). The 300 ns-MD simulations of the AM2TM V27A – spiroadamantyl amine complex embedded in 200 POPC lipids accurately reproduced the location of the ligands and waters found within the pore of the AM2 V27A complex in the crystal structure (PDB ID 6NV1). (Thomaston et al., 2020).

4.1.3. ssNMR and MD simulations

DeGrado, Klein and collaborators in 2011 (Wang et al., 2011) performed 100 ns-MD simulations of drug binding to AM2TM WT with the CHARMM27 force field (Feller and MacKerell, 2000) using as starting structure the crystal structure of AM2TM WT (residues 25–46) with PDB ID 3LBW (Acharya et al., 2010) embedded in POPC bilayers. They designed and developed a series of potent spiranic amine inhibitors targeting not only WT, but also AM2 V27A and L26F mutants. The adamantyl spiro-amine shown in Figs. 7, 16 exhibited *in vitro* antiviral potency (EC_{50}) values like those observed with EP and plaque reduction assays for the inhibition of the WT by amantadine. Its binding to the V27A pore was further demonstrated by MAS ssNMR with AM2TM V27A embedded in DMPC bilayers. (Wang et al., 2011).

Kolocouris, Schmidke, Andreas and collaborators studied in 2023 (Stampolaki et al., 2023) the potencies against influenza A with M2 WT channel of several adamantyl amines and some cage amine analogs and the AM2 L26F, V27A, A30T, G34E mutants that are resistant to amantadine. In ref. 2023, (Stampolaki et al., 2023) compound 61 (Fig. 17), developed by Vazquez and collaborators in 2017, (Rey-Carrizo et al., 2014) exhibited a blockage to AM2 WT, L26F, V27A channels by EP

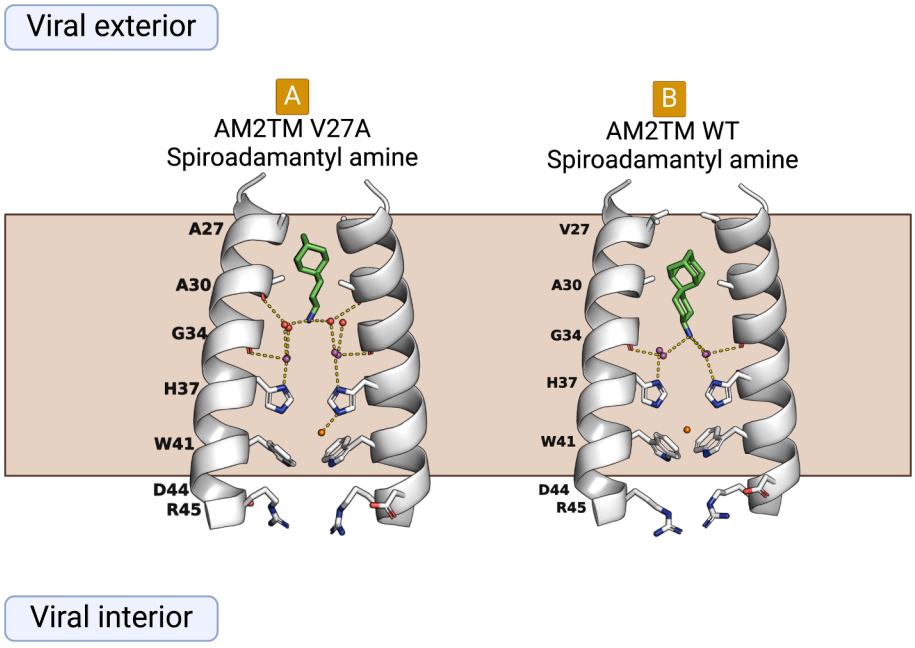

Fig. 16. The mechanism by which the shown spiro-adamantyl amine acts as dual inhibitor of AM2 WT and AM2 V27A explains amantadine drug resistance in the AM2 V27A mutant channel (the front and rear monomer helices are not shown for clarity). (Thomaston et al., 2020) Structures of (A) AM2TM V27A bound to the spiro-adamantyl amine inhibitor (PDB ID 6NV1 (Thomaston et al., 2020), and (B) AM2TM WT bound to the spiro-adamantyl amine inhibitor (PDB ID 6BMZ (Thomaston et al., 2018) are shown. In (A) the ammonium group of the inhibitor when spiroadamantyl amine binds to the AM2TM V27A channel (PDB ID 6NV1 (Thomaston et al., 2020) localizes to the same location as the ammonium of amantadine in the AM2TM WT structure (PDB ID 6BKK (Thomaston et al., 2018). The Val27 to Ala mutation generates more room in the channel pore, which is occupied by the adamantyl group. In (B) the inhibitor attached to the AM2TM WT channel, the four waters in the Ala30 layer are displaced, and the spiro-adamantyl amine inhibitor's adamantyl group binds lower in the channel pore (PDB ID 6BMZ (Thomaston et al., 2018). Consequently, a network of one or two layers of hydrogen-bonded waters is generated for the spiro-adamantyl amine-bound structures according on whether Val or Ala is present at position 27 (waters which are hydrogen bonded to the Ala30 carbonyls are shown with pink spheres and waters that are hydrogen bonded to the Gly34 carbonyls are shown with red spheres). (For interpretation of the references to color in this figure legend, the reader is referred to the web version of this article.)

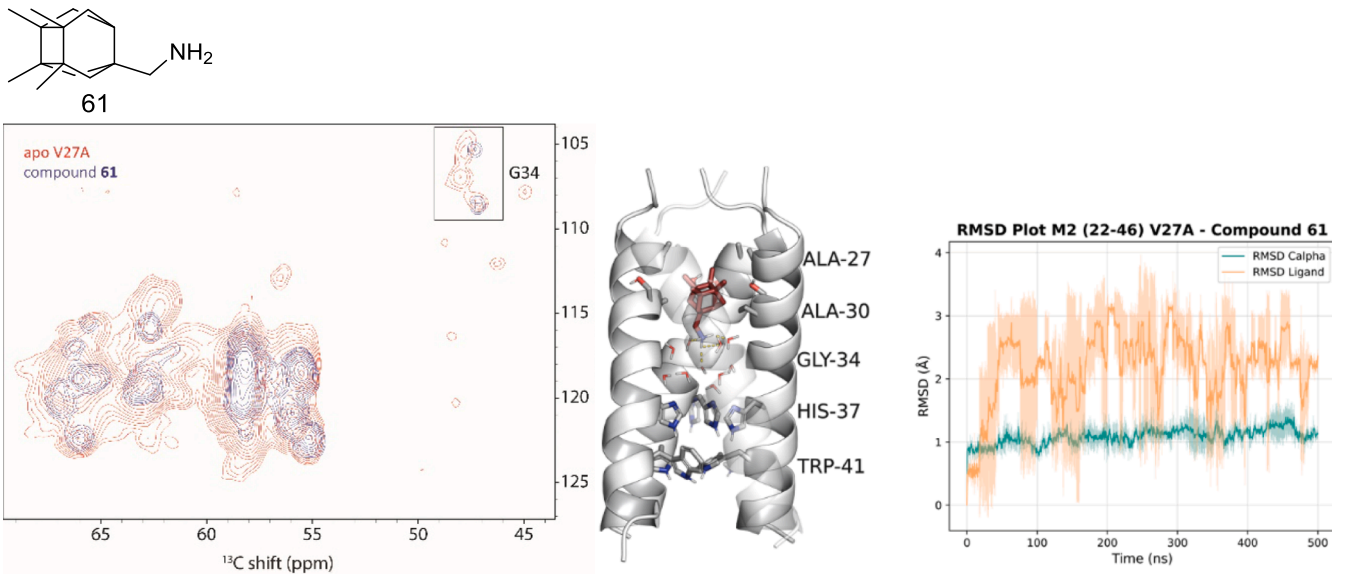

Fig. 17. Slices from 3D (H)CαNH spectra (^{15}N-^{13}Cα projection) of AM2TM V27A and mutant proteins in complex with compound 61 (protein was embedded in DPhPC bilayers with a lipid to protein tetramer molar ratio of 24:1 at pH 7.8) and results from 500 ns-MD simulations for AM2TM-61 complexes embedded in POPC bilayers utilizing the CHARMM36m force field. (Huang et al., 2016) Panel on the left side: the NMR signals of the apo-protein are shown in red and the signals of the complexes of AM2TM with compound 61 are shown in blue. Panel on the center: Average structure of AM2TM V27A from MD simulations; grey cartoon is used to display the AM2TM tetramer, stick representations were used for ligands, waters, and amino acid side chains indicated and cartoon representations was used for the protein backbone (carbons are depicted with grey color for amino acids and ruby color for the ligand, red for oxygen, blue for nitrogen) while the yellow dotted line represents hydrogen bonding between the drug and water molecules. Panel on the right side: RMSD plots of the protein Ca atoms (green line) and of the ligand heavy atoms (orange line) (reproduced from Kolocouris, Schmidke, Andreas and collaborators work in ref. (Stampolaki et al., 2023) with permission by Wiley). (For interpretation of the references to color in this figure legend, the reader is referred to the web version of this article.)

assays and several adamantyl amine analogs blocked AM2 WT and AM2 L26F channels by EP.

The triple blocker 61, (Rey-Carrizo et al., 2014) while having length equal to rimantadine, binds and blocks the AM2 V27A channel due to its larger volume (larger girth) as well as AM2 L26F and AM2 WT as was shown by 500 ns-MD simulations with the CHARMM36m force field (Huang et al., 2016) of AM2CD V27A, AM2CD L26F and AM2CD WT embedded in 50 POPC lipids bilayer. This compound's ammonium group was oriented steadily towards the C-terminus in AM2CD WT, V27A, and L26F channels during the MD simulations and the ligand was stabilized within the AM2 pore by forming an average of three hydrogen bonds with the water that was present between the ligand's ammonium group and His37. Furthermore, by displacing loosely bound waters close to the top of the pore (N-terminal side) the large cage alkyl group stabilized the complex through interactions between the tetramethylcyclobutane ring and residue 27 side chains (Stouffer et al., 2008; Thomaston et al., 2018) and successfully blocked the passage of water molecules, preventing protons from entering the pore and generating conduction. The MAS ssNMR provided information on the contacts of 61 with AM2CD V27A (residues 18–60), AM2CD L26F, AM2CD WT. When the drug was added to the mutant channels, there was a noticeable increase in peak resolution as opposed to the relatively wide peaks in the apo-AM2 V27A and apo-AM2 L26F. This suggests that the protein's conformational flexibility was decreased during the formation of the drug-protein complex. In Fig. 17 are shown representatively results for the AM2CD V27A complex.

4.2. Adamantyl amine drugs against AM2 S31N

4.1.1. MD simulations

The effect of the AM2 S31N mutation to rimantadine binding was analysed in detail by Arkin and collaborators in 2014. (Alhadeff et al., 2014) They ran 100 ns-MD simulations with the GROMOS 53a6 force field (Oostenbrink et al., 2004) for AM2TM WT or S31N in complex to rimantadine in DMPC bilayers. The X-ray structure of the apo-AM2TM WT (PDB ID 3LBW (Acharya et al., 2010) or the solution NMR of the apo-AM2CD S31N (PDB ID 2LY0 (Wang et al., 2013) in complex with M2WJ332 (after deleting the ligand) were used as starting structures for these MD simulations. Then the relaxed structures of the complexes between AM2TM channels and rimantadine were used for subsequent PMF(US) calculations with 10 ns MD simulations (Pastor and MacKerell, 2011) in each window, using 30 and 40 windows separated in *z*-axis by 2 Å intervals. It was observed that while rimantadine has a stable orientation of its ammonium group towards the His37 tetrad in AM2TM, it rotates towards the N-end as previously described along the reaction coordinate (see Fig. 21). These results were reproduced and advanced further in the PMF(US) simulations by Busath, Kolocouris and collaborators in 2015. (Gleed et al., 2015; Gleed and Busath, 2015) They ran 20 MD simulations for the complex if amantadine with PDB ID 2KQT mutated with S31N and the CHARMM36 force field (Huang and Mackerell, 2013) for protein and lipids and CGenFF (Vanommeslaeghe et al., 2010) for the ligand in 94 DMPC lipid bilayer. They also performed 80 ns-MD simulations with the OPLS2005 force field (Thomaston et al., 2017; Wright et al., 2016) based on PDB ID 2KQT (Cady et al., 2010) in complex with amantadine as starting structure embedded in embedded in ~ 80 DMPC lipids bilayer. The MD simulations showed that in contrast to the AM2TM WT complex, the amide side chains of Asn31 cannot incorporate amantadine's bulky adamantyl group inside AM2TM S31N due to repulsive interactions, and amantadine loses the dispersion contacts between the adamantyl group and the isopropyl groups of the Val27 tetrad. As a result, amantadine or rimantadine assume an inverted binding mode by rotating by 180° and pointing their ammonium group to bind with Asn31 amide side chains and waters. Similar results were also observed in the 2D PMF(US) with replica-exchange MD (REMD) for sampling (Gleed et al., 2015) using as collective variable the displacement of the centre of mass of the adamantane cage of amantadine along the z axis (which was approximately parallel to the bilayer normal) from the centre of the plane of the bilayer and the angle formed between the x–y plane and the vector passing through the adamantane centre of mass and NH_3^+ of amantadine.

Klein and coworkers in 2015 also used an amine group probe to map the potential energy minima along the AM2TM S31N pore with PMF(US) calculations. (Gianti et al., 2015) They ran the PMF using metadynamics algorithm for enhanced sampling using as a collective variable the projection of the position of the nitrogen atom of methylammonium or amantadine along the POPC lipid membrane normal. The biasing potential used was composed by Gaussian hills. They found that the local free energy minima along the translocation pathway of positively charged chemical species correspond to the experimentally determined binding sites of inhibitors' cationic ammonium groups including the reversed orientation of amantadine/rimantadine in the S31N mutant, suggesting three sites for cation stabilization along the mutant pore (see Fig. 19 in **Subsection 4.2.1**).

4.1.2. ssNMR and MD simulations

Kolocouris, Cross and collaborators in 2017 (Tzitzoglaki et al., 2017) applied OS ssNMR in ^{15}N-V28, A30, I42-labelled AM2TM WT or AM2TM S31N embedded in DMPC bilayers without and with amantadine or other adamantyl amine blockers of AM2 WT channel. The labels can efficiently sample both channel domains (upper and lower) since residues 28 and 30 are in the AM2TM helix's N-terminal domain while residue 42 is in its C-terminal domain. The structures of the apo-AM2TM S31N and apo-AM2TM WT in DMPC bilayers were found to differ somewhat. The AM2TM S31N data revealed a helical tilt of around 38°, which was higher than the helical tilt seen in the AM2TM WT structure (~32°). This was in line with earlier measurements made by Hong and coworkers in 2010 (Cady et al., 2010) and Cross and coworkers in 2007. (Hu et al., 2007) While the binding of amantadine or 2-propyl-2-adamantylamine to AM2TM WT effected a 10° kink near Gly34 in each helix of the AM2TM WT, (Hu et al., 2007; Cady et al., 2010) no such structural change was observed when these adamantyl amines interact with AM2TM S31N (Table 2). Amantadine or 2-propyl-2-adamantylamine in the AM2TM S31N exhibited a uniform ~ 4° or 7° decrease in the helical tilt compared to the apo-AM2TM S31N effecting a change to the entire helix-helix interface.

When the adamantyl amines were added to the AM2TM S31N sample, the Val27 and Ala30 resonances remained the same, while the isotropic CSPs of ^{15}N in residues Asn31 and Gly34 increased by 1.2 and 2.1 ppm, respectively. The small CSP of the Asn31 and Gly34 residues show a weak drug binding with AM2TM S31N either through formation of direct hydrogen bonds with the backbone carbonyls or indirect hydrogen bonding via water molecules (water bridges). (Wright et al., 2016) The results suggested that Val27 and Ala30 are not involved in binding. Significant ^{15}N and/or ^{13}Cα CSPs at Val27, Ser31, Gly34 have been published when rimantadine binds to AM2TM WT (Andreas et al., 2010; Andreas et al., 2013; Wright et al., 2016) with Ser31 exhibiting a significant 7 ppm shift compared to the apo-AM2TM WT (Wright et al., 2016) (see **Section 2.1.10**).

In ref. (Tzitzoglaki et al., 2017) the increased CSPs and the narrower signal linewidths for the AM2TM WT bound to 2-propyl-2-adamantylamine compared to AM2TM S31N showed reduced dynamics of the S31N channel for residues 31 and 34. In conjuction with the ITC results, it is concluded weaker or less specific binding of the adamantyl amine to the AM2TM S31N occurs. In fact, even though CSPs were seen at residues Asn31 and Gly34 when the adamantyl amine bound to the AM2TM S31N, cross peak intensity did not increase, seen for the AM2FL WT bound to rimantadine. (Wright et al., 2016) Additionally, ssNMR chemical shift changes and MD simulations agreed with a mean orientation of the amino group of the drug molecules towards the N-end in these weaker complexes with this mutant. (Tzitzoglaki et al., 2017) 80 ns-MD simulations with the OPLS2005 force field (Thomaston et al., 2017; Wright et al., 2016) were performed based on PDB ID 2KQT (Cady et al., 2010) in complex with adamantyl amine as starting structure embedded in DMPC lipid bilayers. The results are shown for 2-propyl-2-adamantyl complexes with AM2TM WT (Fig. 18**A**) or S31N (Fig. 18**B**). As discussed in **Subsection 4.1.1**, in the S31N-induced reverse orientation, amantadine forms hydrogen bonds with Asn31 but the adamantyl group forms only weak/transient contacts with Gly34 while amantadine couldn't efficiently block AM2TM S31N in agreement with EP and cell assays. (Tzitzoglaki et al., 2017) This effect of AM2 S31N to amantadine binding was also analysed in detail using PMF(US) calculations by Busath and collaborators in ref. (Gleed and Busath, 2015) or Arkin and collaborators in ref. (Alhadeff et al., 2014) as discussed in **Subsection 4.1.1**.

In ref. (Drakopoulos et al., 2018) Kolocouris and collaborators showed via EP that AM2 S31N's resistance to rimantadine analogs was caused by greater k_{off} rates rather than a difference in k_{on} rates as determined by EP experiments. Putting the kinetic investigations in the frame of molecular interactions, the greater off-rates in AM2 S31N can be attributed to the loss of the adamantyl cage-Val27 pocket hydrophobic interactions, resulting in short residence times within the mutant M2 pore.

4.2. Amantadine-aryl conjugates against AM2 S31N

4.2.1. Solution NMR, MD simulations

DeGrado and collaborators in 2013 (Wang et al., 2013) published a solution NMR structure of AM2TM S31N (residues 19–49) in DPC micelles in complex with a drug molecule, M2J332 (Wang et al., 2013) (PDB ID 2LY0 [173]). M2J332 (Wang et al., 2013) is a representative second generation adamantane-based inhibitor that blocks AM2 S31N-mediated current by EP and replication of M2 S31N virus by antiviral assays (Fig. 19**A,B**). These drugs consist of amantadine moiety connected through a methylene linker with aryl groups. Examples are the conjugates between amantadine and 5-(thiophenyl)oxazolyl (M2J332), (Wang et al., 2013) 5-phenyloxazolyl (M2J352), (Wang et al., 2013) 5-cyclopropyloxazolyl, (Hu et al., 2018; Li et al., 2016) or 3-bromo-thiophenyl groups. (Wu et al., 2014) In ref. (Wang et al., 2013) solution NOE NMR experiments were performed along with 80 ns-MD simulations using the CHARMM36 force field (Huang and Mackerell, 2013) for protein and lipids and CGenFF (Vanommeslaeghe et al., 2010) for the ligand. For the MD simulations they used the X-ray structure of the apo-AM2TM WT (PDB ID 3LBW (Acharya et al., 2010) mutated with S31N and complexed with M2WJ332. For each mutant of M2 (WT and S31N), the drug was tested with the aromatic headgroup either facing toward His37 or away. From this research the structure of M2J332-AM2TM S31N was deposited in the PDB. In PDB ID 2LY0, (Wang et al., 2013) the amantadine moiety's amino group and the 5-(thiophenyl)oxazolyl group are oriented towards the N-end (outward). This is in contrast with amantadine and adamantyl amines analogs which point their amino groups towards the C-end (outward) of the AM2 WT channel (Fig. 19**C-F**). according to the ssNMR observations by Hong and collaborators

Table 2
(A) Mean helical tilt values relative to the bilayer normal from MD simulations of amantadine − AM2TM WT complex or 2-propyl-2-adamantylamine-AM2TM WT complex in DMPC bilayer with respect to bilayer normal.

Ligand	MD simulations N-terminus / C-terminus	ssNMR Experiment N-terminus / C-terminus	PDB IDs 2H95 (Hu et al., 2007) or 2KQT (Cady et al., 2010) N-terminus / C-terminus
amantadine	31° ± 4.6° / 18° ± 4.9°	32 ± 2° / 22° ± 2°	30° / 19°
2-Pr-2-AdNH$_2$	31° ± 5.1° / 19° ± 5.0°	32 ± 2° / 22° ± 2°	

(B) Mean helical tilt values relative to the bilayer normal from MD simulations of amantadine-AM2TM S31N complex or 2-propyl-2-adamantylamine-AM2TM S31N complex in DMPC bilayer with respect to bilayer normal.

Ligand	MD simulations [177]	Experiment (Tzitzoglaki et al., 2017)
amantadine	34 ° ± 4°	38° ± 1°
2-Pr-2-AdNH$_2$	31° ± 6°	33° ± 1°

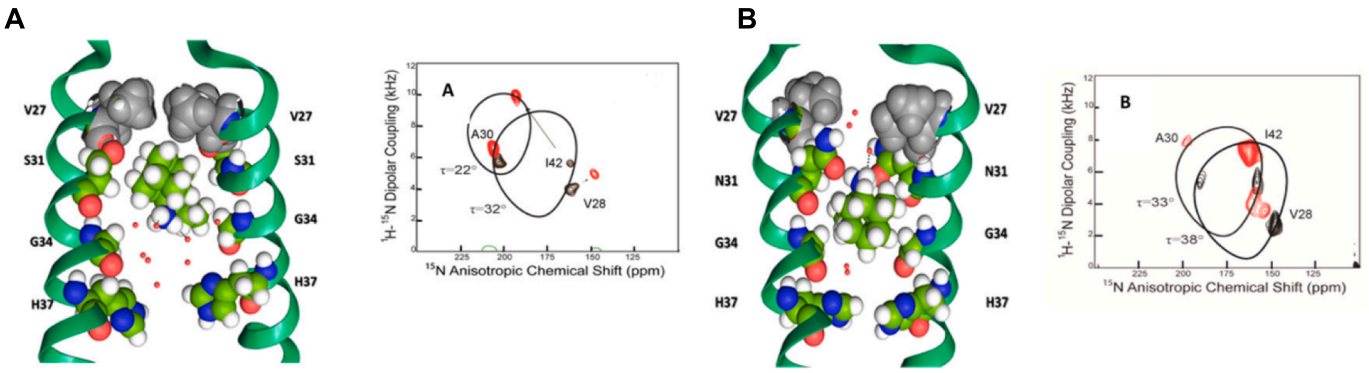

Fig. 18. (A), (B) Results from OS ssNMR (right side in each panel) and MD simulations frames (left side in each panel) from the complexes of 2-propyl-2-adamantyl amine embedded with (A) AM2TM WT, or (B) AM2TM S31N, embedded in DMPC bilayers; in the slices from OS ssNMR spectra in black color are depicted the signals of the apo-protein and in red the signals after addition of the adamantyl amine ligand (black arrows show the chemical shift changes after addition of the adamantyl amine); in the MD simulation frames, are shown for clarity only two helices of the AMTM tetramer; (protein backbone is shown with light green ribbon; Val27, Ser31 or Asn31, Gly34, His37 side chains and ligand's atoms are shown with van der Waals spheres; carbons are depicted with green color; Val27 gate carbons are depicted with grey color; nitrogen with blue color; oxygen with red color; hydrogen with white color). (Tzitzoglaki et al., 2017) (A) The results reveal a tight AM2TM WT-2-propyl-2-adamantyl amine complex with the amino group of the ligand having a C-terminus direction and adamantyl positioned in the V27 hydrophobic pocket, as is shown in the MD simulations frame; there is 10° kink in C-terminus half near Gly34. (B) In the weak AM2TM S31N-2-propyl-2-adamantyl amine complex the adamantyl amine has a propensity for the amino group of the ligand towards the N-terminus orientation due to the disruption of the V27 hydrophobic pocket; the backbone of the protein forms a uniform helical tilt of 32° to the normal bilayer (reproduced from Kolocouris, Cross and collaborators work in ref. (Tzitzoglaki et al., 2017) with permission by American Chemical Society). (For interpretation of the references to color in this figure legend, the reader is referred to the web version of this article.)

(Cady et al., 2011) and X-ray structures by DeGrado, Kolocouris and collaborators. (Thomaston et al., 2018).

DeGrado and collaborators in 2014 (Wu et al., 2014) published another solution NMR structures of AM2TM (residues 19–49) WT (PDB ID MUW (Wu et al., 2014) and S31N (PDB ID 2MUV (Wu et al., 2014) in complex with 2-bromo-5-(1-adamantyl)amimomethyl thiophene in DPC micelles. They suggested with solution NOE NMR experiments and MD simulations (preformed as previously in ref. (Wang et al., 2013) that 2-bromo-5-(1-adamantyl)amimomethyl thiophene blocks AM2 S31N channel-mediated proton current by EP with an orientation of the amantadine amino and 3-bromo-thiophenyl group oriented towards the N-end while it blocks AM2 WT channel by EP with an orientation of the amantadine amino group and 3-bromo-thiophenyl group towards the C-end, as suggested for adamantylamines by Kolocouris, Cross and collaborators (Tzitzoglaki et al., 2017) or by Busath and collaborators in ref. (Gleed and Busath, 2015) or by Arkin and collaborators in ref. (Alhadeff et al., 2014).

4.2.2. *ssNMR*

Hong, DeGrado and collaborators in 2013 (Williams et al., 2013) published a ssNMR study supporting the orientation of the phenyl group towards the N-end for the conjugate between amantadine and 5-phenyl-oxazolyl group, i.e., the 5-phenyl-3-(1-adamantyl)amimomethyl isoxazole (M2J352) (Williams et al., 2013) in agreement with findings by DeGrado and collaborators in 2013. (Wang et al., 2013).

4.2.3. *MD simulations*

Arkin and collaborators in 2014 (Alhadeff et al., 2014) identified the N-(((1-(1-adamantyl)ethyl)amino)carbonothioyl)-3-(2-thienyl)acrylamide (thiophene derivative) and N-(((1-(1-adamantyl)ethyl)amino) carbonothioyl)-nicotinamide (pyridine derivative) as inhibitors of the AM2 S31N channel using their *E. coli* cell-based assay to measure proton conductivity. (Astrahan et al., 2011) In ref. (Alhadeff et al., 2014) MD simulations and PMF(US) calculations were performed with the AM2TM S31N solution NMR structure (PDB ID 2LY0 (Wang et al., 2013) as starting structure, described for rimantadine complexes in **Subsection 4.1.1**. It was shown that the thiophene and pyridine derivatives favorably orient towards the N-end which agrees with the solution NMR-based results for M2WJ332 by DeGrado and collaborators in 2013. (Wang et al., 2013).

Hirokawa, Kawaguchi and collaborators in 2018 (Sakai et al., 2018) performed well-tempered metadynamics simulations with the OPLS3 force field to explore the binding kinetics of AM2TM channel blocker systems embedded in POPC bilayers. With 100 ns-metadynamics simulations (10 runs for each ligand) they examined the blocking of AM2TM WT by amantadine using as starting structure the ssNMR structure of AM2TM WT-amantadine complex solved in DMPC bilayers (PDB ID 2KQT (Cady et al., 2010). They also explored with 100 ns-metadynamics simulations the blocking interactions of AM2TM WT and AM2TM S31N with a dual blocker (amantadine-bromothiophene conjugate) of AM2 WT and AM2 S31N using the solution NMR structure of this inhibitor-AM2TM WT solved in micelles (PDB ID 2MUW (Wu et al., 2014) as their starting structure. The simulations for the entry pathway showed that amantadine is first trapped to a metastable conformation in which it binds Asp24 of AM2TM WT before placed in the minimum energy position observed in the experimental structures. In contrast, amantadine inside AM2 S31N flips, and its ammonium is oriented towards the N-end forming hydrogen bonding interactions with Asn31 amide side chains, as previously described by Kolocouris and collaborators (Tzitzoglaki et al., 2017) or Busath, Kolocouris and collaborators. (Gleed et al., 2015) In contrast to the simulations of amantadine inside the AM2TM WT channel pore, the simulations of the dual blocker (amantadine-bromothiophene conjugate) inside the AM2TM WT showed that the dual inhibitor, likely because of steric hindrance, did not form transient interactions with Asp24 (metastable states).

4.2.4. *EP, mutagenesis experiments and MD simulations*

Wang, Kolocouris and collaborators in 2019 (Musharrafieh et al., 2019) performed serial viral passages against AM2 S31N virus to explore resistance against an interesting AM2 S31N channel blocker, amantadine–5-cyclopropyloxazolyl conjugate. (Hu et al., 2018; Li et al., 2016) The unique drug-resistant mutation, L46P, was discovered that lies outside the drug-binding site, indicating a mechanism of allosteric resistance for the dual mutant S31N/L46P. Interestingly, the channel's sensitivity to amantadine inhibition was unaffected when the L46P mutant was added to AM2 WT. To explore the molecular basis of resistance of AM2 S31N L46P to the amantadine-isoxazole conjugate in ref. (Musharrafieh et al., 2019), MD simulations with CHARMM36 force

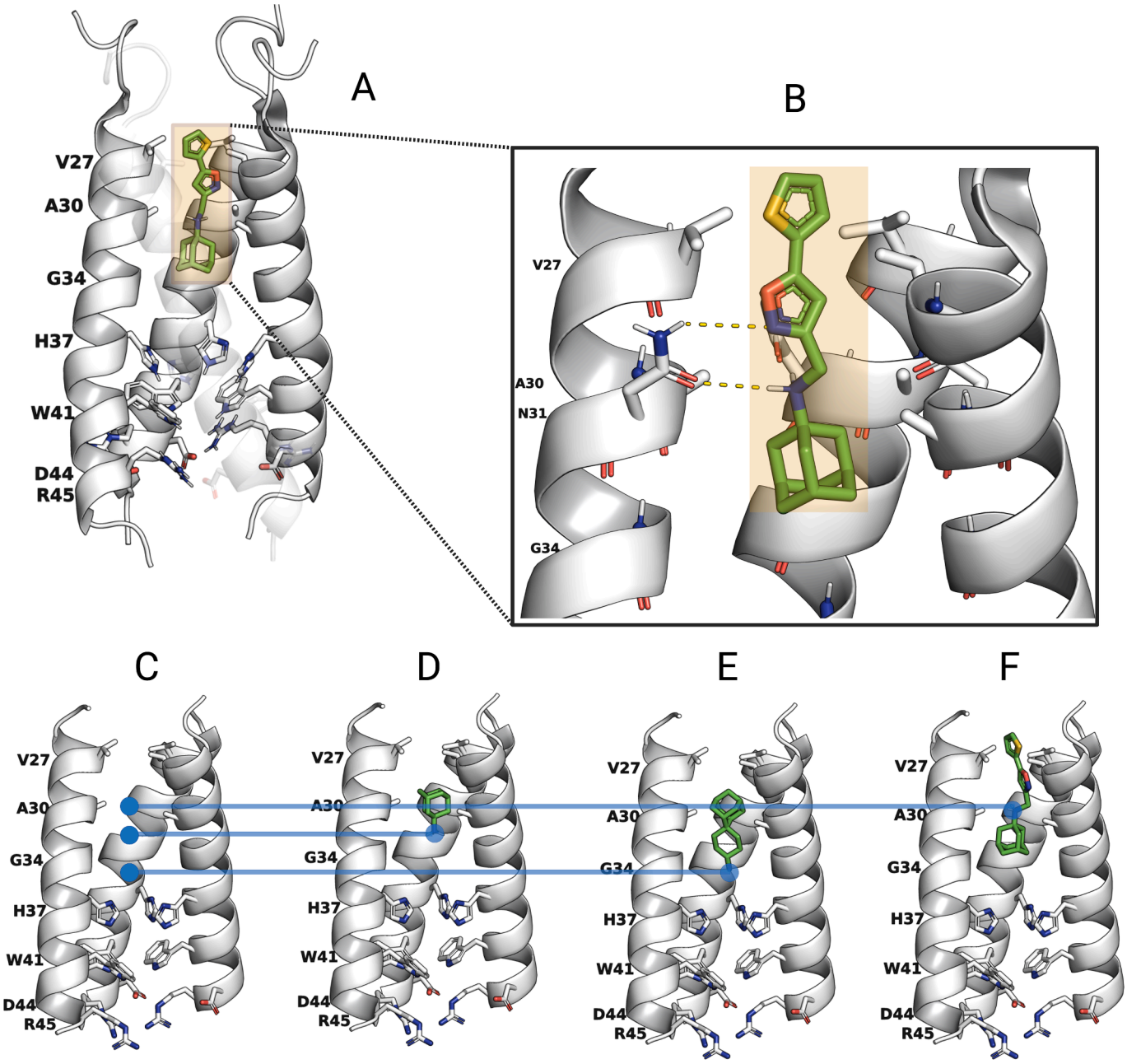

Fig. 19. Suggested inhibition mechanism of AM2 S31N by second generation adamantane-based inhibitors. (A) Binding site of M2WJ332 from solution NMR structure in DPC micelles (PDB ID 2LY0 (Wang et al., 2013): the side chains Val27, Ala30, Asn31, and His37 and the adamantane-based conjugate are represented with sticks; the protein's backbone (one monomer is not shown for clarity) is depicted with opaque ribbons. (B) Interactions of the drug with AM2 S31N pore: one of the Asn31 side chains forms bidentate hydrogen bonds with the drug, and the carbonyls of the amide side chains from another two Asn31 residues can establish water mediated hydrogen bonds with the ammonium group of the M2WJ332 drug. (C) Complex between AM2TM WT (residues 19–49) and an ammonium probe with energy minima close to Ala30 or between Ala30 and Gly34 or between Gly34 and His37 (blue sphere) (D) Complex between AM2TM WT (residues 19–49) and amantadine (PDB ID 6BMZ (Thomaston et al., 2018). (E) Complex between AM2TM WT (residues 19–49) and spiroadamantyl amine (PDB ID 6BMZ (Thomaston et al., 2018). (F) Complex between AM2TM S31N (residues 19–49) and M2WJ332. (C)–(F) Comparison between the calculated density (blue spheres) from MD simulations of nitrogen of the ammonium group sites in the four complexes with AM2TM; the backbone is described with a cartoon representation, and the side chains of residues 27, 30, 37, 41, 44, 45 which point inside the pore lumen are shown with grey sticks; carbons of the ligands are shown with green sticks; nitrogen is shown with blue color; oxygen with red color. (For interpretation of the references to color in this figure legend, the reader is referred to the web version of this article.)

field (Huang and Mackerell, 2013) were performed in the apo-proteins AM2CD S31N L46P, AM2CD S31N, AM2CD L46P, and the complexes between amantadine-isoxazole conjugate and AM2CD S31N L46P or AM2CD S31N and between amantadine and AM2CD L46P embedded in bilayers consisting of ~ 107 POPC lipids. The simulations were performed using the ssNMR starting structure of AM2CD WT (residues 22–62) (PDB ID 2L0J (Sharma et al., (1979) 2010) and the relative coordinates of amantadine from the ssNMR structure with PDB ID 2KQT. (Cady et al., 2010) The MD simulations for the apo-protein have a duration of 1 μs and the MD simulations for the complexes have a duration of 100 ns. It was discovered that the AM2 S31N inhibitor's drug-binding site, covering residues 26–34, was broadened by a

conformational change in the TM residues 22–31 on the N-terminus because of the L46P mutation. However, the resultant conformation of AM2CD S31N/L46P could be blocked by the AM2 WT inhibitor amantadine, between residues 31–34. The approximate Molecular Mechanics Generalized Born (MM-GBSA) binding free energy calculations with OPLS2005 force field showed stronger binding stability for the amantadine–5-cyclopropyloxazolyl conjugate in complex with AM2CD S31N compared with the same inhibitor in complex with AM2CD S31N/L46P, while amantadine showed similar binding free energies for either AM2CD WT or AM2CD L46P. The L46P mutation is the first drug-resistant AM2 mutant that has been experimentally verified to be not inside the pore drug binding site. Thus, these findings collectively showed a distinct mechanism of drug resistance of AM2 S31N via allosteric modulation between S31N and L46P that is lacking in AM2 channels without the S31N mutation.

Wang, Kolocouris and collaborators in 2020 (Musharrafieh et al., 2020) using a combination of EP measurements, antiviral assays in recombinant viruses, and MD simulations suggested the mechanism by which AM2 S31N can develop resistance to amantadine–5-cyclopropyloxazolyl conjugate by investigating the double mutants including the additional mutations V27A, V27F, I32N, G34E, R45H (Musharrafieh et al., 2020) inside the AM2 pore and L46P outside the pore. (Musharrafieh et al., 2019) These double mutants in complex with the inhibitor were embedded in 107 POPC lipids, using as starting structure the AM2CD WT (residues 22–62; PDB ID 2L0J) on which computational mutagenesis was performed. (Sharma et al., (1979) 2010) Multiple additive force fields were tested including the OPLS2005 force field, ff99sb, (Lindorff-Larsen et al., 2010) and CHARMM36 force field. (Huang and Mackerell, 2013) The simulations of the complexes demonstrated that these mutations increase the pore's diameter and hydration. MM-GBSA calculations with OPLS2005 force field were also performed to approximately rank the binding free energies. The results from the calculations showed that the complexes of resistant M2 (S31N/V27A, S31N/V27F, S31N/G34E, S31N/R45H) with the amantadine-5-cyclopropyloxazolyl conjugate have more positive binding free energies compared to its stable complex with AM2CD S31N.

Kolocouris, Busath and collaborators in 2020 (Tzitzoglaki et al., 2020) or Kolocouris and collaborators in 2022 (Tzitzoglaki et al., 2022) developed synthetic adamantyl amine-aryl conjugates for inhibition of influenza A M2 WT and mutants. Conjugates 1 to 6 (Tzitzoglaki et al., 2020) were used as sensitive probes to understand the structural features needed for an inhibitor to block the WT or S31N AM2 channels and viruses (Fig. 20**A**). The girth and length of the adamantane adduct (found in compounds 4 and 5) as well as the length between the adamantyl and the first ring of the aryl headgroup (found in compounds 2 and 3) significantly influenced the binding kinetics on AM2 S31N assessed using EP. The 80 ns- or 100 ns-MD simulations using OPLS2005 force field on Desmond MD engine or ff14sb (Lindorff-Larsen et al., 2010) on the Amber engine or CHARMM36 (Huang and Mackerell, 2013) on the NAMD engine revealed that all six compounds (1 to 6) may bind in the AM2 S31N channel with the adamantyl group between Val27 and Gly34 and the aryl group pointing out of the channel with the phenyl (or isoxazole in compound 6) embraced by the side chains of the Val27 cluster. (Thomaston et al., 2017; Wright et al., 2016; Samways et al., 2023; Feller and MacKerell, 2000). MM-PBSA calculations with ff14sb (Lindorff-Larsen et al., 2010) were also performed based on the ssNMR structure with PDB ID 2KQT. (Cady et al., 2010) Compared to the amantadine-based conjugates 1 and 6 that block by EP the M2 S31N channel, the addition of only one saturated carbon between adamantyl and amine groups in compound 2 hampers the blocking efficiency. Similarly, conjugate 3 in which a longer spacer was introduced between the aryl group and adamantyl group as well as conjugates 4 and 5 with a diamantyl or triamantyl group did not block AM2 S31N channel. In contrast to the inactive blockers 2 to 5, which had much lower k_{on} and higher k_{off} against AM2 S31N channel, the phenyl and isoxazolyl groups in the active blockers 1 and 6 against AM2 S31N demonstrated high k_{on}/low k_{off} and high k_{on}/high k_{off} rates, respectively (Fig. 20**B**). By binding in the stretch between Val27–His37, compounds 1 to 5 inwardly oriented block the AM2 WT channel, with high k_{on} and low k_{off} rates. Approximate predictions that agreed well were realized by steered-MD simulations for 10 ns with CHARMM36 force field (Huang and Mackerell, 2013)using the NAMD engine.

Kolocouris and collaborators in 2021 (Kolokouris et al., 2021) applied 200 ns-MD simulations on the AM2CD (residues 22–62) or AM2TM constructs, WT or S31N, in complex with adamantyl amines or the amantadine 5-cyclopropyloxazolyl conjugate embedded in 60 or 120

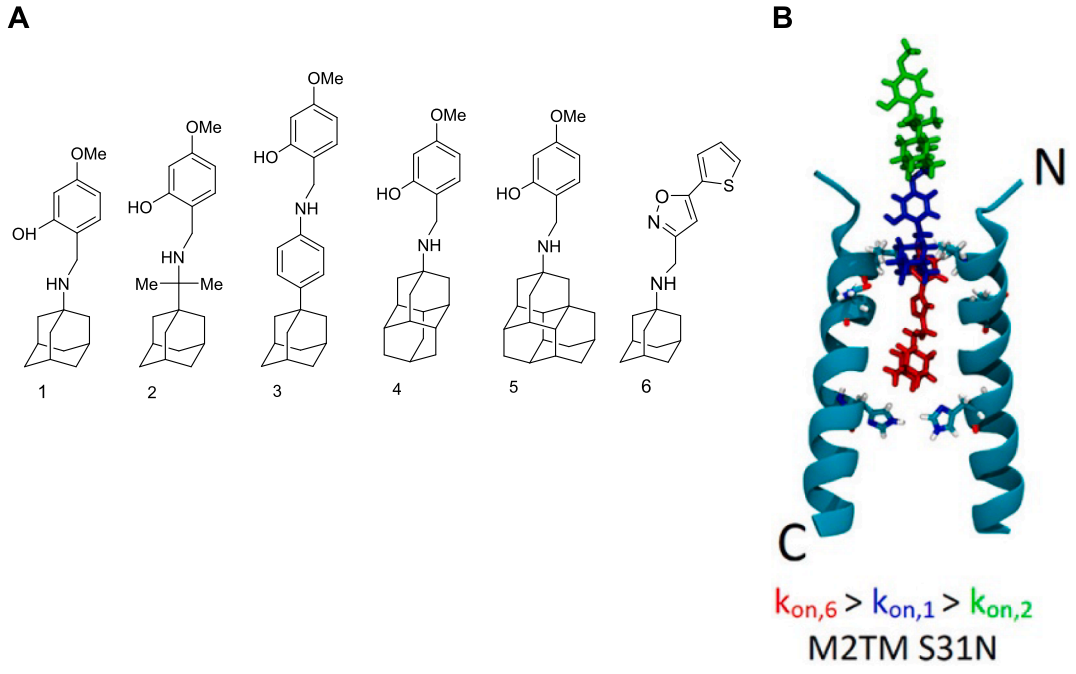

Fig. 20. (A) Compounds 1 to 6 were employed as probes to investigate binding to AM2 WT and AM2 S31N channels. (B) Exit pathway from AM2TM S31 as resulted by steered-MD simulations of AM2TM S31N complexes embedded in POPC bilayers using the CHARMM36 force field. (Huang and Mackerell, 2013).

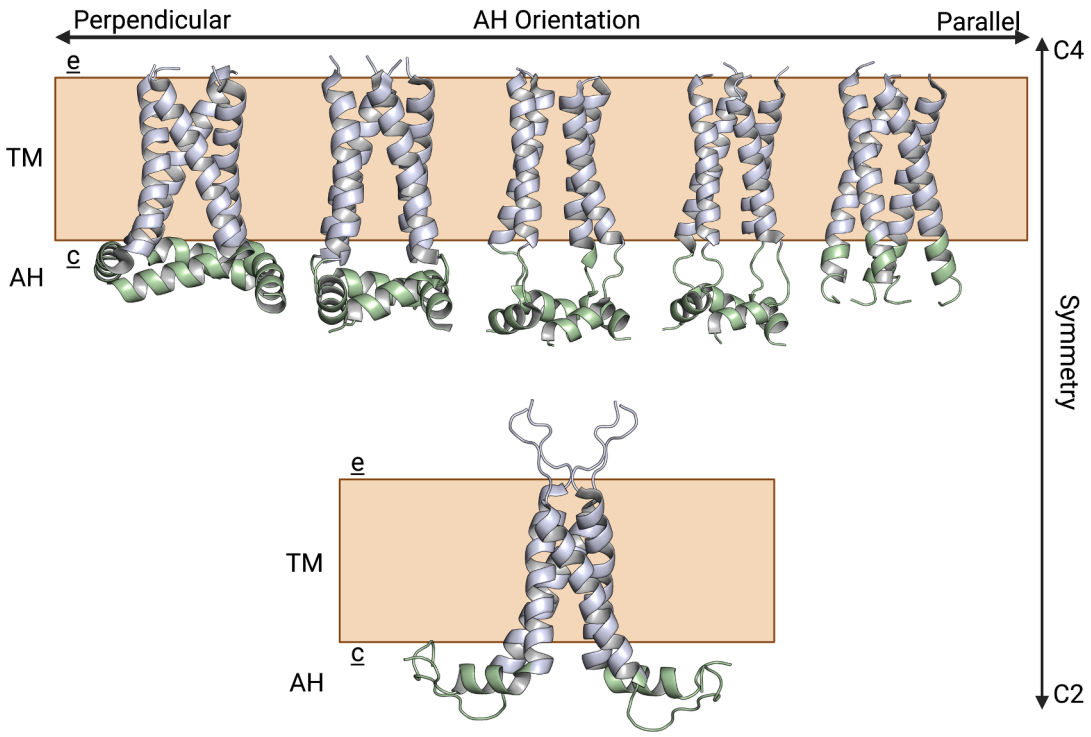

Fig. 21. Selected published AM2CD structures categorized by orientation of AHs (horizontal arrow) or by tetramer symmetry (vertical arrow). In the top row are shown structures with C4 symmetry and with AHs oriented nearly vertically to the TM α-helices in structures solved by ssNMR in phospholipid bilayers (PDB ID PDB ID 2L0J (Sharma et al., (1979) 2010); residues 22–62) and solution NMR in DHPC micelles (PDB ID 2KWX (Pielak and Chou, 2010); residues 18–60) or extended in the cytoplasmic region solved by solution NMR in DHPC micelles (PDB IDs 2RLF, (Schnell and Chou, 2008) 2KIH (Pielak et al., 2009); residues 18–60) or forming continuous helices with TM helices (PDB ID 6OUG (Thomaston et al., 2020); residues 21–61) solved by X-ray crystallography in MNG-3-C8 detergent environment. AHs are colored yellow, whereas the TM backbone is colored grey. In the bottom row is shown the structure PDB ID 2 N70 (Andreas and L., Reese, M., T. Eddy, M., Gelev, V., Zhe Ni, Q., A. Miller, E., Emsley, L., Pintacuda, G., J. Chou, J., G. Griffin, R. , 2015) solved by ssNMR in phospholipid bilayer with C2 tetramer symmetry (e: extracellular, c: cytoplasmic; TM region shown with white ribbons; AH region shown with green ribbons). (For interpretation of the references to color in this figure legend, the reader is referred to the web version of this article.)

or 200 POPC lipids bilayer. The simulations used the PDB ID 2L0J (Sharma et al., (1979) 2010) and 2KQT (Cady et al., 2010) for AM2CD (residues 22–62) and AM2TM, respectively, and were performed with both OPLS2005 and CHARMM36 (Huang and Mackerell, 2013) force fields. It was demonstrated that these force fields correctly calculate the AM2 pore structure and interactions within the pore, including the position of the adamantane channel blocker, the structure of the two layers of the waters in AM2TM and AM2CD channels, and the blocking or passage of water or chloride anions from the AM2 pore when a channel blocker is present. It was shown that for complexes of AM2TM or AM2CD S31N with 3-cyclopropyl-5-(3-hydroxyladamant-1-ylmethyl)-isoxazole, 100–130 POPC lipids surrounding the protein are needed to produce an adequately stiff M2 bundle where waters passage is blocked by the ligand.

4.3. Development of new assays for compound screening

Due to the importance of influenza A virus infections, new assays for the detection of AM2 channel blockers have been developed. Thus, Arkin and collaborators reported in 2011 (Astrahan et al., 2011) an *Escherichia coli* cell-based assay that was used to measure proton conductivity. The membrane permeability to protons may be examined using bacteria that express pHluorin, a pH-sensitive green fluorescent protein. There are two excitation maxima in the emission of pHluorin at 520 nm: 390 nm and 466 nm, whose ratio varies with pH. As a result, one may directly connect the fluorescence ratio to the proton concentration by utilizing a calibration curve. In contrast to bacteria that bear an empty vector or when an inhibitor is present, any bacteria that express a proton-conducting channel will show a significant shift in the fluorescence ratio, demonstrating channel AM2 channel activity. The assay is convenient to screen potential inhibitors of influenza A M2 WT and M2 mutants (Astrahan et al., 2011) as also reported by Willemoës, Lindorff-Larsen and collaborators in 2018 (Santner et al., 2018; Santner et al., 2018) or other viroporins as reported by Arkin and collaborators in 2020, 2021. (Singh Tomar and Arkin, 2020; Tomar et al., 2021) Griffin and collaborators reported in 2020 (Scott et al., 2020) another *in vitro* functional assay, an indirect liposome dye release assay for viroporin activity.

5. Discussion and conclusions — Future challenges

5.1. The application of molecular biophysics to investigate structure and function of AM2

This review article would like to highlight that although a commercial drug (amantadine, rimantadine) is used for treatment of a disease, its mechanism of action can remain untargeted for several decades until its determination. We described this research adventure for the fifty years after “Symmetrel’s” approval or prophylaxis. The structural biology work, MD simulation findings, functional characterization of influenza A M2 and mutants, and the complexes with inhibitors triggered intensive research to explain the mechanism of action of adamantane-based drugs and possibly the development of new ones.

5.1.1. Biophysical experiments in model AM2 constructs and membranes

Cross and collaborators in 2022 (Wright and A., Paulino, J., A. Cross, T. , 2022) using MAS ssNMR in DOPC/DOPE bilayers and tetramer: phospholipid ratio = 1:120 argued against the dimer-of-dimers

symmetry, as being a non-native structure formed mainly in the much denser protein samples of tetramer: phospholipid ratio = 1:24 used by Griffin and coworkers (Andreas et al., 2010; Andreas et al., 2012; Andreas and L., Reese, M., T. Eddy, M., Gelev, V., Zhe Ni, Q., A. Miller, E., Emsley, L., Pintacuda, G., J. Chou, J., G. Griffin, R. , 2015) or Andreas and coworkers. (Movellan et al., 2020; Tekwani Movellan et al., 2023) Nevertheless, in a MAS ssNMR study of AM2CD S31N (residues 18–60) reconstituted in either DPhPC or DOPC/DOPE lipid bilayers with samples having an even higher tetramer:phospholipid ratio of 1:180, (Stampolaki et al., 2024)Andreas and collaborators in 2024 (Stampolaki et al., 2024) revealed the dimer-of-dimers symmetry for the whole TM domain. It will be interesting to investigate further the dimers of dimers structure in the complexes of AM2CD with inhibitors.

Still a detailed atomistic experimental structure (X-ray or cryo-EM) of AM2CD without or with an inhibitor is missing. The only such structure available is the X-ray structure of the mutant AM2CD V27A (residues 21–61) in complex to spiro-adamantylamine, reported by Thomaston, Kolocouris, DeGrado and collaborators in 2020 (PDB ID 6OUG (Thomaston et al., 2020). The C-terminus of the channel in PDB ID 6OUG (Thomaston et al., 2020) has a different conformation in the X-ray crystal structure (Fig. 21) than in the solution NMR produced by Chou and collaborators between 2008–2010 (Schnell and Chou, 2008; Pielak et al., 2009; Pielak and Chou, 2010) or ssNMR structures reported by Cross and collaborators in 2010 (Sharma et al., (1979) 2010) or Griffin and collaborators in 2015. (Andreas and L., Reese, M., T. Eddy, M., Gelev, V., Zhe Ni, Q., A. Miller, E., Emsley, L., Pintacuda, G., J. Chou, J., G. Griffin, R. , 2015) In PDB ID 6OUG (Thomaston et al., 2020) the C-terminus of the channel is not tilted relative to the AM2TM V27A construct (PDB ID 6NV1 (Thomaston et al., 2020). The cytosolic amphipathic helix of M2 is predicted by several NMR studies to have a secondary α-helical structure, with either a turn or a disordered area joining the cyto helix to the TM region.

In the ssNMR of apo-AM2CD WT in phospholipid bilayers (PDB ID 2L0J) this turn is ~ 90° (Fig. 21). In these NMR structures, the turn/disordered area starts at residues Phe48 (2L0J, (Sharma et al., (1979) 2010) 2 N70 (Andreas and L., Reese, M., T. Eddy, M., Gelev, V., Zhe Ni, Q., A. Miller, E., Emsley, L., Pintacuda, G., J. Chou, J., G. Griffin, R. , 2015) or Leu46 (2KWX, 2RLF, 2KIH). (Schnell and Chou, 2008; Pielak et al., 2009; Pielak and Chou, 2010) The juxta-membrane domain that connects the TM and cytosolic helices has a conformation that is sensitive to solubilizing conditions, according to solution NMR studies. (Claridge et al., 2013) Therefore, the lipid mimetic or crystal contacts at the channel's C-terminus in PDB ID 6OUG (Thomaston et al., 2020) may have an impact on the conformation of the monomer helices from residues 47 to 56. Interestingly, in the structure of the M2CD V27A (PDB ID 6OUG (Thomaston et al., 2020) the Asp44, Arg45 and Phe48 tetrad residues all face the aqueous pore and are well-positioned to interact with protons exiting the AM2 channel after passing through the protonable His37 gate. Residue Phe48 forms f cation-π interactions with Arg45 in this conformation.

In ref. (Rey-Carrizo et al., 2014) the triple blocker 61 of AM2 V27A, L26F and WT was studied against AM2CD V27A, AM2CD L26F and AM2CD WT with MS ssNMR and MD simulations. While the MAS ssNMR showed interactions with AM2CD L26F, AM2CD V27A could not identify binding for AM2CD WT, even though TEVC revealed blocking, and an inhibitory activity was also shown in cells. Possibly, the slow kinetics of drug binding to AM2CD WT (Tekwani Movellan et al., 2023) can explain the discrepancy (see **Subsection 3.2.2**). Additionally, although binding of amantadine to AM2TM WT has been detected by MAS ssNMR (Cady et al., 2010) and US/PMF simulations have demonstrated that amantadine enters through the Val27 gate, (Gleed et al., 2015) ssNMR has previously partially detected the binding of amantadine to AM2CD WT (residues 22–61) in DMPC bilayers while no binding was observed in a VM membrane (see **Subsection 3.2.2**). (Cady et al., 2011) Thus still the constructs and membrane models used requited interpretation.

5.1.2. MD simulations

It must be noted that the time scale of the MD simulations in some studies reported in this review were in the range of only tens to hundreds of ns. With the advent of graphics processing unit (GPU) technology, MD simulations of several hundreds of ns have been reported with AM2TM or AM2CD and reported in this review article. Binding and conformational changes of virus proteins and life-cycle phenomena, e.g., transportation of ions by ion channel or disassembly of viral capsids and viruses budding, may require all-atom (AA) MD simulations running for several microseconds (μs) and distinct methodologies or coarse-grained (CG) MD simulations, respectively. Indeed, other than unbiased AA MD, other sophisticated methodologies can provide examples triggering further applications of AM2 or related proteins and their interactions. For example, Voth and collaborators applied in 2022 (Watkins and L., F. DeGrado, W., A. Voth, G. , 2022) 800 ns-MD simulations with CHARMM36 force field (Huang and Mackerell, 2013) as well as MS-RMD and QM/MM MD simulations with an explicit, reactive excess proton to calculate the free energy difference required for proton transport between AM2 WT and the AM2 D44N mutant and study the dynamic behavior of D44N at a molecular-level. In contrast to the asymmetric inward proton conduction in the AM2 WT channel, Voth and collaborators showed in 2022 (Watkins and L., F. DeGrado, W., A. Voth, G. , 2022) that proton transport and activation from the viral interior is possible in AM2 D44N due to the increased hydration around the His37 tetrad that diminishes the effect of the His37 charge on the channel's water structure. Subsequently, Lazaridis in 2023 (Lazaridis, 2023) reported with MD simulations using the CHARMM36 force field (Huang and Mackerell, 2013) that Asp44 uses strong electrostatic interactions to trap the hydronium in an outward direction. Additionally, Asp44 and Trp41 prevent outward Grotthus hopping by orienting the hydronium to point inward. Consequently, the inward direction has a reduced effective barrier. (Lazaridis, 2023).

Interestingly, Bhargava and Chodhury in 2022 (Chowdhury and Bhargava, 2022) ran MD simulations to understand the conformational changes required for the activation of the influenza B M2 (BM2) ion channel, bearing the critical HxxxW motif for proton conduction, like AM2 WT (His37 and Trp41 in AM2, His19 and Trp23 in BM2). In ref. (Chowdhury and Bhargava, 2022) ~ 1 μs-MD simulations with CHARMM36 force field for the protein (Huang and Mackerell, 2013) and lipids (Klauda et al., 2010) were performed at various protonation states of BM2 embedded in a lipid bilayer consisting of POPC/POPG/cholesterol and ~ 120 lipids. It was described that protonation of the His residues increases the tilt angle and the intra-helix distance needed for activation of the channel. (Chowdhury and Bhargava, 2022) The processes behind the symmetric proton conductance of the influenza BM2 proton channel and the participation of a second histidine (His27) cluster are still unknown, even though the channel is crucial for viral replication. In a recent work, Voth and collaborators in 2024 (Yue et al., 2024) studied the pH-dependent conformational transition of BM2 WT and its critical H27A mutant channel embedded in ~ 160 POPC or POPE lipids bilayer using membrane-enabled continuous constant-pH MD simulations. The protein was modeled with the CHARMM22 force field (MacKerell et al., 1998) with CMAP (grid-based energy correction term) corrections, (MacKerell et al., 2004) while lipids were represented by the CHARMM36 force field. (Klauda et al., 2010) The transition occurs at lower pH levels than AM2, driven by electrostatic repulsions between His19 and the a priori protonated His27. According to the simulations, the channel is activated as the first histidine (His19) is protonated.

The inhibition of the NGC induced by the AM2-cholesterol complex is necessary for the budding of the virus and can be targeted by lipophilic drugs. Thus, Kolocouris and collaborators in 2021 (Kolokouris et al., 2021) used MD simulations to study cholesterol binding in atomic detail. Following the cholesterol docking in the AHs region of M2CD (residues 22–62), the docking poses were inserted in in 20 Å POPC/cholesterol lipid buffer and AA MD simulations were run. The experimentally determined cholesterol binding sites were identified from these MD

simulations. In longer AA MD simulations in scrambled membranes with cholesterol not previously docked, the experimentally reported cholesterol binding sites at the TM and AH interface were also captured. Using residence time kinetic modeling, long-residency (low k_{off}) cholesterol sites were identified within the lot of noisy, transient cholesterol binding events. Further, this methodology was able to recover another set of novel cholesterol sites situated in the clefts between adjacent TM helices that have yet to be reported. These sites were calculated to have an order of magnitude lower k_{off} compared to those on the AH interface, suggesting that higher-sensitivity NMR experiments may be required for their experimental observation. New ssNMR studies with appropriately labelled-AM2CD are required to confirm these predicted cholesterol sites.

Kolocouris and collaborators applied in 2024 (Kolokouris and Kalenderoglou, 2024) CG MD simulations using the Martini 2 coarse-grained force field (Marrink et al., 2007; Monticelli et al., 2008; Herzog et al., 2016) in systems that include multicopy AM2CD embedded in bilayers to increase both the sampling and translational findings of the simulations. Kolocouris and collaborators tracked (Kolokouris and Kalenderoglou, 2024) the clustering and spatial localization of AM2 in regions of increased NGC, required physiologically for viral budding. This was previously studied by Voth and collaborators in 2018 (Madsen et al., 2018) with CG MD simulations using a custom ultra-CG parameterization procedure. Long time-scale dynamics of AM2 can be explored with other CG methodologies, such as GoMartini (Poma et al., 2017) and Go-like force fields, (Poma et al., 2021) SIRAH (Machado et al., 2019) and SPICA (Yamada et al., 2023) force fields. (Herzog et al., 2016) Hong and collaborators showed in 2022 (Sutherland et al., 2022) with ssNMR that cholesterol drives both AM2 channel clustering and NGC generation in POPE bilayers. In ref. (Kolokouris and Kalenderoglou, 2024) Kolocouris and collaborators report that cholesterol stabilized the formation of M2 channel clusters, specifically by filling and bridging the conical gap between M2 channels at specific sites in the N-terminals of adjacent channels or via the C-terminal region of TM and AHs, the latter sites displaying longer interaction time and higher stability (Fig. 22).

PMF/US calculations suggested that when cholesterols occupied the identified interfacial binding sites between two M2 channels, the dimer was stabilized by 11 kJ/mol. It was demonstrated that the cholesterol bridged M2 channels can exert lateral force on the surrounding membrane to induce the necessary NGC profile which permits the spontaneous scission of the catenoid membrane neck and leads to viral buds and scission. These results can inspire novel routes for the inhibition of the NGC that is necessary for the budding of influenza A virus but also of other viruses. Indeed, the effect of cholesterol interaction with the trimeric HIV fusion protein gp41 in membranes was investigated by Hong and collaborators in 2020 (Kwon et al., 2020) using ssNMR and AA 500 ns-MD simulations.

5.2. Challenges for design of new antivirals

Possibly the failure of the second generation of the adamantane-based drugs to enter the market despite intense efforts mainly from DeGrado (Wang et al., 2013; Wu et al., 2014; Wang et al., 2013) and Wang (Wang et al., 2013; Wang et al., 2013; Hu et al., 2018; Wang et al., 2018; Hu et al., 2017; Wu et al., 2014; Musharrafieh et al., 2019; Li et al., 2016; Li et al., 2017; Musharrafieh et al., 2020; Cáceres et al., 2021) and collaborators may be due to their rapid metabolism and rapid emergence of mutant viruses. We discuss possible new strategies of inhibition of influenza A virus, that implicate AM2, other than proton blockage, and possibly new classes of compounds. It is interesteting that non-adamantane compounds were previously identified by DeGrado and collaborators in 2013 using high-throughput yeast growth restoration assay. (Balgi et al., 2013) Also, it is worth noting that pinanamine-aryl conjugates can inhibit hemagglutinin instead of AM2 channel as showed by Hu, Yand and collaborators in 2018, (Zhao et al., 2018) and further investigated computationally by Luque and collaborators in 2024. (Townsend et al., 2021).

Despite their disordered structure, the N-terminal ectodomain strengthens AM2′s α-helical content, while the C-terminal cytoplasmic tail (after the AH) modifies the TM helix conformation's equilibrium in favor of proton binding. The dynamics and conformation of the structurally ordered TM domains that are functionally significant appear to be modulable by the structurally disordered extramembrane domain. It is yet unknown if the cytoplasmic domain may change the drug binding affinity or whether the ectodomain can change the His37 proton conduction equilibrium, but mutations in this domain appear to influence drug binding allosterically. Thus a communication network between the ectodomain and the TM domain is expected.

The findings from recent studies on AM2 might direct trials to develop antivirals that target various targets. Results from nMS revealed that the physiologically active oligomer (tetramer) (Chen et al., 2008) is most affected by the lipid environment. This suggests that AM2 may normally exist as a mixture of several oligomeric states that can be changed to the channel's active oligomer (tetramer) at low pH. Effective influenza treatments may thus be made possible by a better knowledge of how M2CD and FL (WT and S31N) oligomerize in various lipid environments leading to the discovery of drugs that alter the oligomeric

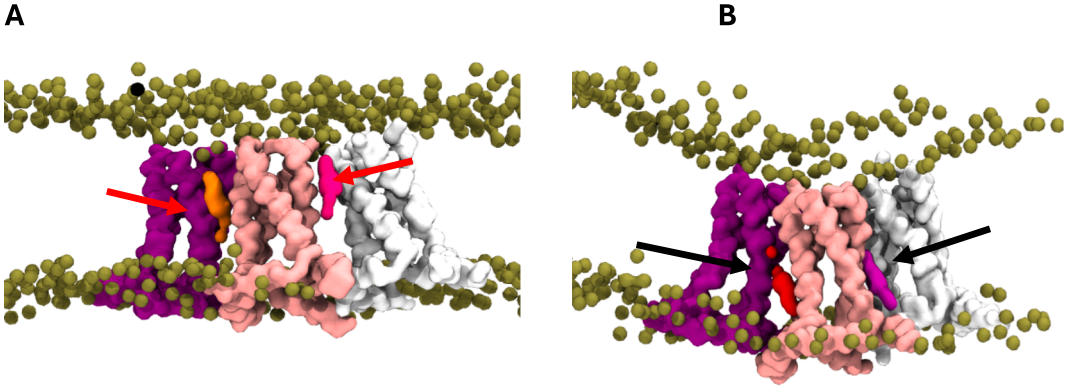

Fig. 22. Cholesterol mediating clustering of AM2CD (residues 22–62) proteins as was shown by recent 10 μs-CG MD simulations. (Kolokouris and Kalenderoglou, 2024) (A) Densities occupied by cholesterol close to M2AH are shown with black arrows. Interestingly the same positions were predicted with 1 μs-AA MD simulations in scrambled membranes. (Kolokouris et al., 2021) The cholesterol densities at the bottom bilayer leaflets matched the experimental models of cholesterol binding found experimentally using ssNMR by Cross and collaborators in 2016 (Ekanayake et al., 2016) or Hong and collaborators in 2017, 2018. (Elkins et al., 2017; Elkins et al., 2018) (B) Densities occupied by new cholesterol sites close to M2AH are shown with red arrows. (For interpretation of the references to color in this figure legend, the reader is referred to the web version of this article.)

state of drug-resistant mutant strains.

Lamb and collaborators by measuring the budding of virus-like particles in 2008 (Rossman and Lamb, 2011) showed that for influenza A that lacks ESCRT machinery, AM2 mediates virus budding. According to biochemical and functional investigations conducted by Lamb and colleagues in 2010, 2011, (Rossman et al., 2010; Rossman et al., 2010; Martyna and Rossman, 2014) or subsequently by Rossman and colleagues in 2010, 2011, 2014, (Rossman et al., 2010; Rossman et al., 2010; Martyna et al., 2017; Nguyen et al., 2008) AM2 cannot stimulate viral budding and vesicle fission in the absence of AHs. (Kim et al., 2019)The synergistic conformational coupling of AH and TM domains in defining AM2CD WT conformation required for membrane deformation in the presence of cholesterol was suggested. (Nguyen et al., 2008)Thus, inhibiting the coupling between AH and TM may offer a way to design novel anti-influenza A drugs. Furthermore, Howald, DeGrado, and coworkers demonstrated (Kim et al., 2019) using EPR and EP tests in AM2 WT that the mutation of Lys49 to Cys in the AH abolishes channel function in AM2CD WT. Examining this effect may provide novel drugs targeting a different binding site to the classical orthosteric pore blockers.

The positive effect of cholesterol in virus budding has been described. (Rossman et al., 2010) Cross and collaborators in 2016 (Ekanayake et al., 2016) with ssNMR revealed that cholesterol has a binding site on M2FL and that Phe54 mostly likely interacts with cholesterol. Additionally, cholesterol may form hydrogen bonding interactions with the carbonyl oxygen of Ser50 that replaces the native Cys that gets palmitoylated. Hong and collaborators explored in 2017 (Elkins et al., 2017; Elkins et al., 2018) binding of cholesterol to AM2CD (residues 22–61) and suggested that AM2CD structure (PDB ID 2L0J (Sharma et al., (1979) 2010) has an interhelical void that forms an optimum van der Waals cavity in a region with large separation between TM and AH helices. In this interhelical crevice cholesterol binds AM2CD next to the natural Cys50 palmitoylation site (Ser50 in studied AM2CD) as described previously. Interactions with the palmitoyl group Cys50 in the native protein may help to further stabilize cholesterol binding. Hong and collaborators in 2018 (Elkins et al., 2017; Elkins et al., 2018) used AM2(22–97) and showed that the cholesterol *iso*-octyl tail interacts with membrane facing Ile39 in the TM domain, while the cholesterol polar head lies close to Phe47 at the beginning of AH. Inhibiting the cholesterol-induced stabilization of AM2CD through cholesterol-competing lipophilic ligands provides an exciting opportunity for drug design in the field.

The importance of the putative AM1-AM2 connection (Petrich et al., 2021) for several AM2 functions in the influenza A infection cycle (e.g., virus assembly and budding) suggests that its disruption may also present a target for antivirals. Chiantia suggested in 2021 (Chen et al., 2008) that M1(1–67) interacts with M2 in a 1:2 stoichiometry, while Lamb and collaborators proposed in 2008 (Tietjen et al., 2024) that SMREEY (residues 71–77) of AM2 C-terminus (AM2CT) participate in binding with AM1. AM2CT has high flexibility and along with the significant negative charge which can cause electrostatic repulsion increases its potential as a hub for protein–protein interactions. Analogs of the SMREEY peptide could block interaction with AM1.

Kolocouris, Teigen, and collaborators reported in 2024 (Torres et al., 2013) the testing of 36 amantadine analogs against the replication of a panel of influenza A viruses containing either M2 S31N or M2 WT. It was found that several analogs, primarily those with sizeable lipophilic adducts, inhibited up to three M2 S31N-containing viruses (including Calif/09 S31N) with activities at least 5-fold higher than rimantadine, without blocking M2FL S31N proton currents or modulating endosomal pH. Mechanistic insights were exploited. It was shown that a subset of analogs inhibits the cellular entry of infectious influenza A virus. Conversely, an overlapping subset of the most lipophilic analogs disrupt viral AM2-AM1 protein colocalization required for intracellular viral assembly and budding. This contrasts with amantadine which binds to the pore of the AM2TM channel and does not interact with AM1. (Torres et al., 2013) These results indicate that amantadine analogs act on multiple, complementary mechanisms to inhibit replication of AM2 S31N viruses. (Torres et al., 2013) Cage amine analogs that can block cellular entry of infectious influenza A virus have also been developed by Vazquez and coworkers. (Mould et al., 2003) Thus, amine drugs may be also repurposed to mechanistically target other aspects if the influenza life cycle, e.g. the AM2-AM1 dimerization where nMS can be particularly useful in screening.

Other viroporins such as the influenza BM2, (Wilson et al., 2004) SARS CoV2 E, (Torres et al., 2007; Cabrera-Garcia et al., 2021; Toft-Bertelsen et al., 2021; Verdiá-Báguena et al., 2012; Ouyang et al., 2013) hepatitis p7, (Griffin et al., 2003; Townsend et al., 2024) or HIV vpu. [245,246] are being under active research. Viroporin researchers are sure to be inspired by the methodologies, insights and approaches used for AM2.

CRediT authorship contribution statement

Kyriakos Georgiou: Writing – review & editing, Software, Data curation. **Dimitrios Kolokouris:** Visualization, Writing – review & editing. **Antonios Kolocouris:** Writing – review & editing, Writing – original draft, Visualization, Validation, Supervision, Resources, Project administration, Methodology, Investigation, Funding acquisition, Formal analysis, Conceptualization.

Declaration of competing interest

The authors declare the following financial interests/personal relationships which may be considered as potential competing interests: Antonios Kolocouris reports financial support was provided by Chiesi Hellas SA. If there are other authors, they declare that they have no known competing financial interests or personal relationships that could have appeared to influence the work reported in this paper.

Acknowledgements

We thank Chiesi Hellas for supporting this research (SARG/NKUA; grant No 10354).

Appendix A. Supplementary material

Supplementary data to this article can be found online at https://doi.org/10.1016/j.yjsbx.2025.100122.

Data availability

No data was used for the research described in the article.

References

Abed, Y., Goyette, N., Boivin, G., 2005. Generation and characterization of recombinant influenza A (H1N1) viruses harboring amantadine resistance mutations. Antimicrob. Agents Chemother. 49 (2), 556–559. https://doi.org/10.1128/AAC.49.2.556-559.2005.

Acharya, R., Carnevale, V., Fiorin, G., Levine, B.G., Polishchuk, A.L., Balannik, V., Samish, I., Lamb, R.A., Pinto, L.H., DeGrado, W.F., Klein, M.L., 2010. Structure and mechanism of proton transport through the transmembrane tetrameric M2 protein bundle of the influenza A virus. PNAS 107 (34), 15075–15080. https://doi.org/10.1073/pnas.1007071107.

Aldrich, P.E., Hermann, E.C., Meier, W.E., Paulshock, M., Prichard, W.W., Snyder, J.A., Watts, J.C., 1971. Antiviral agents. 2. structure-activity relationships of compounds related to 1-adamantanamine. J. Med. Chem. 14 (6), 535–543. https://doi.org/10.1021/jm00288a019.

Aledavood, E., Selmi, B., Estarellas, C., Masetti, M., 2022. From acid activation mechanisms of proton conduction to design of inhibitors of the M2 proton channel of In Fl Uenza A. Virus 8 (796229), 1–21. https://doi.org/10.3389/fmolb.2021.796229.

Alhadeff, R., Assa, D., Astrahan, P., Krugliak, M., Arkin, I.T., 2014. Computational and experimental analysis of drug binding to the influenza M2 channel. Biochim. Biophys. Acta 1838 (4), 1068–1073. https://doi.org/10.1016/j.bbamem.2013.07.033.

Andreas, L.B., Eddy, M.T., Pielak, R.M., Chou, J., Griffin, R.G., 2010. Magic angle spinning NMR investigation of influenza A M218–60 : support for an allosteric mechanism of inhibition. J. Am. Chem. Soc. 132 (32), 10958–10960. https://doi.org/10.1021/ja101537p.

Andreas, L.B., Eddy, M.T., Chou, J.J., Griffin, R.G., 2012. Magic-angle-spinning NMR of the drug resistant S31N M2 proton transporter from influenza A. J. Am. Chem. Soc. 134 (17), 7215–7218. https://doi.org/10.1021/ja3003606.

Andreas, L.B., Barnes, A.B., Corzilius, B., Chou, J.J., Miller, E.A., Caporini, M., Rosay, M., Griffin, R.G., 2013. Dynamic nuclear polarization study of inhibitor binding to the M2 18–60 proton transporter from influenza A. Biochemistry 52 (16), 2774–2782. https://doi.org/10.1021/bi400150x.

B. Andreas, L.; Reese, M.; T. Eddy, M.; Gelev, V.; Zhe Ni, Q.; A. Miller, E.; Emsley, L.; Pintacuda, G.; J. Chou, J.; G. Griffin, R. Structure and Mechanism of the Influenza A M218–60 Dimer of Dimers. *J Am Chem Soc* **2015**, *137* (47), 14877–14886. https://doi.org/10.1021/jacs.5b04802.

Astrahan, P., Arkin, I.T., 2011. Resistance characteristics of influenza to amino-adamantyls. Biochim. Biophys. Acta Biomembr. 1808 (2), 547–553. https://doi.org/10.1016/j.bbamem.2010.06.018.

Astrahan, P., Flitman-Tene, R., Bennett, E.R., Krugliak, M., Gilon, C., Arkin, I.T., 2011. Quantitative analysis of influenza M2 channel blockers. Biochim. Biophys. Acta Biomembr. 1808 (1), 394–398. https://doi.org/10.1016/j.bbamem.2010.08.021.

Balannik, V., Wang, J., Ohigashi, Y., Jing, X., Magavern, E., Lamb, R.A., DeGrado, W.F., Pinto, L.H., 2009. Design and pharmacological characterization of inhibitors of amantadine-resistant mutants of the M2 ion channel of influenza A virus. Biochemistry 48 (50), 11872–11882. https://doi.org/10.1021/bi9014488.

Balannik, V., Carnevale, V., Fiorin, G., Levine, B.G., Lamb, R.A., Klein, M.L., DeGrado, W. F., Pinto, L.H., 2010. Functional studies and modeling of pore-lining residue mutants of the influenza A virus M2 ion channel. Biochemistry 49 (4), 696–708. https://doi.org/10.1021/bi901799k.

Balgi, A.D., Wang, J., Cheng, D.Y.H., Ma, C., Pfeifer, T.A., Shimizu, Y., Anderson, H.J., Pinto, L.H., Lamb, R.A., DeGrado, W.F., Roberge, M., 2013. Inhibitors of the influenza A virus M2 proton channel discovered using a high-throughput yeast growth restoration assay. PLoS One 8 (2), e55271. https://doi.org/10.1371/journal.pone.0055271.

Barniol-Xicota, M., Gazzarrini, S., Torres, E., Hu, Y., Wang, J., Naesens, L., Moroni, A., Vázquez, S., 2017. Slow but steady wins the race: dissimilarities among new dual inhibitors of the wild-type and the V27A mutant M2 channels of influenza A virus. J. Med. Chem. 60 (9), 3727–3738. https://doi.org/10.1021/acs.jmedchem.6b01758.

Berendsen, H.J.C., van der Spoel, D., van Drunen, R., 1995. GROMACS: A message-passing parallel molecular dynamics implementation. Comput. Phys. Commun. 91 (1–3), 43–56. https://doi.org/10.1016/0010-4655(95)00042-E.

Berger, O., Edholm, O., Jähnig, F., 1997. Molecular dynamics simulations of a fluid bilayer of dipalmitoylphosphatidylcholine at full hydration, constant pressure, and constant temperature. Biophys. J. 72 (5), 2002–2013. https://doi.org/10.1016/S0006-3495(97)78845-3.

Bright, R.A., Medina, M.J., Xu, X., Perez-Oronoz, G., Wallis, T.R., Davis, X.M., Povinelli, L., Cox, N.J., Klimov, A.I., 2005. Incidence of adamantane resistance among influenza A (H3N2) viruses isolated worldwide from 1994 to 2005: a cause for concern. Lancet 366 (9492), 1175–1181. https://doi.org/10.1016/S0140-6736(05)67338-2.

Brown, A.N., McSharry, J.J., Weng, Q., Driebe, E.M., Engelthaler, D.M., Sheff, K., Keim, P.S., Nguyen, J., Drusano, G.L., 2010. In vitro system for modeling influenza A virus resistance under drug pressure. Antimicrob. Agents Chemother. https://doi.org/10.1128/AAC.01385-09.

Cabrera-Garcia, D., Bekdash, R., Abbott, G.W., Yazawa, M., Harrison, N.L., 2021. The envelope protein of SARS-CoV-2 increases intra-golgi PH and forms a cation channel that is regulated by PH. J. Physiol. 599 (11), 2851–2868. https://doi.org/10.1113/JP281037.

Cáceres, C.J., Hu, Y., Cárdenas-García, S., Wu, X., Tan, H., Carnaccini, S., Gay, L.C., Geiger, G., Ma, C., Zhang, Q.Y., Rajao, D., Perez, D.R., Wang, J., 2021. Rational design of a deuterium-containing M2-S31N channel blocker UAWJ280 with in vivo antiviral efficacy against both oseltamivir sensitive and -resistant influenza A viruses. Emerg. Microbes Infect. https://doi.org/10.1080/22221751.2021.1972769.

Cady, S.D., Hong, M., 2008. Amantadine-induced conformational and dynamical changes of the influenza M2 transmembrane proton channel. PNAS 105 (5), 1483–1488. https://doi.org/10.1073/pnas.0711500105.

Cady, S.D., Hong, M., 2009. Effects of amantadine on the dynamics of membrane-bound influenza A M2 transmembrane peptide studied by NMR relaxation. J. Biomol. NMR 45 (1–2), 185–196. https://doi.org/10.1007/s10858-009-9352-9.

Cady, S.D., Goodman, C., Tatko, C.D., DeGrado, W.F., Hong, M., 2007. Determining the orientation of uniaxially rotating membrane proteins using unoriented samples: A 2H, 13C, and 15N solid-state NMR investigation of the dynamics and orientation of a transmembrane helical bundle. J. Am. Chem. Soc. 129 (17), 5719–5729. https://doi.org/10.1021/ja070305e.

Cady, S.D., Mishanina, T.V., Hong, M., 2009. Structure of amantadine-bound M2 transmembrane peptide of influenza A in lipid bilayers from magic-angle-spinning solid-state NMR: the role of Ser31 in amantadine binding. J. Mol. Biol. 385 (4), 1127–1141. https://doi.org/10.1016/j.jmb.2008.11.022.

Cady, S.D., Schmidt-Rohr, K., Wang, J., Soto, C.S., DeGrado, W.F., Hong, M., 2010. Structure of the amantadine binding site of influenza M2 proton channels in lipid bilayers. Nature 463 (7281), 689–692. https://doi.org/10.1038/nature08722.

Cady, S., Wang, T., Hong, M., 2011. Membrane-dependent effects of a cytoplasmic helix on the structure and drug binding of the influenza virus M2 protein. J. Am. Chem. Soc. 133 (30), 11572–11579. https://doi.org/10.1021/ja202051n.

Cady, S.D., Wang, J., Wu, Y., Degrado, W.F., Hong, M., 2011. Specific binding of adamantane drugs and direction of their polar amines in the pore of the influenza M2 transmembrane domain in lipid bilayers and dodecylphosphocholine micelles determined by NMR spectroscopy. J. Am. Chem. Soc. 133 (12), 4274–4284. https://doi.org/10.1021/ja102581n.

Chee, F.C., Guy, A., Biggin, P.C., 2008. Distribution and dynamics of adamantanes in a lipid bilayer. Biophys. J. 95 (12), 5627–5636. https://doi.org/10.1529/biophysj.108.139477.

Chen, B.J., Leser, G.P., Jackson, D., Lamb, R.A., 2008. The influenza virus M2 protein cytoplasmic tail interacts with the M1 protein and influences virus assembly at the site of virus budding. J. Virol. 82 (20), 10059–10070. https://doi.org/10.1128/jvi.01184-08.

Chizhmakov, I.V., Geraghty, F.M., Ogden, D.C., Hayhurst, A., Antoniou, M., Hay, A.J., 1996. Selective proton permeability and PH regulation of the influenza virus M2 channel expressed in mouse erythroleukaemia cells. J. Physiol. 494 (Pt 2), 329–336. https://doi.org/10.1113/jphysiol.1996.sp021495.

Chizhmakov, I.V., Ogden, D.C., Geraghty, F.M., Hayhurst, A., Skinner, A., Betakova, T., Hay, A.J., 2003. Differences in conductance of M2 proton channels of two influenza viruses at low and high PH. J. Physiol. https://doi.org/10.1113/jphysiol.2002.028910.

Chowdhury, U.D., Bhargava, B.L., 2022. Understanding the conformational changes in the influenza B M2 ion channel at various protonation states. Biophys. Chem. 289, 106859. https://doi.org/10.1016/j.bpc.2022.106859.

Claridge, J.K., Aittoniemi, J., Cooper, D.M., Schnell, J.R., 2013. Isotropic bicelles stabilize the juxtamembrane region of the influenza M2 protein for solution NMR studies. Biochemistry 52 (47), 8420–8429. https://doi.org/10.1021/bi401035m.

Cristian, L., Lear, J.D., DeGrado, W.F., 2003. Use of thiol-disulfide equilibria to measure the energetics of assembly of transmembrane helices in phospholipid bilayers. Proc. Natl. Acad. Sci. 100 (25), 14772–14777. https://doi.org/10.1073/pnas.2536751100.

Cross, T.A., Dong, H., Sharma, M., Busath, D.D., Zhou, H.X., 2012. M2 protein from influenza A: from multiple structures to biophysical and functional insights. Curr. Opin. Virol. Elsevier B.V. 128–133. https://doi.org/10.1016/j.coviro.2012.01.005.

Czabotar, P.E., Martin, S.R., Hay, A.J., 2004. Studies of structural changes in the M2 proton channel of influenza a virus by tryptophan fluorescence. Virus Res. https://doi.org/10.1016/j.virusres.2003.10.004.

Dong, G., Peng, C., Luo, J., Wang, C., Han, L., Wu, B., Ji, G., He, H., 2015. Adamantane-resistant influenza a viruses in the world (1902-2013): frequency and distribution of M2 gene mutations. PLoS One 10 (3), 1–20. https://doi.org/10.1371/journal.pone.0119115.

Drakopoulos, A., Tzitzoglaki, C., Ma, C.C., Freudenberger, K., Hoffmann, A., Hu, Y., Gauglitz, G.G., Schmidtke, M., Wang, J., Kolocouris, A., 2017. Affinity of rimantadine enantiomers against influenza A/M2 protein revisited. ACS Med. Chem. Lett. 8 (2), 145–150. https://doi.org/10.1021/acsmedchemlett.6b00311.

Drakopoulos, A., Tzitzoglaki, C., McGuire, K., Hoffmann, A., Ma, C., Freudenberger, K., Konstantinidi, A., Kolocouris, D., Hutterer, J., Gauglitz, G., Wang, J., Schmidtke, M., Busath, D.D., Kolocouris, A., Kolokouris, D., Ma, C., Freudenberger, K., Hutterer, J., Gauglitz, G., Wang, J., Schmidtke, M., Busath, D.D., Kolocouris, A., 2018. Unraveling the binding, proton blockage, and inhibition of influenza M2 WT and S31N by rimantadine variants. ACS Med. Chem. Lett. 9 (3), 198–203. https://doi.org/10.1021/acsmedchemlett.7b00458.

Duff, K.C., Ashley, R.H., 1992. The transmembrane domain of influenza A M2 protein forms amantadine-sensitive proton channels in planar lipid bilayers. Virology 190 (1), 485–489. https://doi.org/10.1016/0042-6822(92)91239-Q.

Duff, K.C., Kelly, S.M., Price, N.C., Bradshaw, J.P., 1992. The secondary structure of influenza A M2 transmembrane domain A circular dichroism study. FEBS Lett. 311 (3), 256–258. https://doi.org/10.1016/0014-5793(92)81114-2.

Duff, K.C., Gilchrist, P.J., Saxena, A.M., Bradshaw, J.P., 1994. Neutron diffraction reveals the site of amantadine blockade in the influenza A M2 ion channel. Virology. https://doi.org/10.1006/viro.1994.1345.

Duong-Ly, K.C., Nanda, V., Degrado, W.F., Howard, K.P., 2005. The conformation of the pore region of the M2 proton channel depends on lipid bilayer environment. Protein Sci. 14 (4), 856–861. https://doi.org/10.1110/ps.041185805.

Ekanayake, E.V., Fu, R., Cross, T.A., 2016. Structural influences: cholesterol, drug, and proton binding to full-length influenza A M2 protein. Biophys. J. 110 (6), 1391–1399. https://doi.org/10.1016/j.bpj.2015.11.3529.

Elkins, M.R., Williams, J.K., Gelenter, M.D., Dai, P., Kwon, B., Sergeyev, I.V., Pentelute, B.L., Hong, M., 2017. Cholesterol-binding site of the influenza M2 protein in lipid bilayers from solid-state NMR. PNAS 114 (49), 12946–12951. https://doi.org/10.1073/pnas.1715127114.

Elkins, M.R., Sergeyev, I.V., Hong, M., 2018. Determining cholesterol binding to membrane proteins by cholesterol 13C labeling in yeast and dynamic nuclear polarization NMR. J. Am. Chem. Soc. 140 (45), 15437–15449. https://doi.org/10.1021/jacs.8b09658.

Feller, S.E., MacKerell, A.D., 2000. An improved empirical potential energy function for molecular simulations of phospholipids. J. Phys. Chem. B 104 (31), 7510–7515. https://doi.org/10.1021/jp0007843.

Furuse, Y., Suzuki, A., Oshitani, H., 2009. Large-scale sequence analysis of M gene of influenza A viruses from different species: mechanisms for emergence and spread of amantadine resistance. Antimicrob. Agents Chemother. 53 (10), 4457–4463. https://doi.org/10.1128/AAC.00650-09.

Furuse, Y., Suzuki, A., Kamigaki, T., Oshitani, H., 2009. Evolution of the M gene of the influenza A virus in different host species: large-scale sequence analysis. Virol. J. 6 (1), 67. https://doi.org/10.1186/1743-422X-6-67.

Garcia, V., Aris-Brosou, S., 2014. Comparative dynamics and distribution of influenza drug resistance acquisition to protein M2 and neuraminidase inhibitors. Mol. Biol. Evol. 31 (2), 355–363. https://doi.org/10.1093/molbev/mst204.

Georgieva, E.R., Borbat, P.P., Norman, H.D., Freed, J.H., 2015. Mechanism of influenza A M2 transmembrane domain assembly in lipid membranes. Sci. Rep. 5 (1), 11757. https://doi.org/10.1038/srep11757.

Georgieva, E.R., Borbat, P.P., Grushin, K., Stoilova-McPhie, S., Kulkarni, N.J., Liang, Z., Freed, J.H., 2016. Conformational response of influenza A M2 transmembrane domain to amantadine drug binding at low PH (PH 5.5). Front. Physiol. 7. https://doi.org/10.3389/fphys.2016.00317.

Georgiou, K., Kolocouris, A., 2025. Conformational heterogeneity and structural features for function of the prototype viroporin influenza AM2. Biochim. Biophys. Acta (BBA) - B Biomembr. 1867 (1), 184387. https://doi.org/10.1016/j.bbamem.2024.184387.

Georgiou, K., Konstantinidi, A., Hutterer, J., Freudenberger, K., Kolarov, F., Lambrinidis, G., Stylianakis, I., Stampelou, M., Gauglitz, G., Kolocouris, A., 2024. Accurate calculation of affinity changes to the close state of influenza A M2 transmembrane domain in response to subtle structural changes of adamantyl amines using free energy perturbation methods in different lipid bilayers. Biochim. Biophys. Acta (BBA) - B Biomembr. 1866 (2), 184258. https://doi.org/10.1016/j.bbamem.2023.184258.

Gianti, E., Carnevale, V., Degrado, W.F., Klein, M.L., Fiorin, G., 2015. Hydrogen-bonded water molecules in the M2 channel of the influenza a virus guide the binding preferences of ammonium-based inhibitors. J. Phys. Chem. B 119 (3), 1173–1183. https://doi.org/10.1021/jp506807y.

Gkeka, P., Eleftheratos, A.-S., Kolocouris, A., Cournia, Z., Eleftheratos, S., Kolocouris, A., Cournia, Z., 2013. Free energy calculations reveal the origin of binding preference for aminoadamantane blockers of influenza A/M2TM pore. J. Chem. Theory Comput. 9 (2), 1272–1281. https://doi.org/10.1021/ct300899n.

Gleed, M.L., Busath, D.D., 2015. Why bound amantadine fails to inhibit proton conductance according to simulations of the drug-resistant influenza A M2 (S31N). J. Phys. Chem. B 119, 1225–1231. https://doi.org/10.1021/jp508545d.

Gleed, M.L., Ioannidis, H., Kolocouris, A., Busath, D.D., 2015. Resistance-mutation (N31) effects on drug orientation and channel hydration in amantadine-bound influenza A M2. J. Phys. Chem. B 119 (35), 11548–11559. https://doi.org/10.1021/acs.jpcb.5b05808.

Griffin, S.D.C., Beales, L.P., Clarke, D.S., Worsfold, O., Evans, S.D., Jaeger, J., Harris, M. P.G., Rowlands, D.J., Klenk, H.D., 2003. The P7 protein of hepatitis C virus forms an ion channel that is blocked by the antiviral drug, amantadine. FEBS Lett. 175–184. https://doi.org/10.1016/S0014-5793(02)03851-6.

Gu, R.-X., Liu, L.A., Wei, D.-Q., Du, J.-G., Liu, L., Liu, H., 2011. Free energy calculations on the two drug binding sites in the M2 proton channel. J. Am. Chem. Soc. 133 (28), 10817–10825. https://doi.org/10.1021/ja1114198.

Hay, A.J., Wolstenholme, A.J., Skehel, J.J., Smith, M.H., 1985. The molecular basis of the specific anti-influenza action of amantadine. EMBO J. 4 (11), 3021–3024. https://doi.org/10.1002/j.1460-2075.1985.tb04038.x.

Herzog, F.A., Braun, L., Schoen, I., Vogel, V., 2016. Improved side chain dynamics in MARTINI simulations of protein–lipid interfaces. J. Chem. Theory Comput. 12, 2446–2458.

Holsinger, L.J., Alams, R., 1991. Influenza virus M2 integral membrane protein is a homotetramer stabilized by formation of disulfide bonds. Virology. https://doi.org/10.1016/0042-6822(91)90115-R.

Holsinger, L.J., Nichani, D., Pinto, L.H., Lamb, R.A., 1994. Influenza A virus M2 ion channel protein: a structure-function analysis. J. Virol. 68 (3), 1551–1563. https://doi.org/10.1128/jvi.68.3.1551-1563.1994.

Holsinger, L.J., Shaughnessy, M.A., Micko, A., Pinto, L.H., Lamb, R.A., 1995. Analysis of the posttranslational modifications of the influenza virus M2 protein. J. Virol. 69 (2), 1219–1225. https://doi.org/10.1128/jvi.69.2.1219-1225.1995.

Homeyer, N., Ioannidis, H., Kolarov, F., Gauglitz, G., Zikos, C., Kolocouris, A., Gohlke, H., 2016. Interpreting thermodynamic profiles of aminoadamantane compounds inhibiting the M2 proton channel of influenza A by free energy calculations. J. Chem. Inf. Model. 56, 110–126. https://doi.org/10.1021/acs.jcim.5b00467.

Hu, J., Fu, R., Nishimura, K., Zhang, L., Zhou, H.X., Busath, D.D., Vijayvergiya, V., Cross, T.A., 2006. Histidines, heart of the hydrogen ion channel from influenza A virus: toward an understanding of conductance and proton selectivity. PNAS 103 (18), 6865–6870. https://doi.org/10.1073/pnas.0601944103.

Hu, J., Asbury, T., Achuthan, S., Li, C., Bertram, R., Quine, J.R., Fu, R., Cross, T.A., 2007. Backbone structure of the amantadine-blocked trans-membrane domain M2 proton channel from influenza A virus. Biophys. J. 92 (12), 4335–4343. https://doi.org/10.1529/biophysj.106.090183.

Hu, J., Fu, R., Cross, T.A., 2007. The chemical and dynamical influence of the anti-viral drug amantadine on the M2 proton channel transmembrane domain. Biophys. J. 93 (1), 276–283. https://doi.org/10.1529/biophysj.106.102103.

Hu, Y., Hau, R.K., Wang, Y., Tuohy, P., Zhang, Y., Xu, S., Ma, C., Wang, J., 2018. Structure-property relationship studies of influenza A virus AM2-S31N proton channel blockers. ACS Med. Chem. Lett. 9 (11), 1111–1116. https://doi.org/10.1021/acsmedchemlett.8b00336.

Hu, F., Luo, W., Cady, S.D., Hong, M., 2011. Conformational plasticity of the influenza A M2 transmembrane helix in lipid bilayers under varying PH, drug binding, and membrane thickness. Biochim. Biophys. Acta Biomembr. 1808 (1), 415–423. https://doi.org/10.1016/j.bbamem.2010.09.014.

Hu, Y., Musharrafieh, R., Ma, C., Zhang, J., Smee, D.F., DeGrado, W.F., Wang, J., 2017. An M2-V27A channel blocker demonstrates potent in vitro and in vivo antiviral activities against amantadine-sensitive and -resistant influenza A viruses. Antiviral Res. https://doi.org/10.1016/j.antiviral.2017.01.006.

Huang, J., Mackerell, A.D., 2013. CHARMM36 all-atom additive protein force field: validation based on comparison to NMR data. J. Comput. Chem. 34 (25), 2135–2145. https://doi.org/10.1002/jcc.23354.

Huang, J., Rauscher, S., Nawrocki, G., Ran, T., Feig, M., De Groot, B.L., Grubmüller, H., MacKerell, A.D., 2016. CHARMM36m: an improved force field for folded and intrinsically disordered proteins. Nat. Methods. https://doi.org/10.1038/nmeth.4067.

Ioannidis, H., Drakopoulos, A., Tzitzoglaki, C., Homeyer, N., Kolarov, F., Gkeka, P., Freudenberger, K., Liolios, C., Gauglitz, G., Cournia, Z., Gohlke, H., Kolocouris, A., 2016. Alchemical free energy calculations and isothermal titration calorimetry measurements of aminoadamantanes bound to the closed state of influenza A/M2TM. J. Chem. Inf. Model. 56 (5). https://doi.org/10.1021/acs.jcim.6b00079.

Jalily, P.H., Duncan, M.C., Fedida, D., Wang, J., Tietjen, I., 2020. Put a cork in it: plugging the M2 viral ion channel to sink influenza. Antiviral Res. 178, 104780. https://doi.org/10.1016/j.antiviral.2020.104780.

Jin, H., Leser, G.P., Zhang, J., Lamb, R.A., 1997. Influenza virus hemagglutinin and neuraminidase cytoplasmic tails control particle shape. EMBO J. 16 (6), 1236–1247. https://doi.org/10.1093/emboj/16.6.1236.

Jing, X., Ma, C., Ohigashi, Y., Oliveira, F.A., Jardetzky, T.S., Pinto, L.H., Lamb, R.A., 2008. Functional studies indicate amantadine binds to the pore of the influenza A virus M2 proton-selective ion channel. PNAS 105 (31), 10967–10972. https://doi.org/10.1073/pnas.0804958105.

Kaminski, G.A., Friesner, R.A., Tirado-Rives, J., Jorgensen, W.L., 2001. Evaluation and reparametrization of the OPLS-AA force field for proteins via comparison with accurate quantum chemical calculations on peptides. J. Phys. Chem. B 105 (28), 6474–6487. https://doi.org/10.1021/jp003919d.

Kellokumpu, S., 2019. Golgi PH, ion and redox homeostasis: how much do they really matter? Front. Cell Dev. Biol. 7, 93. https://doi.org/10.3389/fcell.2019.00093.

Khurana, E., Devane, R.H., Dal Peraro, M., Klein, M.L., 2011. Computational study of drug binding to the membrane-bound tetrameric M2 peptide bundle from influenza A virus. Biochim. Biophys. Acta Biomembr. 1808 (2), 530–537. https://doi.org/10.1016/j.bbamem.2010.03.025.

Kim, G., Raymond, H.E., Herneisen, A.L., Wong-Rolle, A., Howard, K.P., 2019. The distal cytoplasmic tail of the influenza A M2 protein dynamically extends from the membrane. Biochim. Biophys. Acta Biomembr. 1861 (8), 1421–1427. https://doi.org/10.1016/j.bbamem.2019.05.021.

Klauda, J.B., Venable, R.M., Freites, J.A., O'Connor, J.W., Tobias, D.J., Mondragon-Ramirez, C., Vorobyov, I., MacKerell, A.D., Pastor, R.W., 2010. Update of the charmm all-atom additive force field for lipids: validation on six lipid types. J. Phys. Chem. B 114, 7830–7843.

Kolocouris, A., Hansen, R.K., Broadhurst, R.W., 2004. Interaction between an amantadine analogue and the transmembrane portion of the influenza A M2 protein in liposomes probed by 1H NMR spectroscopy of the ligand. J. Med. Chem. 47 (20). https://doi.org/10.1021/jm0496685.

Kolocouris, A., Zikos, C., Broadhurst, R.W., 2007. 19F NMR detection of the complex between amantadine and the receptor portion of the influenza A M2 ion channel in DPC micelles. Bioorg. Med. Chem. Lett. 17 (14). https://doi.org/10.1016/j.bmcl.2007.04.100.

Kolocouris, A., Tzitzoglaki, C., Johnson, F.B., Zell, R., Wright, A.K., Cross, T.A., Tietjen, I., Fedida, D., Busath, D.D., 2014. Aminoadamantanes with persistent in vitro efficacy against H1N1 (2009) influenza A. J. Med. Chem. 57 (11), 4629–4639. https://doi.org/10.1021/jm500598u.

Kolokouris, D.; Kalenderoglou E., I.; Duncan, A.; Sansom S. P., M.; Kolocouris, A. *The Role of Cholesterol in M2 Clustering and Viral Budding Explained*; 2024. https://doi.org/10.1021/acs.jctc.4c01026.

Kolokouris, D., Kalenderoglou, I.E., Kolocouris, A., 2021. Inside and out of the pore: comparing interactions and molecular dynamics of influenza A M2 viroporin complexes in standard lipid bilayers. J. Chem. Inf. Model. 61 (11), 5550–5568. https://doi.org/10.1021/acs.jcim.1c00264.

Kolokouris, D., Kalenderoglou, I.E., Duncan, A.L., Corey, R.A., Sansom, M.S.P., Kolocouris, A., 2024. The role of cholesterol in M2 clustering and viral budding explained. J. Chem. Theory Comput. https://doi.org/10.1021/acs.jctc.4c01026.

Konstantinidi, A., Naziris, N., Chountoulesi, M., Kiriakidi, S., Sartori, B., Kolokouris, D., Amentisch, H., Mali, G., Ntountaniotis, D., Demetzos, C., Mavromoustakos, T., Kolocouris, A., 2018. Comparative perturbation effects exerted by the influenza A M2 WT protein inhibitors amantadine and the spiro[Pyrrolidine-2,2′-Adamantane] variant AK13 to membrane bilayers studied using biophysical experiments and molecular dynamics simulations. J. Phys. Chem. B 122 (43), 9877–9895. https://doi.org/10.1021/acs.jpcb.8b07071.

Konstantinidi, A., Chountoulesi, M., Naziris, N., Sartori, B., Amenitsch, H., Mali, G., Čendak, T., Plakantonaki, M., Triantafyllakou, I., Tselios, T., Demetzos, C., Busath, D.D.D., Mavromoustakos, T., Kolocouris, A., 2020. The boundary lipid around DMPC-spanning influenza A M2 transmembrane domain channels: its structure and potential for drug accommodation. Biochim. Biophys. Acta (BBA) - B Biomembr. 1862 (3), 183156. https://doi.org/10.1016/j.bbamem.2019.183156.

Kumar, G., Sakharam, K.A., 2024. Tackling influenza A virus by M2 ion channel blockers: latest progress and limitations. Eur. J. Med. Chem. 267, 116172. https://doi.org/10.1016/j.ejmech.2024.116172.

Kwon, B., Hong, M., 2016. The influenza M2 ectodomain regulates the conformational equilibria of the transmembrane proton channel: insights from solid-state nuclear magnetic resonance. Biochemistry 55 (38), 5387–5397. https://doi.org/10.1021/acs.biochem.6b00727.

Kwon, B., Mandal, T., Elkins, M.R., Oh, Y., Cui, Q., Hong, M., 2020. Cholesterol interaction with the trimeric HIV fusion protein Gp41 in lipid bilayers investigated by solid-state NMR spectroscopy and molecular dynamics simulations. J. Mol. Biol. 432 (16), 4705–4721. https://doi.org/10.1016/j.jmb.2020.06.017.

Lamb, R.A., Zebedee, S.L., Richardson, C.D., 1985. Influenza virus M2 protein is an integral membrane protein expressed on the infected-cell surface. Cell. https://doi.org/10.1016/0092-8674(85)90211-9.

Lan, Y., Zhang, Y., Dong, L., Wang, D., Huang, W., Xin, L., Yang, L., Zhao, X., Li, Z., Wang, W., Li, X., Xu, C., Yang, L., Guo, J., Wang, M., Peng, Y., Gao, Y., Guo, Y., Wen, L., Jiang, T., Shu, Y., 2010. A comprehensive surveillance of adamantane resistance among human influenza A virus isolated from mainland China between 1956 and 2009. Antivir. Ther. 15 (6), 853–859. https://doi.org/10.3851/IMP1656.

Lazaridis, T., 2023. Molecular origins of asymmetric proton conduction in the influenza M2 channel. Biophys. J. 122 (1), 90–98. https://doi.org/10.1016/j.bpj.2022.11.029.

Leonov, H., Astrahan, P., Krugliak, M., Arkin, I.T., 2011. How do aminoadamantanes block the influenza M2 channel, and how does resistance develop? J. Am. Chem. Soc. 133 (25), 9903–9911. https://doi.org/10.1021/ja202288m.

Li, F., Ma, C., Degrado, W.F., Wang, J., 2016. Discovery of highly potent inhibitors targeting the predominant drug-resistant S31N mutant of the influenza A virus M2 proton channel. J. Med. Chem. 59 (3), 1207–1216. https://doi.org/10.1021/acs.jmedchem.5b01910.

Li, F., Ma, C., Hu, Y., Wang, Y., Wang, J., 2016. Discovery of potent antivirals against amantadine-resistant influenza A viruses by targeting the M2-S31N proton channel. ACS Infect. Dis. 2 (10), 726–733. https://doi.org/10.1021/acsinfecdis.6b00130.

Li, F., Hu, Y., Wang, Y., Ma, C., Wang, J., 2017. Expeditious Lead optimization of isoxazole-containing influenza A virus M2-S31N inhibitors using the Suzuki – Miyaura cross-coupling reaction. J. Med. Chem. 60, 1580–1590. https://doi.org/10.1021/acs.jmedchem.6b01852.

Li, C., Qin, H., Gao, F.P., Cross, T.A., 2007. Solid-state NMR characterization of conformational plasticity within the transmembrane domain of the influenza A M2 proton channel. Biochim. Biophys. Acta Biomembr. 1768 (12), 3162–3170. https://doi.org/10.1016/j.bbamem.2007.08.025.

Li, D., Saito, R., Suzuki, Y., Sato, I., Zaraket, H., Dapat, C., Caperig-Dapat, I.M., Suzuki, H., 2009. In vivo and in vitro alterations in influenza A/H3N2 Virus M2 and hemagglutinin genes: effect of passage in MDCK-SIAT1 cells and conventional MDCK cells. J. Clin. Microbiol. https://doi.org/10.1128/JCM.00892-08.

Li, C., Yi, M., Hu, J., Zhou, H.-X., Cross, T.A., 2008. Solid-state NMR and MD simulations of the antiviral drug amantadine solubilized in DMPC bilayers. Biophys. J. 94 (4), 1295–1302. https://doi.org/10.1529/biophysj.107.112482.

Liang, R., Li, H., Swanson, J.M.J., Voth, G.A., 2014. Multiscale simulation reveals a multifaceted mechanism of proton permeation through the influenza A M2 proton channel. PNAS 111 (26), 9396–9401. https://doi.org/10.1073/pnas.1401997111.

Liang, R., Swanson, J.M.J., Madsen, J.J., Hong, M., De Grado, W.F., Voth, G.A., 2016. Acid activation mechanism of the influenza A M2 proton channel. PNAS 113 (45), E6955–E6964. https://doi.org/10.1073/pnas.1615471113.

Liao, S.Y., Yang, Y., Tietze, D., Hong, M., 2015. The influenza M2 cytoplasmic tail changes the proton-exchange equilibria and the backbone conformation of the transmembrane histidine residue to facilitate proton conduction. J. Am. Chem. Soc. 137 (18), 6067–6077. https://doi.org/10.1021/jacs.5b02510.

Liao, S.Y., Lee, M., Hong, M., 2019. Interplay between membrane curvature and protein conformational equilibrium investigated by solid-state NMR. J. Struct. Biol. https://doi.org/10.1016/j.jsb.2018.02.007.

Lin, T.I., Schroeder, C., 2001. Definitive assignment of proton selectivity and attoampere unitary current to the M2 ion channel protein of influenza A virus. J. Virol. 75 (8), 3647–3656. https://doi.org/10.1128/JVI.75.8.3647-3656.2001.

Lindorff-Larsen, K., Piana, S., Palmo, K., Maragakis, P., Klepeis, J.L., Dror, R.O., Shaw, D. E., 2010. Improved side-chain torsion potentials for the amber Ff99SB protein force field. Proteins Struct. Funct. Bioinf. 78 (8), 1950–1958. https://doi.org/10.1002/prot.22711.

Llabrés, S., Juárez-Jiménez, J., Masetti, M., Leiva, R., Vázquez, S., Gazzarrini, S., Moroni, A., Cavalli, A., Luque, F.J., 2016. Mechanism of the pseudoirreversible binding of amantadine to the M2 proton channel. J. Am. Chem. Soc. 138 (47), 15345–15358. https://doi.org/10.1021/jacs.6b07096.

Ma, C.; Polishchuk, a L.; Ohigashi, Y.; Stouffer, a L.; Schon, a; Magavern, E.; Jing, X.; Lear, J. D.; Freire, E.; Lamb, R. a; DeGrado, W. F.; Pinto, L. H. Identification of the Functional Core of the Influenza A Virus A/M2 Proton-Selective Ion Channel. *Proc Natl Acad Sci U S A* **2009**, *106*, 12283–12288. https://doi.org/0905726106 [pii] \r10.1073/pnas.0905726106 [doi].

Ma, C.; Polishchuk, A. L.; Ohigashi, Y.; Stouffer, A. L.; Schon, A.; Magavern, E.; Jing, X.; Lear, J. D.; Freire, E.; Lamb, R. A.; DeGrado, W. F.; Pinto, L. H. Identification of the Functional Core of the Influenza A Virus A/M2 Proton-Selective Ion Channel. *Proc Natl Acad Sci U S A* **2009**, *106* (30), 12283–12288. https://doi.org/0905726106 [pii]\r10.1073/pnas.0905726106 [doi].

Ma, C., Polishchuk, A.L., Ohigashi, Y., Stouffer, A.L., Schön, A., Magavern, E., Jing, X., Lear, J.D., Freire, E., Lamb, R.A., DeGrado, W.F., Pinto, L.H., 2009. Identification of the functional core of the influenza A virus A/M2 proton-selective ion channel. Proc. Natl. Acad. Sci. 106 (30), 12283–12288. https://doi.org/10.1073/pnas.0905726106.

Ma, C., Polishchuk, A.L., Ohigashi, Y., Stouffer, A.L., Schö, A., Magavern, E., Jing, X., Lear, J.D., Freire, E., Lamb, R.A., Degrado, W.F., Pinto, L.H., 2009. Identification of the functional core of the influenza A virus A/M2 proton-selective ion channel. PNAS 106 (30), 12283–12288.

Machado, M.R., Barrera, E.E., Klein, F., Sóñora, M., Silva, S., Pantano, S., 2019. The SIRAH 2.0 force field: altius, forties, Citius. J. Chem. Theory Comput. 15 (4), 2719–2733. https://doi.org/10.1021/acs.jctc.9b00006.

MacKerell, A.D., Bashford, D., Bellott, M., Dunbrack, R.L., Evanseck, J.D., Field, M.J., Fischer, S., Gao, J., Guo, H., Ha, S., Joseph-McCarthy, D., Kuchnir, L., Kuczera, K., Lau, F.T.K., Mattos, C., Michnick, S., Ngo, T., Nguyen, D.T., Prodhom, B., Reiher, W. E., Roux, B., Schlenkrich, M., Smith, J.C., Stote, R., Straub, J., Watanabe, M., Wiórkiewicz-Kuczera, J., Yin, D., Karplus, M., 1998. All-atom empirical potential for molecular modeling and dynamics studies of proteins. J. Phys. Chem. B 102 (18), 3586–3616. https://doi.org/10.1021/jp973084f.

Mackerell, A.D., Feig, M., Brooks, C.L., 2004. Extending the treatment of backbone energetics in protein force fields: limitations of gas-phase quantum mechanics in reproducing protein conformational distributions in molecular dynamics simulation. J. Comput. Chem. https://doi.org/10.1002/jcc.20065.

MacKerell, A.D., Feig, M., Brooks, C.L., 2004. Improved treatment of the protein backbone in empirical force fields. J. Am. Chem. Soc. 126 (3), 698–699. https://doi.org/10.1021/ja036959e.

Madsen, J.J., Grime, J.M.A.A., Rossman, J.S., Voth, G.A., 2018. Entropic forces drive clustering and spatial localization of influenza A M2 during viral budding. Proc. Natl. Acad. Sci. 115 (37), E8595–E8603. https://doi.org/10.1073/pnas.1805443115.

Mandala, V.S., Liao, S.-Y., Kwon, B., Hong, M., 2017. Structural basis for asymmetric conductance of the influenza M2 proton channel investigated by solid-state NMR spectroscopy. J. Mol. Biol. 429 (14), 2192–2210. https://doi.org/10.1016/j.jmb.2017.05.015.

Marrink, S.J., Risselada, H.J., Yefimov, S., Tieleman, D.P., De Vries, A.H., 2007. The MARTINI force field: coarse grained model for biomolecular simulations. J. Phys. Chem. B 111 (27), 7812–7824. https://doi.org/10.1021/jp071097f.

Martin, K., Heleniust, A., 1991. Nuclear transport of influenza virus ribonucleoproteins: the viral matrix protein (M1) promotes export and inhibits import. Cell 67 (1), 117–130. https://doi.org/10.1016/0092-8674(91)90576-K.

Martyna, A., Bahsoun, B., Badham, M.D., Srinivasan, S., Howard, M.J., Rossman, J.S., 2017. Membrane remodeling by the M2 amphipathic helix drives influenza virus membrane scission. Sci. Rep. 7 (1), 44695. https://doi.org/10.1038/srep44695.

Martyna, A., Rossman, J., 2014. Alterations of membrane curvature during influenza virus budding. Biochem. Soc. Trans. 42 (5), 1425–1428. https://doi.org/10.1042/BST20140136.

Monticelli, L., Kandasamy, S.K., Periole, X., Larson, R.G., Tieleman, D.P., Marrink, S.J., 2008. The MARTINI coarse-grained force field: extension to proteins. J. Chem. Theory Comput. 4 (5), 819–834. https://doi.org/10.1021/ct700324x.

Mould, J.A., Drury, J.E., Frings, S.M., Kaupp, U.B., Pekosz, A., Lamb, R.A., Pinto, L.H., 2000. Permeation and activation of the M2 ion channel of influenza A virus. J. Biol. Chem. 275 (40), 31038–31050. https://doi.org/10.1074/jbc.M003663200.

Mould, J.A., Paterson, R.G., Takeda, M., Ohigashi, Y., Venkataraman, P., Lamb, R.A., Pinto, L.H., 2003. Influenza B virus BM2 protein has ion channel activity that conducts protons across membranes. Dev. Cell 5, 175–184. https://doi.org/10.1016/S1534-5807(03)00190-4.

Movellan, K.T., Wegstroth, M., Overkamp, K., Leonov, A., Becker, S., Andreas, L.B., 2020. Imidazole-imidazole hydrogen bonding in the PH-sensing histidine side chains of influenza A M2. J. Am. Chem. Soc. 142 (6), 2704–2708. https://doi.org/10.1021/jacs.9b10984.

Musharrafieh, R., Lagarias, P.I., Ma, C., Tan, G.S., Kolocouris, A., Wang, J., 2019. The L46P mutant confers a novel allosteric mechanism of resistance toward the influenza A virus M2 S31N proton channel blockers. Mol. Pharmacol. 96 (2), 148–157. https://doi.org/10.1124/mol.119.116640.

Musharrafieh, R., Ma, C., Wang, J., 2020. Discovery of M2 channel blockers targeting the drug-resistant double mutants M2-S31N/L26I and M2-S31N/V27A from the influenza A viruses. Eur. J. Pharm. Sci. 141, 105124. https://doi.org/10.1016/j.ejps.2019.105124.

Musharrafieh, R., Lagarias, P., Ma, C., Hau, R., Romano, A., Lambrinidis, G., Kolocouris, A., Wang, J., 2020. Investigation of the drug resistance mechanism of M2-S31N channel blockers through biomolecular simulations and viral passage experiments. ACS Pharmacol. Transl. Sci. 3 (4), 666–675. https://doi.org/10.1021/acsptsci.0c00018.

Nguyen, P.A., Soto, C.S., Polishchuk, A., Caputo, G.A., Tatko, C.D., Ma, C., Ohigashi, Y., Pinto, L.H., Degrado, W.F., Howard, K.P., 2008. PH-induced conformational change of the influenza M2 protein C-terminal domain. Biochemistry. https://doi.org/10.1021/bi801315m.

Nishimura, K., Kim, S., Zhang, L., Cross, T.A., 2002. The closed state of a H+ channel helical bundle combining precise orientational and distance restraints from solid state NMR. Biochemistry 41 (44), 13170–13177. https://doi.org/10.1021/bi0262799.

Ohigashi, Y., Ma, C., Jing, X., Balannick, V., Pinto, L.H., Lamb, R.A., 2009. An amantadine-sensitive chimeric BM2 ion channel of influenza B virus has implications for the mechanism of drug inhibition. PNAS 106 (44), 18775–18779. https://doi.org/10.1073/pnas.0910584106.

Okada, A., Miura, T., Takeuchi, H., 2001. Protonation of histidine and histidine-tryptophan interaction in the activation of the M2 ion channel from influenza A virus. Biochemistry. https://doi.org/10.1021/bi0028441.

Oostenbrink, C., Villa, A., Mark, A.E., Van Gunsteren, W.F., 2004. A biomolecular force field based on the free enthalpy of hydration and solvation: the GROMOS force-field parameter sets 53A5 and 53A6. J. Comput. Chem. 25, 1656–1676.

Ouyang, B., Xie, S., Berardi, M.J., Zhao, X., Dev, J., Yu, W., Sun, B., Chou, J.J., 2013. Unusual architecture of the P7 channel from hepatitis C virus. Nature. https://doi.org/10.1038/nature12283.

Paget, J., Danielle Iuliano, A., Taylor, R.J., Simonsen, L., Viboud, C., Spreeuwenberg, P., 2022. Estimates of mortality associated with seasonal influenza for the European union from the GLaMOR project. Vaccine 40 (9), 1361–1369. https://doi.org/10.1016/j.vaccine.2021.11.080.

Park, E.K., Castrucci, M.R., Portner, A., Kawaoka, Y., 1998. The M2 ectodomain is important for its incorporation into influenza A virions. J. Virol. https://doi.org/10.1128/jvi.72.3.2449-2455.1998.

Pastor, R.W., MacKerell, A.D., 2011. Development of the CHARMM force field for lipids. J. Phys. Chem. Lett. 2 (13), 1526–1532. https://doi.org/10.1021/jz200167q.

Petrich, A., Dunsing, V., Bobone, S., Chiantia, S., 2021. Influenza A M2 recruits M1 to the plasma membrane: a fluorescence fluctuation microscopy study. Biophys. J. 120 (24), 5478–5490. https://doi.org/10.1016/j.bpj.2021.11.023.
Pielak, R.M., Chou, J.J., 2010. Solution NMR structure of the V27A drug resistant mutant of influenza A M2 channel. Biochem. Biophys. Res. Commun. 401 (1), 58–63. https://doi.org/10.1016/j.bbrc.2010.09.008.
Pielak, R.M., Chou, J.J., 2010. Flu channel drug resistance: a tale of two sites. Protein Cell 1 (3), 246–258. https://doi.org/10.1007/s13238-010-0025-y.
Pielak, R.M., Chou, J.J., 2011. Influenza M2 proton channels. Biochim. Biophys. Acta - B Biomembr. 522–529. https://doi.org/10.1016/j.bbamem.2010.04.015.
Pielak, R.M., Schnell, J.R., Chou, J.J., 2009. Mechanism of drug inhibition and drug resistance of influenza A M2 channel. PNAS 106 (18), 7379–7384. https://doi.org/10.1073/pnas.0902548106.
Pielak, R.M., Oxenoid, K., Chou, J.J., 2011. Structural investigation of rimantadine inhibition of the AM2-BM2 chimera channel of influenza viruses. Structure 19 (11), 1655–1663. https://doi.org/10.1016/j.str.2011.09.003.
Pinto, L.H., Lamb, R.A., 2007. Controlling influenza virus replication by inhibiting its proton channel. Mol. Biosyst. 3 (1), 18–23. https://doi.org/10.1039/b611613m.
Pinto, L.H., Holsinger, L.J., Lamb, R.A., 1992. Influenza virus M2 protein has ion channel activity. Cell 69 (3), 517–528. https://doi.org/10.1016/0092-8674(92)90452-I.
Pinto, L.H., Dieckmann, G.R., Gandhi, C.S., Papworth, C.G., Braman, J., Shaughnessy, M. A., Lear, J.D., Lamb, R.A., DeGrado, W.F., 1997. A functionally defined model for the M2 proton channel of influenza A virus suggests a mechanism for its ion selectivity. PNAS 94 (21), 11301–11306. https://doi.org/10.1073/pnas.94.21.11301.
Pinto, L.H., Lamb, R.A., 2006. The M2 proton channels of influenza A and B viruses. J. Biol. Chem. 8997–9000. https://doi.org/10.1074/jbc.R500020200.
Poma, A.B., Cieplak, M., Theodorakis, P.E., 2017. Combining the MARTINI and structure-based coarse-grained approaches for the molecular dynamics studies of conformational transitions in proteins. J. Chem. Theory Comput. 13 (3), 1366–1374. https://doi.org/10.1021/acs.jctc.6b00986.
Poma, A.B., Thu, T.T.M., Tri, L.T.M., Nguyen, H.L., Li, M.S., 2021. Nanomechanical stability of Aβ tetramers and fibril-like structures: molecular dynamics simulations. J. Phys. Chem. B 125 (28), 7628–7637. https://doi.org/10.1021/acs.jpcb.1c02322.
Rey-carrizo, M., Torres, E., Ma, C., Barniol-xicota, M., Wang, J., Wu, Y., Naesens, L., Degrado, W.F., Lamb, R.A., Pinto, L.H., Vázquez, S., Va, S., 2013. 3-azatetracyclo [5.2.1.15,8.01,5]undecane derivatives: from wild-type inhibitors of the M2 ion channel of influenza A virus to derivatives with potent activity against the V27A mutant. J. Med. Chem. 56, 9265–9274. https://doi.org/10.1021/jm401340p.
Rey-Carrizo, M., Barniol-Xicota, M., Ma, C., Frigolé-Vivas, M., Torres, E., Naesens, L., Llabrés, S., Juárez-Jiménez, J., Luque, F.J., Degrado, W.F., Lamb, R.A., Pinto, L.H., Vázquez, S., 2014. Easily accessible polycyclic amines that inhibit the wild-type and amantadine-resistant mutants of the M2 channel of influenza A virus. J. Med. Chem. 57 (13), 5738–5747. https://doi.org/10.1021/jm5005804.
Rey-Carrizo, M., Gazzarrini, S., Llabrés, S., Frigolé-Vivas, M., Juárez-Jiménez, J., Font-Bardia, M., Naesens, L., Moroni, A., Luque, F.J., Vázquez, S., 2015. New polycyclic dual inhibitors of the wild type and the V27A mutant M2 channel of the influenza A virus with unexpected binding mode. Eur. J. Med. Chem. 96, 318–329. https://doi.org/10.1016/j.ejmech.2015.04.030.
Rizzo, R.C., Jorgensen, W.L., 1999. OPLS all-atom model for amines: resolution of the amine hydration problem. J. Am. Chem. Soc. 121 (20), 4827–4836. https://doi.org/10.1021/ja984106u.
Rosenberg, M.R., Casarotto, M.G., 2010. Coexistence of two adamantane binding sites in the influenza A M2 ion channel. PNAS 107 (31), 13866–13871. https://doi.org/10.1073/pnas.1002051107.
Rossman, J.S., Jing, X., Leser, G.P., Lamb, R.A., 2010. Influenza virus M2 protein mediates ESCRT-independent membrane scission. Cell 142 (6), 902–913. https://doi.org/10.1016/j.cell.2010.08.029.
Rossman, J.S., Jing, X., Leser, G.P., Balannik, V., Pinto, L.H., Lamb, R.A., 2010. Influenza virus M2 ion channel protein is necessary for filamentous virion formation. J. Virol. 84 (10), 5078–5088. https://doi.org/10.1128/JVI.00119-10.
Rossman, J.S., Lamb, R.A., 2011. Influenza virus assembly and budding. Virology 411 (2), 229–236. https://doi.org/10.1016/j.virol.2010.12.003.
Sakaguchi, T., Tu, Q., Pinto, L.H., Lamb, R.A., 1997. The active oligomeric state of the minimalistic influenza virus M2 ion channel is a tetramer. PNAS 94 (10), 5000–5005. https://doi.org/10.1073/pnas.94.10.5000.
Sakai, Y., Kawaguchi, A., Nagata, K., Hirokawa, T., 2018. Analysis by metadynamics simulation of binding pathway of influenza virus M2 channel blockers. Microbiol. Immunol. 62 (1), 34–43. https://doi.org/10.1111/1348-0421.12561.
Salom, D., Hill, B.R., Lear, J.D., DeGrado, W.F., 2000. PH-dependent tetramerization and amantadine binding of the transmembrane helix of M2 from the influenza A virus. Biochemistry 39 (46), 14160–14170. https://doi.org/10.1021/bi001799u.
Samways, M.L., Bruce Macdonald, H.E., Taylor, R.D., Essex, J.W., 2023. Water networks in complexes between proteins and FDA-approved drugs. J. Chem. Inf. Model. 63 (1), 387–396. https://doi.org/10.1021/acs.jcim.2c01225.
Santner, P., Martins, J.M.D.S., Laursen, J.S., Behrendt, L., Riber, L., Olsen, C.A., Arkin, I. T., Winther, J.R., Willemoës, M., Lindorff-Larsen, K., 2018. A Robust Proton Flux (PHlux) assay for studying the function and inhibition of the influenza A M2 proton channel. Biochemistry. https://doi.org/10.1021/acs.biochem.8b00721.
Santner, P., Martins, J.M.D.S., Kampmeyer, C., Hartmann-Petersen, R., Laursen, J.S., Stein, A., Olsen, C.A., Arkin, I.T., Winther, J.R., Willemoës, M., Lindorff-Larsen, K., 2018. Random mutagenesis analysis of the influenza A M2 proton channel reveals novel resistance mutants. Biochemistry. https://doi.org/10.1021/acs.biochem.8b00722.
Schnell, J.R., Chou, J.J., 2008. Structure and mechanism of the M2 proton channel of influenza A virus. Nature 451 (7178), 591–595. https://doi.org/10.1038/nature06531.
Schroeder, C., Heider, H., Möncke-Buchner, E., Lin, T.I., 2005. The influenza virus ion channel and maturation cofactor M2 is a cholesterol-binding protein. Eur. Biophys. J. 34 (1), 52–66. https://doi.org/10.1007/s00249-004-0424-1.
Scott, C., Kankanala, J., Foster, T.L., Goldhill, D.H., Bao, P., Simmons, K., Pingen, M., Bentham, M., Atkins, E., Loundras, E., Elderfield, R., Claridge, J.K., Thompson, J., Stilwell, P.R., Tathineni, R., McKimmie, C.S., Targett-Adams, P., Schnell, J.R., Cook, G.P., Evans, S., Barclay, W.S., Foster, R., Griffin, S., 2020. Site-Directed M2 proton channel inhibitors enable synergistic combination therapy for rimantadine-resistant pandemic influenza. PLoS Pathog. https://doi.org/10.1371/JOURNAL.PPAT.1008716.
Sharma, M.; Yi, M.; Dong, H.; Qin, H.; Peterson, E.; Busath, D. D.; Zhou, H.-X.; Cross, T. A. Insight into the Mechanism of the Influenza A Proton Channel from a Structure in a Lipid Bilayer. *Science (1979)* **2010**, *330* (6003), 509–512. https://doi.org/10.1126/science.1191750.
Shimbo, K., Brassard, D.L., Lamb, R.A., Pinto, L.H., 1996. Ion Selectivity and activation of the M2 ion channel of influenza virus. Biophys. J. 70 (3), 1335–1346. https://doi.org/10.1016/S0006-3495(96)79690-X.
Singh Tomar, P.P., Arkin, I.T., 2020. SARS-CoV-2 E protein is a potential ion channel that can be inhibited by gliclazide and memantine. Biochem. Biophys. Res. Commun. 530 (1), 10–14. https://doi.org/10.1016/j.bbrc.2020.05.206.
Skehel, J.J., Hay, A.J., Armstrong, J.A., 1978. On the mechanism of inhibition of influenza virus replication by amantadine hydrochloride. J. Gen. Virol. 38 (1), 97–110. https://doi.org/10.1099/0022-1317-38-1-97.
Sprenger, K.G., Jaeger, V.W., Pfaendtner, J., 2015. The General AMBER Force Field (GAFF) can accurately predict thermodynamic and transport properties of many ionic liquids. J. Phys. Chem. B 119 (18), 5882–5895. https://doi.org/10.1021/acs.jpcb.5b00689.
Stamatiou, G., Kolocouris, A., Kolocouris, N., Fytas, G., Foscolos, G.B., Neyts, J., De Clercq, E., 2001. Novel 3-(2-Adamantyl)pyrrolidines with potent activity against influenza A virus - identification of aminoadamantane derivatives bearing two pharmacophoric amine groups. Bioorg. Med. Chem. Lett. 11 (16). https://doi.org/10.1016/S0960-894X(01)00388-2.
Stampolaki, M.; Varkey, A.; Nimerovsky, E.; Leonov A; Becker S; Andreas, L. *Seeing Double: The Persistent Dimer-of-Dimers Structure of Drug Resistant Influenza A M2*; 2024. https://doi.org/10.26434/chemrxiv-2024-v4rrs.
Stampolaki, M., Hoffmann, A., Tekwani, K., Georgiou, K., Tzitzoglaki, C., Ma, C., Becker, S., Schmerer, P., Döring, K., Stylianakis, I., Turcu, A.L., Wang, J., Vázquez, S., Andreas, L.B., Schmidtke, M., Kolocouris, A., 2023. A study of the activity of adamantyl amines against mutant influenza A M2 channels identified a polycyclic cage amine triple blocker, explored by molecular dynamics simulations and solid-state NMR**. ChemMedChem. https://doi.org/10.1002/cmdc.202300182.
Stouffer, A.L., Nanda, V., Lear, J.D., DeGrado, W.F., 2005. Sequence determinants of a transmembrane proton channel: an inverse relationship between stability and function. J. Mol. Biol. 347 (1), 169–179. https://doi.org/10.1016/j.jmb.2005.01.023.
Stouffer, A.L., Ma, C., Cristian, L., Ohigashi, Y., Lamb, R.A., Lear, J.D., Pinto, L.H., DeGrado, W.F., 2008. The interplay of functional tuning, drug resistance, and thermodynamic stability in the evolution of the M2 proton channel from the influenza A virus. Structure. https://doi.org/10.1016/j.str.2008.04.011.
Stouffer, A.L., Acharya, R., Salom, D., Levine, A.S., Di Costanzo, L., Soto, C.S., Tereshko, V., Nanda, V., Stayrook, S., DeGrado, W.F., 2008. Structural basis for the function and inhibition of an influenza virus proton channel. Nature 451 (7178), 596–599. https://doi.org/10.1038/nature06528.
Sugrue, R.J., Belshe, R.B., Hay, A.J., 1990. Palmitoylation of the influenza a virus M2 protein. Virology 179 (1), 51–56. https://doi.org/10.1016/0042-6822(90)90272-S.
Sugrue, R.J., Hay, A.J., 1991. Structural characteristics of the M2 protein of influenza a viruses: evidence that it forms a tetrameric channel. Virology 180 (2), 617–624. https://doi.org/10.1016/0042-6822(91)90075-M.
Sutherland, M., Tran, N., Hong, M., 2022. Clustering of tetrameric influenza M2 peptides in lipid bilayers investigated by 19F solid-state NMR. Biochim. Biophys. Acta (BBA) - B Biomembr. 1864 (7), 183909. https://doi.org/10.1016/j.bbamem.2022.183909.
Tang, Y., Zaitseva, F., Lamb, R.A., Pinto, L.H., 2002. The gate of the influenza virus M2 proton channel is formed by a single tryptophan residue. J. Biol. Chem. 277 (42), 39880–39886. https://doi.org/10.1074/jbc.M206582200.
Tekwani Movellan, K., Wegstroth, M., Overkamp, K., Leonov, A., Becker, S., Andreas, L. B., 2023. Real-time tracking of drug binding to influenza A M2 reveals a high energy barrier. J. Struct. Biol. X 8, 100090. https://doi.org/10.1016/j.yjsbx.2023.100090.
Thomaston, J.L., Woldeyes, R.A., Nakane, T., Yamashita, A., Tanaka, T., Koiwai, K., Brewster, A.S., Barad, B.A., Chen, Y., Lemmin, T., Uervirojnangkoorn, M., Arima, T., Kobayashi, J., Masuda, T., Suzuki, M., Sugahara, M., Sauter, N.K., Tanaka, R., Nureki, O., Tono, K., Joti, Y., Nango, E., Iwata, S., Yumoto, F., Fraser, J.S., DeGrado, W.F., 2017. XFEL structures of the influenza M2 proton channel: room temperature water networks and insights into proton conduction. PNAS 114, 13357–13362. https://doi.org/10.1073/pnas.1705624114.
Thomaston, J.L., Polizzi, N.F., Konstantinidi, A., Wang, J., Kolocouris, A., Degrado, W.F., 2018. Inhibitors of the M2 proton channel engage and disrupt transmembrane networks of hydrogen-bonded waters. J. Am. Chem. Soc. 140 (45), 15219–15226. https://doi.org/10.1021/jacs.8b06741.
Thomaston, J.L., Polizzi, N.F., Konstantinidi, A., Wang, J., Kolocouris, A., Degrado, W.F., 2018. Inhibitors of the M2 proton channel engage and disrupt transmembrane networks of hydrogen-bonded waters. J. Am. Chem. Soc. 45, 15219–15226. https://doi.org/10.1021/jacs.8b06741.
Thomaston, J.L., Konstantinidi, A., Liu, L., Lambrinidis, G., Tan, J., Caffrey, M., Wang, J., Degrado, W.F., Kolocouris, A., 2020. X-ray crystal structures of the influenza M2 proton channel drug-resistant V27A mutant bound to a spiro-adamantyl amine

inhibitor reveal the mechanism of adamantane resistance. Biochemistry 59 (4), 627–634. https://doi.org/10.1021/acs.biochem.9b00971.
Thomaston, J.L., Samways, M.L., Konstantinidi, A., Ma, C., Hu, Y., Bruce Macdonald, H. E., Wang, J., Essex, J.W., Degrado, W.F., Kolocouris, A., 2021. Rimantadine binds to and inhibits the influenza A M2 proton channel without enantiomeric specificity. Biochemistry 60 (32), 2471–2482. https://doi.org/10.1021/acs.biochem.1c00437.
Tian, C., Gao, P.F., Pinto, L.H., Lamb, R.A., Cross, T.A., 2003. Initial structural and dynamic characterization of the M2 protein transmembrane and amphipathic helices in lipid bilayers. Protein Sci. 12 (11), 2597–2605. https://doi.org/10.1110/ps.03168503.
Tian, C., Kasavajhala, K., Belfon, K.A.A., Raguette, L., Huang, H., Migues, A.N., Bickel, J., Wang, Y., Pincay, J., Wu, Q., Simmerling, C., 2020. Ff19SB: amino-acid-specific protein backbone parameters trained against quantum mechanics energy surfaces in solution. J. Chem. Theory Comput. 16 (1), 528–552. https://doi.org/10.1021/acs.jctc.9b00591.
Tietjen, I.; Kwan, D. C.; Petrich, A.; Zell, R.; Antoniadou, I. T.; Gavriilidou, A.; Tzitzoglaki, C.; Rallis, M.; Fedida, D.; Sureda, F. X.; Mestdagh, C.; Naesens, L. M. J.; Chiantia, S.; Johnson, F. B.; Kolocouris, A. Antiviral Mechanisms and Preclinical Evaluation of Amantadine Analogs That Continue to Inhibit Influenza A Viruses with M2 S31N-Based Drug Resistance. *bioRxiv* **2024**, 2024.09.09.612141. https://doi.org/10.1101/2024.09.09.612141.
Toft-Bertelsen, T. L.; Jeppesen, M. G.; Tzortzini, E.; Xue, K.; Giller, K.; Becker, S.; Mujezinovic, A.; Bentzen, B. H.; B. Andreas, L.; Kolocouris, A.; Kledal, T. N.; Rosenkilde, M. M. Amantadine Inhibits Known and Novel Ion Channels Encoded by SARS-CoV-2 in Vitro. *Commun Biol* **2021**, *4* (1), 1–10. https://doi.org/10.1038/s42003-021-02866-9.
Tomar, P.P.S., Krugliak, M., Arkin, I.T., 2021. Blockers of the Sars-Cov-2 3a channel identified by targeted drug repurposing. Viruses. https://doi.org/10.3390/v13030532.
Torres, E., Fernández, R., Miquet, S., Font-Bardia, M., Vanderlinden, E., Naesens, L., Vázquez, S., 2012. Synthesis and anti-influenza a virus activity of 2,2-dialkylamantadines and related compounds. ACS Med. Chem. Lett. 3 (12), 1065–1069. https://doi.org/10.1021/ml300279b.
Torres, E., Duque, M.D., Vanderlinden, E., Ma, C., Pinto, L.H., Camps, P., Froeyen, M., Vázquez, S., Naesens, L., 2013. Role of the viral hemagglutinin in the anti-influenza virus activity of newly synthesized polycyclic amine compounds. Antiviral Res. 99 (3), 281–291. https://doi.org/10.1016/j.antiviral.2013.06.006.
Torres, E., Leiva, R., Gazzarrini, S., Rey-Carrizo, M., Frigolé-Vivas, M., Moroni, A., Naesens, L., Vázquez, S., 2014. Azapropellanes with anti-influenza a virus activity. ACS Med. Chem. Lett. https://doi.org/10.1021/ml500108s.
Torres, J., Maheswari, U., Parthasarathy, K., Ng, L., Liu, D.X., Gong, X., 2007. Conductance and amantadine binding of a pore formed by a lysine-flanked transmembrane domain of SARS coronavirus envelope protein. Protein Sci. 16 (9), 2065–2071. https://doi.org/10.1110/ps.062730007.
Townsend, J.A., Sanders, H.M., Rolland, A.D., Park, C.K., Horton, N.C., Prell, J.S., Wang, J., Marty, M.T., 2021. Influenza AM2 channel oligomerization is sensitive to its chemical environment. Anal. Chem. 93 (48), 16273–16281. https://doi.org/10.1021/acs.analchem.1c04660.
Townsend, J.A., Fapohunda, O., Wang, Z., Pham, H., Taylor, M.T., Kloss, B., Park, S.H., Opella, S., Aspinwall, C.A., Marty, M.T., 2024. Differences in oligomerization of the SARS-CoV-2 envelope protein, poliovirus VP4, and HIV Vpu. Biochemistry 63 (3), 241–250. https://doi.org/10.1021/acs.biochem.3c00437.
Tu, Q., Pinto, L.H., Luo, G., Shaughnessy, M.A., Mullaney, D., Kurtz, S., Krystal, M., Lamb, R.A., 1996. Characterization of inhibition of M2 ion channel activity by BL-1743, an inhibitor of influenza A virus. J. Virol. https://doi.org/10.1128/jvi.70.7.4246-4252.1996.
Tzitzoglaki, C., Wright, A., Freudenberger, K., Hoffmann, A., Tietjen, I., Stylianakis, I., Kolarov, F., Fedida, D., Schmidtke, M., Gauglitz, G., Cross, T.A., Kolocouris, A., 2017. Binding and proton blockage by amantadine variants of the influenza M2WT and M2S31N explained. J. Med. Chem. 60 (5), 1716–1733. https://doi.org/10.1021/acs.jmedchem.6b01115.
Tzitzoglaki, C., Wright, A., Freudenberger, K., Hoffmann, A., Tietjen, I., Stylianakis, I., Kolarov, F., Fedida, D., Schmidtke, M., Gauglitz, G., Cross, T.A., Kolocouris, A., 2017. Binding and proton blockage by amantadine variants of the influenza M2 $_{WT}$ and M2 $_{S31N}$ explained. J. Med. Chem. 60 (5), 1716–1733. https://doi.org/10.1021/acs.jmedchem.6b01115.
Tzitzoglaki, C., McGuire, K., Lagarias, P., Konstantinidi, A., Hoffmann, A., Fokina, N.A., Ma, C.C., Papanastasiou, I.P., Schreiner, P.R., Vázquez, S., Schmidtke, M., Wang, J., Busath, D.D., Kolocouris, A., Vazquez, S., Schmidtke, M., Wang, J., Busath, D.D., Kolocouris, A., 2020. Chemical probes for blocking of influenza A M2 wild-type and S31N channels. ACS Chem. Biol. 15 (9), 2331–2337. https://doi.org/10.1021/acschembio.0c00553.
Tzitzoglaki, C., Hoffmann, A., Turcu, A.L., Schmerer, P., Ma, C., Laros, G., Liolios, C., José, B., Wang, J., Vázquez, S., Schmidtke, M., Kolocouris, A., 2022. Amantadine variant – aryl conjugates that inhibit multiple M2 mutant – amantadine resistant influenza a viruses. Eur. J. Med. Chem. Rep. 6 (September), 100083. https://doi.org/10.1016/j.ejmcr.2022.100083.
Vanommeslaeghe, K., Hatcher, E., Acharya, C., Kundu, S., Zhong, S., Shim, J., Darian, E., Guvench, O., Lopes, P., Vorobyov, I., Mackerell, A.D., 2010. CHARMM general force field: a force field for drug-like molecules compatible with the CHARMM all-atom additive biological force fields. J. Comput. Chem. 31, 671–690. https://doi.org/10.1002/jcc.21367.
Verdiá-Báguena, C., Nieto-Torres, J.L., Alcaraz, A., DeDiego, M.L., Torres, J., Aguilella, V.M., Enjuanes, L., 2012. Coronavirus E protein forms ion channels with functionally and structurally-involved membrane lipids. Virology 432 (2), 485–494. https://doi.org/10.1016/j.virol.2012.07.005.
Wang, J.; Qiu, J. X.; Soto, C.; F., W.; DeGrado; Degrado, W. F. Structural and Dynamic Mechanisms for the Function and Inhibition of the M2 Proton Channel from Influenza A Virus. *Curr Opin Struct Biol* **2011**, *21* (1), 68–80. https://doi.org/10.1016/j.sbi.2010.12.002.
Wang, Y., Hu, Y., Xu, S., Zhang, Y., Musharrafieh, R., Hau, R.K., Ma, C., Wang, J., 2018. In vitro pharmacokinetic optimizations of AM2-S31N channel blockers led to the discovery of slow-binding inhibitors with potent antiviral activity against drug-resistant influenza A viruses. J. Med. Chem. 61 (3), 1074–1085. https://doi.org/10.1021/acs.jmedchem.7b01536.
Wang, J., Kim, S., Kovacs, F., Cross, T.A., 2001. Structure of the transmembrane region of the M2 protein H+ channel. Protein Sci. 10 (11), 2241–2250. https://doi.org/10.1110/ps.17901.
Wang, J., Schnell, J.R., Chou, J.J., 2004. Amantadine partition and localization in phospholipid membrane: a solution NMR study. Biochem. Biophys. Res. Commun. 324 (1), 212–217. https://doi.org/10.1016/j.bbrc.2004.09.039.
Wang, J., Ma, C., Fiorin, G., Carnevale, V., Wang, T., Hu, F., Lamb, R.A., Pinto, L.H., Hong, M., Klein, M.L., Degrado, W.F., 2011. Molecular dynamics simulation directed rational design of inhibitors targeting drug-resistant mutants of influenza A virus M2. J. Am. Chem. Soc. 133 (32), 12834–12841. https://doi.org/10.1021/ja204969m.
Wang, C., Takeuchi, K., Pinto, L.H., Lamb, R.A., 1993. Ion channel activity of influenza A virus M2 protein: characterization of the amantadine block. J. Virol. 67 (9), 5585–5594. https://doi.org/10.1128/jvi.67.9.5585-5594.1993.
Wang, C., Lamb, R.A., Pinto, L.H., 1994. Direct measurement of the influenza A virus M2 protein ion channel activity in mammalian cells. Virology. https://doi.org/10.1006/viro.1994.1628.
Wang, J., Wu, Y., Ma, C., Fiorin, G., Wang, J., Pinto, L.H., Lamb, R.A., Klein, M.L., DeGrado, W.F., 2013. Structure and inhibition of the drug-resistant S31N mutant of the M2 ion channel of influenza A virus. PNAS 110 (4), 1315–1320. https://doi.org/10.1073/pnas.1216526110.
Wang, J., Ma, C., Wang, J., Jo, H., Canturk, B., Fiorin, G., Pinto, L.H., Lamb, R.A., Klein, M.L., DeGrado, W.F., 2013. Discovery of novel dual inhibitors of the wild-type and the most prevalent drug-resistant mutant, S31N, of the M2 proton channel from influenza A virus. J. Med. Chem. 56 (7), 2804–2812. https://doi.org/10.1021/jm301538e.
Wang, J.J., Wu, Y., Ma, C., Fiorin, G., Pinto, L.H., Lamb, R.A., Klein, M.L., Degrado, W.F., 2013. Structure and inhibition of the drug-resistant S31N mutant of the M2 ion channel of influenza A virus. PNAS 110 (4), 1315–1320. https://doi.org/10.1073/pnas.1216526110.
Watkins, L.C., Degrado, W.F., Voth, G.A., 2020. Influenza A M2 inhibitor binding understood through mechanisms of excess proton stabilization and channel dynamics. J. Am. Chem. Soc. 142 (41), 17425–17433. https://doi.org/10.1021/jacs.0c06419.
C. Watkins, L.; F. DeGrado, W.; A. Voth, G. Multiscale Simulation of an Influenza A M2 Channel Mutant Reveals Key Features of Its Markedly Different Proton Transport Behavior. *J Am Chem Soc* **2022**, *144* (2), 769–776. https://doi.org/10.1021/jacs.1c09281.
Watkins, L.C., Liang, R., Swanson, J.M.J., DeGrado, W.F., Voth, G.A., 2019. Proton-induced conformational and hydration dynamics in the influenza A M2 channel. J. Am. Chem. Soc. 141 (29), 11667–11676. https://doi.org/10.1021/jacs.9b05136.
Williams, J.K., Tietze, D., Wang, J., Wu, Y., Degrado, W.F., Hong, M., 2013. Drug-induced conformational and dynamical changes of the S31N mutant of the influenza M2 proton channel investigated by solid-state NMR. J. Am. Chem. Soc. 135 (26), 9885–9897. https://doi.org/10.1021/ja4041412.
Wilson, L., Mckinlay, C., Gage, P., Ewart, G., 2004. SARS Coronavirus E protein forms cation-selective ion channels. Virology 330 (1), 322–331. https://doi.org/10.1016/j.virol.2004.09.033.
Wright, A.K., Batsomboon, P., Dai, J., Hung, I., Zhou, H.X., Dudley, G.B., Cross, T.A., 2016. Differential binding of rimantadine enantiomers to influenza A M2 proton channel. J. Am. Chem. Soc. 138 (5), 1506–1509. https://doi.org/10.1021/jacs.5b13129.
K. Wright, A.; Paulino, J.; A. Cross, T. Emulating Membrane Protein Environments—How Much Lipid Is Required for a Native Structure: Influenza S31N M2. *J Am Chem Soc* **2022**, *144* (5), 2137–2148. https://doi.org/10.1021/jacs.1c10174.
Wu, Y., Canturk, B., Jo, H., Ma, C., Gianti, E., Klein, M.L., Pinto, L.H., Lamb, R.A., Fiorin, G., Wang, J., Degrado, W.F., 2014. Flipping in the pore: discovery of dual inhibitors that bind in different orientations to the wild-type versus the amantadine-resistant S31n mutant of the influenza a virus M2 proton channel. J. Am. Chem. Soc. 136 (52), 17987–17995. https://doi.org/10.1021/ja508461m.
Wu, Y., Voth, G.A., 2005. A computational study of the closed and open states of the influenza A M2 proton channel. Biophys. J. 89 (4), 2402–2411. https://doi.org/10.1529/biophysj.105.066647.
Yamada, T., Miyazaki, Y., Harada, S., Kumar, A., Vanni, S., Shinoda, W., 2023. Improved protein model in SPICA force field. J. Chem. Theory Comput. 19 (23), 8967–8977. https://doi.org/10.1021/acs.jctc.3c01016.
Yang, Y., Dong, H., Zhou, H.-X., 2021. Effects of cholesterol on the partitioning of a drug molecule in lipid bilayers. J. Phys. Chem. B 125 (20), 5338–5345. https://doi.org/10.1021/acs.jpcb.1c02436.
Yi, M., Cross, T.A., Zhou, H.X., 2008. A secondary gate as a mechanism for inhibition of the M2 proton channel by amantadine. J. Phys. Chem. B 112 (27), 7977–7979. https://doi.org/10.1021/jp800171m.
Yi, M., Cross, T.A., Zhou, H.-X.-X., 2009. Conformational heterogeneity of the M2 proton channel and a structural model for channel activation. PNAS 106 (32), 13311–13316. https://doi.org/10.1073/pnas.0906553106.

Yue, Z., Wu, J., Teng, D., Wang, Z., Voth, G.A., 2024. Activation of the influenza B M2 proton channel (BM2). Biochemistry 63 (22), 3011–3019. https://doi.org/10.1021/acs.biochem.4c00607.

Zhang, R., Cross, T.A., Fu, R., 2021. Detecting water-protein chemical exchange in membrane-bound proteins/peptides by solid-state NMR spectroscopy. Magn. Reson. Lett. https://doi.org/10.1016/j.mrl.2021.09.002.

Zhao, X., Li, R., Zhou, Y., Xiao, M., Ma, C., Yang, Z., Zeng, S., Du, Q., Yang, C., Jiang, H., Hu, Y., Wang, K., Mok, C.K.P., Sun, P., Dong, J., Cui, W., Wang, J., Tu, Y., Yang, Z., Hu, W., 2018. Discovery of highly potent pinanamine-based inhibitors against amantadine- and oseltamivir-resistant influenza A viruses. J. Med. Chem. 61 (12), 5187–5198. https://doi.org/10.1021/acs.jmedchem.8b00042.